NOTE TO USERS

Page(s) not included in the original manuscript and are unavailable from the author or university. The manuscript was scanned as received.

126-132

This reproduction is the best copy available.

UMI®

uOttawa

L'Université canadienne
Canada's university

FACULTÉ DES ÉTUDES SUPÉRIEURES ET POSTOCTORALES

uOttawa

L'Université canadienne
Canada's university

FACULTY OF GRADUATE AND POSDOCTORAL STUDIES

Aurelian Tanase

AUTEUR DE LA THÈSE / AUTHOR OF THESIS

M.A.Sc. (Mechanical Engineering)

GRADE / DEGREE

Department of Mechanical Engineering

FACULTÉ, ÉCOLE, DÉPARTEMENT / FACULTY, SCHOOL, DEPARTMENT

Improved Methodology for Deriving the Critical Heat Flux Look-up Table

TITRE DE LA THÈSE / TITLE OF THESIS

Dr. Shui-Chih Cheng

DIRECTEUR (DIRECTRICE) DE LA THÈSE / THESIS SUPERVISOR

D. C. Groeneveld

CO-DIRECTEUR (CO-DIRECTRICE) DE LA THÈSE / THESIS CO-SUPERVISOR

EXAMINATEURS (EXAMINATRICES) DE LA THÈSE / THESIS EXAMINERS

Dr. W. Hallett

Dr. S. Tavoularis

Gary W. Slater

Le Doyen de la Faculté des études supérieures et postdoctorales / Dean of the Faculty of Graduate and Postdoctoral Studies

IMPROVED METHODOLOGY FOR DERIVING THE CRITICAL HEAT FLUX LOOK-UP TABLE

Aurelian Tanase

A thesis submitted to the Faculty of Graduate and Postdoctoral Studies

in partial fulfillment of the requirements for the degree of

MASTER OF APPLIED SCIENCE

in Mechanical Engineering

Ottawa-Carleton Institute for Mechanical and Aerospace Engineering

University of Ottawa

Ottawa, Canada

May 2007

Your file Votre référence
ISBN: 978-0-494-49282-6
Our file Notre référence
ISBN: 978-0-494-49282-6

ABSTRACT

A literature review on critical heat flux (CHF) prediction methods confirmed that the CHF look-up table (LUT) has many advantages over the other prediction methods: it covers the widest range of flow conditions, it is the most accurate CHF prediction method and it is computationally very efficient. The LUT has been included in the major thermalhydraulics and safety analysis computer codes.

The LUT accuracy has increased over the years, although several areas have been identified where further improvements are desirable. These areas include (i) the screening of the experimental data, (ii) effect of the heated channel diameter and length on the CHF, and (iii) difficulties in predicting the CHF in the limiting quality region in LUT, at low flow/low pressure conditions and in the very high dryout quality range.

This thesis describes the various improvements that have been made to the LUT derivation. In addition to the improvements in the LUT derivation methodology, a new visual analysis technique that allows simultaneous LUT trend visualization and comparison in all parametric directions has been developed. Based on the findings and improvements in the LUT derivation methodology, a new version of the LUT has been developed.

The error analysis revealed that refined data screening and removal of outliers is an effective method for improving the CHF LUT accuracy. Because the majority of the experimental data were obtained for diameters close to the standard 8 mm ID, a better correction of diameter effect on the CHF does not significantly affect the overall LUT accuracy, although it appears to be very important at specific conditions such as low flow or extreme diameters.

ACKNOWLEDGEMENTS

I would like to express my gratitude and sincere appreciations to my advisors, Professor S.C. Cheng and Professor D.C. Groeneveld .Their guidance and continuous support, encouragement and care greatly contributed to the completion and the quality of this thesis.

My appreciation is extended to my colleagues and friends at the Thermalhydraulic Research Team from the University of Ottawa for their advice, help and enjoyable work atmosphere.

I am deeply indebted to my family for their goodwill, patience and moral support offered during this study.

TABLE OF CONTENTS

LIST OF TABLES

LIST OF FIGURES

NOMENCLATURE

Bo	boiling number=q" $\cdot h_{fg}^{-1} \cdot G^{-1}$
c_p	specific heat ($J \cdot kg^{-1} \cdot K^{-1}$)
D	tube diameter (mm)
G	mass flux ($kg \cdot m^{-2} \cdot s^{-1}$)
g	gravity constant ($m\ s^{-2}$)
h	enthalpy ($kJ \cdot kg^{-1}$)
h_{fg}	latent heat of vaporization = H_g - H_f ($kJ \cdot kg^{-1}$)
Δh_{in}	enthalpy of inlet sub-cooling ($kJ \cdot kg^{-1}$)
j	superficial velocity ($m \cdot s^{-1}$)
K	pressure loss coefficient
k	thermal conductivity ($W \cdot m^{-1} \cdot K^{-1}$)
L	heated length (m)
M	Mach number
$\dot{m}$	mass flow rate ($kg \cdot s^{-1}$)
P	pressure (kPa)
q"	surface heat flux ($kW \cdot m^{-2}$)
q_c	critical heat flux ($kW \cdot m^{-2}$)
Re	Reynolds number=$G \cdot D \cdot \mu^{-1}$
T	temperature (°C)
ΔT_{sat}	temperature difference = T_{sat} - T_{in} (°C)
ΔT_{sub}	temperature difference = T_{sat} - T_{out} (°C)
x	thermodynamic quality (-)
x_c	critical thermodynamic quality(-)
z	axial location (mm)
We	Weber number =$G^2 \cdot D \cdot \rho_f^{-1} \cdot \sigma^{-1}$

Greek letters

ε	obstruction-area ratio
ρ	density ($kg \cdot m^{-3}$)
σ	surface tension ($N \cdot m^{-1}$)
μ	dynamic viscosity ($Pa \cdot s$)

Subscripts

avg	average
act	actual
CRIT	critical
f	saturated liquid
g	saturated vapour
i	inside
in	inlet
max	maximum
NB	nucleate boiling
o	outside
out	outlet
R	freon
sat	saturation
sub	sub-cooled
TP	two phase
W	water

ABBREVIATIONS

AECL	Atomic Energy of Canada Limited
CHF	critical heat flux
CHFR	critical heat flux ratio
CHF LUT	critical heat flux look-up table
DNBR	departure from nucleate boiling ratio
CANDU	Canadian Deuterium Uranium Reactor
DNB	departure from nucleate boiling
DSM	direct substitution method
EOHL	end of heated length
HB	heat balance
HBM	heat balance method
ID	tube inside diameter
KAIST	Korea Advanced Institute of Science and Technology
LQR	limiting quality region
LPLF	low pressure low flow
LUT	look-up table
OD	tube outside diameter
ONB	onset of nucleate boiling
PDO	post dryout
PU	Purdue University
UO	University of Ottawa

1. INTRODUCTION

1.1 Objectives

The current study focuses on the improvement of the critical heat flux look-up table (CHF LUT) derivation, and ensures that the parametric trends correctly reflect our latest understanding of the CHF phenomena associated with these trends. This is accomplished by performing a) a detailed review of relevant information, b) an appraisal of the experimental database and where appropriate, phenomenological and theoretical justification of the observed trends, and c) a systematic review of the CHF LUT derivation steps.

1.2. Background

Critical heat flux is one of the most important limiting parameter that affects the performance of nuclear reactors, boilers, heat exchangers, etc. The CHF LUT has been successfully used for more than thirty years for prediction of CHF for different applications (such as the design of boilers or cooling systems, the design and thermal analysis of nuclear fuel bundles, and the safety analysis of nuclear reactors) as a superior alternative to empirical or semi-empirical correlations or CHF models.
The complexity of two-phase flow phenomena associated with the CHF has prevented the derivation of a reliable theoretical model for predicting the CHF; therefore the more promising CHF prediction methods rely primarily on experimental data.

The continuous demand for cleaner energy systems requires the improvement of power plants efficiency without reduction of operation or safety margins. This goal can be achieved by reducing the uncertainty in prediction of different limiting parameters, one of the most important being the CHF.

The current trends in the field of safety analysis and design of nuclear reactors are oriented toward development of "best-estimate" computer codes, which use the most accurate prediction methods available. Furthermore, the derivation of nuclear fuel safety criteria requires accurate prediction of the CHF phenomena.
Those needs explain the proliferation of CHF prediction methods: currently more than 700 CHF correlations and models can be found in the literature.

The CHF LUT contains the state-of-the art experimental data and knowledge on CHF, covering the range of practical interest for most applications. Each new CHF LUT version has a better accuracy and more reliable parametric trends than previous versions. In spite of the above mentioned progress there is still space for improvement, such as better screening of the experimental data, the prediction of CHF at extreme flow conditions, and the effect of flow geometry on CHF. These improvements are addressed in this thesis.
An improved CHF prediction accuracy would have a significant impact in operation of all types of boiling heat exchangers.

1.3 Outline

A literature survey on the CHF prediction methods, history and development of the CHF LUT has been performed and it is summarized in Chapter 2.

Chapter 3 presents the main steps of LUT derivation, describes the outstanding issues and explores the ways of overcoming them.

Chapter 4 presents an improved methodology for verification of the experimental data, including a new multi-parametric data and LUT visualization technique. The enlarged CHF database and its impact on the LUT error assessment are included also.

A literature review and the state-of-the-art research on the diameter and the heated length effects are discussed on Chapters 5 and 6, respectively. A new method for predicting the diameter effect and a correlation for diameter correction factor are proposed and assessed.

Chapter 7 presents the limiting quality region (LQR) and the methods of embedding LQR in the CHF LUT.

Critical heat flux at extreme conditions, namely low pressure low flow, high pressures and high qualities are included in Chapter 8. The main findings of this study are summarized and discussed in Chapter 9.

2. GENERAL REVIEW OF THE RESEARCH OF CRITICAL HEAT FLUX IN TUBES

2.1 Pool Boiling

Collier and Thome (1996) define pool boiling as "boiling from a heated surface submerged in a large volume of stagnant liquid". Based on the bulk liquid temperature, one can distinguish between two types of pool boiling: *subcooled pool boiling*, when the bulk liquid is below the boiling point (saturation temperature) and *saturated pool boiling*, when bulk liquid is at the saturation temperature. The result of pool boiling heat transfer experiments are generally plotted as surface heat flux (q") versus heater wall temperature (T_w) or wall superheat (T_w-T_{sat}). A typical pool boiling curve for water at atmospheric pressure is shown in Figure 2-1.

Region AB represents natural convection, where no phase change takes place. Heat transfer occurs by mixing hot liquid layer formed by heat conduction in the immediate proximity of a heated wall and the cold bulk liquid. The difference in density between those two liquid layers creates buoyancy forces that mix and circulate the liquid in the vicinity of the heated wall. In the natural convection region the heat transfer coefficient is relatively low.

At point B, the wall temperature is high enough to start vapour nucleation on the surface. At the onset of nucleate boiling (ONB) the heat transfer coefficient increases, thus lowering the surface temperature for the same surface heat flux (from B to B', Figure 2-1) . For water at high pressures the wall superheat at ONB is generally less than 1K. Much higher temperature differences may occur for water at low pressure and liquid metals.

Path B'C represents the nucleate boiling region. It is characterized by high or very high heat transfer coefficients at moderate wall superheats. In this regime heat is transferred primarily

by phase change (nucleation) and by the increased turbulence induced by the nucleation process.

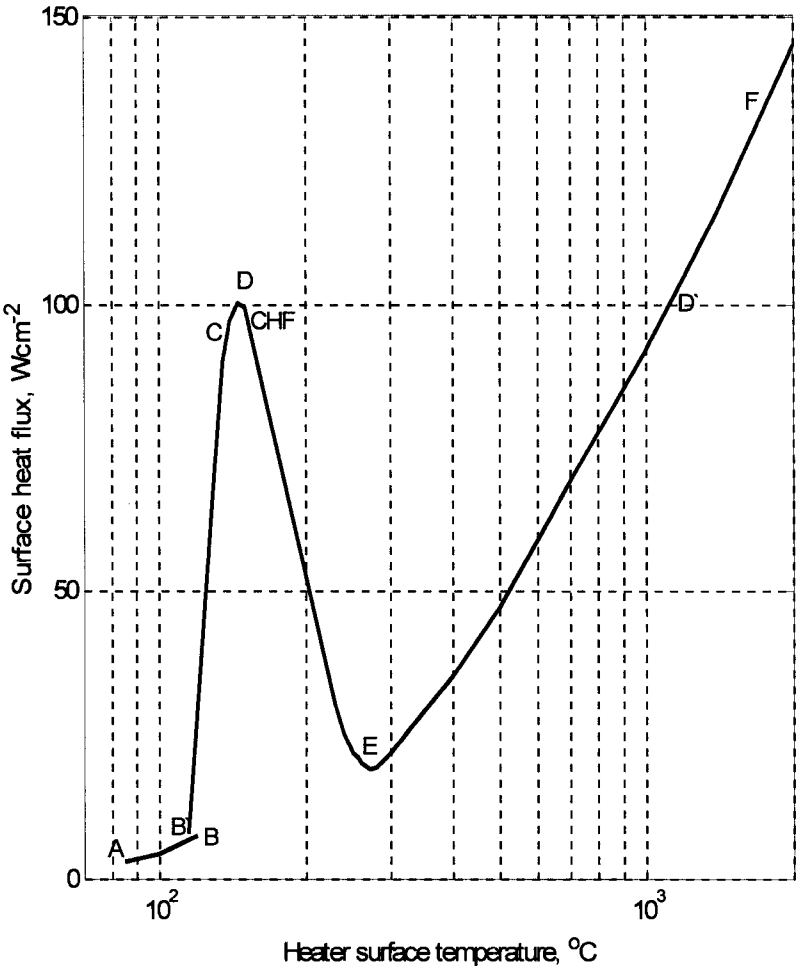

Figure 2-1 Pool boiling curve for water at atmospheric pressure

Nucleate boiling heat transfer is a very efficient way to remove heat because the phase change requires a large amount of heat – latent heat – at an almost constant temperature. At low heat fluxes, there are only few nucleation sites at the heated surface. As heat flux increases, the density of nucleation sites increases, and the bubbles start to coalesce, generating vapour patches and columns.

The critical heat flux (point D) is the point where the nucleate boiling reaches its upper limits. It is caused by the interaction between liquid and vapour streams, which prevents liquid being supplied to the nearby heating surface. Zuber's model (1959) for pool boiling on a infinite, horizontal, upward-facing heating plate describes the hydrodynamic flow pattern as a square array of vapour jets leaving the heated plate. Liquid phase flows between the vapour jets replace the vapour masses escaping from the surface of the plate. The CHF occurs when the vapour-liquid interface becomes unstable (Helmholtz instability).

From a CHF point there are two possible scenarios, depending on how the surface is heated:

a) For heat flux controlled systems (e.g. fuel bundles, electric heaters, boilers), when the heat flux exceeds CHF, the wall surface temperature experiences a sudden and large increase (path D-D'). D' corresponds to film boiling heat transfer, characterized by relatively low heat transfer coefficients, produced by conduction and/or natural convection in the vapour film covering the heated surface and radiation heat transfer. In this regime the heated surface temperature is very high and physical burnout to the heated surface may occur.

b) For temperature controlled systems (e.g. very high thermal inertia, condensation heaters) as soon as CHF is reached and surface temperature is increased, the surface heat flux decreases (DE), because of an unstable vapour blanket over the heating surface. The surface is intermittently cooled by liquid.

EF is the film boiling region, where a stable vapour film is cooling the heating surface. Vapour is released periodically in the form of regularly spaced bubbles.

2.2 Flow Boiling

In a vertical, uniformly heated channel, there are several typical flow patterns (see Figure 2-2), depending on the inlet flow conditions and inner surface heat flux. The flow patterns are:

- single phase liquid
- bubbly flow or flow with nucleation at the heated wall
- inverted annular
- transition
- dispersed droplet
- single phase vapour

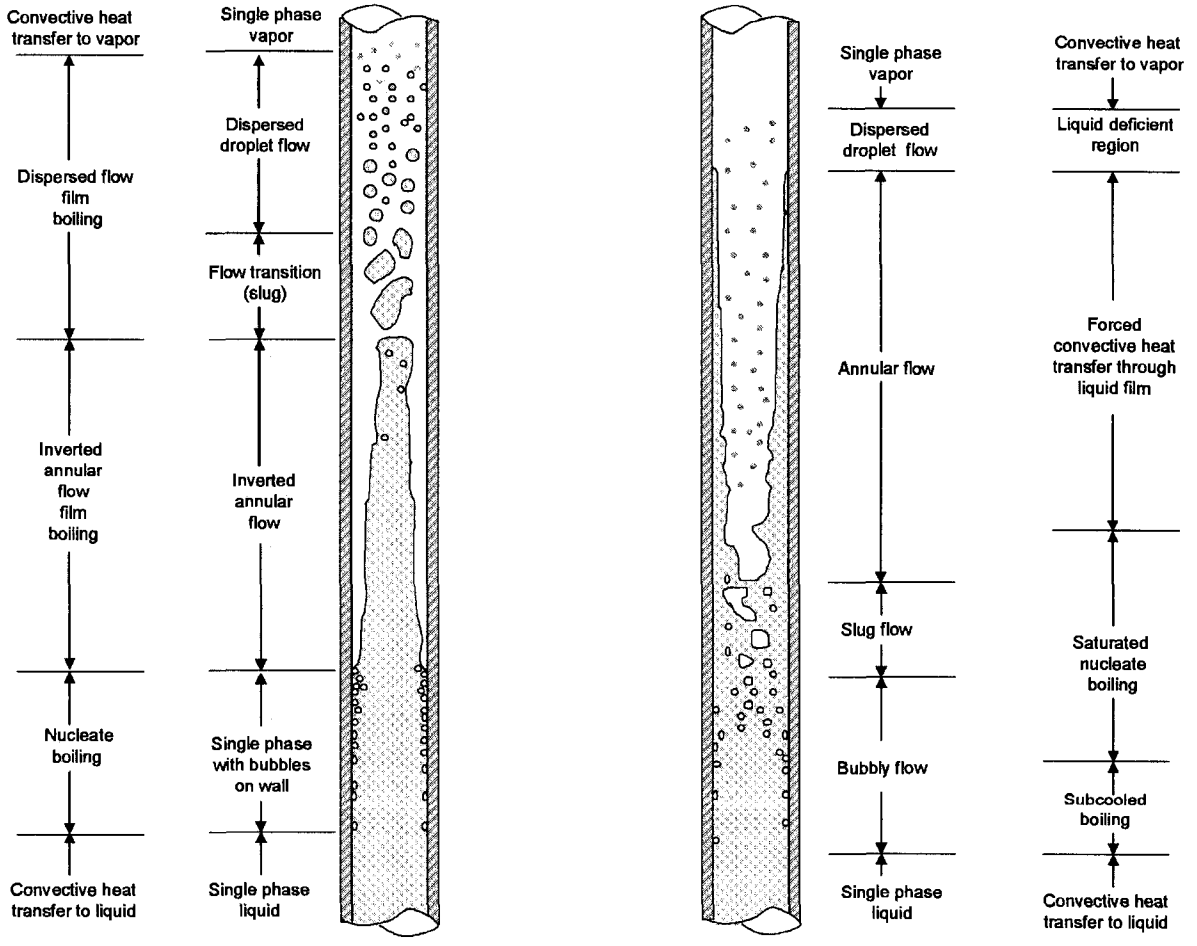

Figure 2-2 Regions of heat transfer and flow patterns for convective boiling

They are described in more detail below:

Single phase liquid

Single phase liquid is encountered as long as the inside channel wall temperature is below saturation, at saturation or even slightly above saturation. Heat transfer occurs mainly by forced convection and conduction inside the boundary layer. In this flow regime heat transfer coefficient is relatively low and depends strongly on fluid velocity.

Nucleate boiling

In the nucleate boiling regime two scenarios are possible: *subcooled nucleate boiling*, when the bulk fluid temperature is below saturation and *saturated nucleate boiling*, when the bulk liquid is at saturation temperature.

In nucleate boiling, either subcooled or saturated, heat is transferred by two mechanisms:

- convective heat transfer, for that part of the heating surface not covered with bubbles.
- nucleation and bubble generation, for the heating surface covered with bubbles.

Just beyond the onset of nucleate boiling (ONB) region, convection is predominant, but as the number of nucleation sites increases, nucleation becomes more important. In the "fully developed" nucleate boiling region, the whole surface is covered with bubbles and the convection component is reduced to zero.

During subcooled nucleate boiling the wall temperature is always a few degrees above saturation. The liquid near the wall is at a higher temperature than the rest of the liquid and at certain spots of the heating wall (nucleation sites), vapour bubbles start to grow. When the buoyancy and drag forces become greater than surface tension forces, the bubbles detach from the surface and become entrained in the subcooled core. Here they release the heat and collapse. Generation and growth of vapour bubbles require a significant amount of heat, while the bubble temperature remains practically constant. This is the main reason for having very high heat transfer coefficients, for both natural and forced nucleate boiling: heat is removed from the heating surface through vapour bubbles. Moreover, the growth, the

detachment and the movement of the bubbles, enhance mixing between cold and hot liquid regions, improving further the convective heat transfer coefficient.

During saturated nucleate boiling, the vapour bubbles that detach from the heating surface do not collapse, they travel downstream and some of them coalesce, forming bigger, irregular bubbles called "slugs".

There are cases when nucleation can occur in the bulk liquid, and this is caused mainly by a sudden decrease in fluid pressure, the bulk fluid temperature exceeding saturation (i.e. flashing). Impurities and dissolved gases can act as preferential nucleation sites where bubbles can growing around these particles. This type of nucleation is more significant at low pressure, due to higher pressure drop and the much larger difference in specific volume between vapour and liquid.

Slug flow

In the bubbly flow regime, especially when the bubble population increases, the bubbles will coalesce, forming bigger bubbles of irregular shape, called "slugs". The slugs travel at a much higher velocity than the liquid. As the liquid upstream of the slug moves downstream, a flow stagnation or even reversal may be observed in the liquid film. This is particularly important in heated channels where due to a lower liquid film velocity more bubbles may be generated in the liquid film. If the surface heat flux is high, the liquid film could break down, leading to dryout conditions.

Churn flow

Churn flow has a similar structure as the slug flow, but the liquid velocity is much higher. In slug flow, if the vapour velocity increases, a transition to churn flow might be possible. The flow consists of irregular shaped pockets of vapour with liquid bridging across the flow area. The interface liquid-vapour is wavy. Unlike slug flow, the liquid velocity is much higher, leading to an increase of heat transfer coefficient, hence suppressing the bubble generation at the heating surface.

Annular flow

Annular flow occurs when the liquid bridges from churn flow collapse and a continuous vapour core and entrained liquid droplets flow in the middle area of the channel, while a liquid film flows near the heating surface. Usually, the velocity of the vapour core is higher than the liquid film velocity. The interface between liquid and vapour core can be wavy or smooth, depending on the flow conditions. A smooth interface is characteristic for low flow, while for high flows it becomes wavy. A wavy interface increases the amount of liquid entrained by the vapour phase. A higher wave amplitude will result in a higher entrainment rate, and therefore increase the droplet concentration in the vapour core. A fraction of droplets, due to random turbulent flow, will deposit back in the liquid film. For any flow conditions there can be equilibrium between entrainment and deposition rates, and as a result an equilibrium droplet concentration exists.

Inverted annular flow

Inverted annular flow occurs only at high wall temperatures where the surface is covered by a vapour blanket. It is usually preceded by a bubble-crowding type of CHF phenomenon with low void fraction (Leung, 1994). During subcooled boiling the vapour bubble generation at the heating surface is so intense that the attached bubbles start to coalesce and form big vapour blankets near heating surface. Inverted annular flow has a reverse structure of annular flow, with a continuous liquid core surrounded by a thin blanket of vapour film. Due to unstable conditions, a wavy liquid-vapour interface is formed. At high mass velocities, droplet entrainment may be encountered. Evaporation and entrainment of the liquid core decrease the liquid core size, finally leading it to breaking up into droplets. The heat is transferred by conduction, convection and radiation through the vapour film. Due to the low thermal conductivity of vapour phase, this regime has relatively low heat transfer coefficients.

Dispersed flow film boiling

Dispersed flow film boiling contains a mixture of vapour core and liquid droplets. It can be preceded either by inverted annular flow or annular flow with a high entrainment rate. In this flow regime the heat transfer coefficient is relatively low, but the entrained droplets are

a contributing source of heat removal as they lower the vapour temperature. The presence of flow obstacles or turbulence promoters significantly increases the droplet deposition rates and enhances the heat transfer coefficient (Leung et al. 2004, Kim et al., 1991).

Single phase forced convection to vapour

This flow regime follows the dispersed flow film boiling when all liquid is evaporated (x>1); it is very similar to single phase convection to liquid, although the heat transfer coefficients are much lower due to poor heat transport properties of the vapour. The heat is transferred by forced convection and radiation to vapour.

2.3 The Boiling Map

Boiling maps are useful tools to present qualitatively the variation of heat flux or heat transfer coefficient as a function of thermodynamic quality or heated length.

In the single phase convective heat transfer region, the heat transfer coefficient has moderate values and increases slightly because of fluid property modifications with heating. When subcooled nucleate boiling starts, the heat transfer coefficient increases linearly up to x=0, due to nucleation.

Figure 2-3 shows schematically the heat transfer regimes as a function of heat flux (heat flux increases from i to vii). As one can notice, at relatively low heat fluxes the heat transfer regime shifts from single-phase convective heat transfer to liquid to nucleate boiling (subcooled and saturated) and to two phase forced convective heat transfer. The CHF mechanism associate with this heat transfer regime is dryout. In the liquid deficient region the heat transfer is relatively poor, but the physical burnout of the heat transfer surface usually occurs at high heat fluxes.

At relatively high surface heat fluxes, the nucleate boiling regime changes directly to film boiling, through the DNB mechanism.

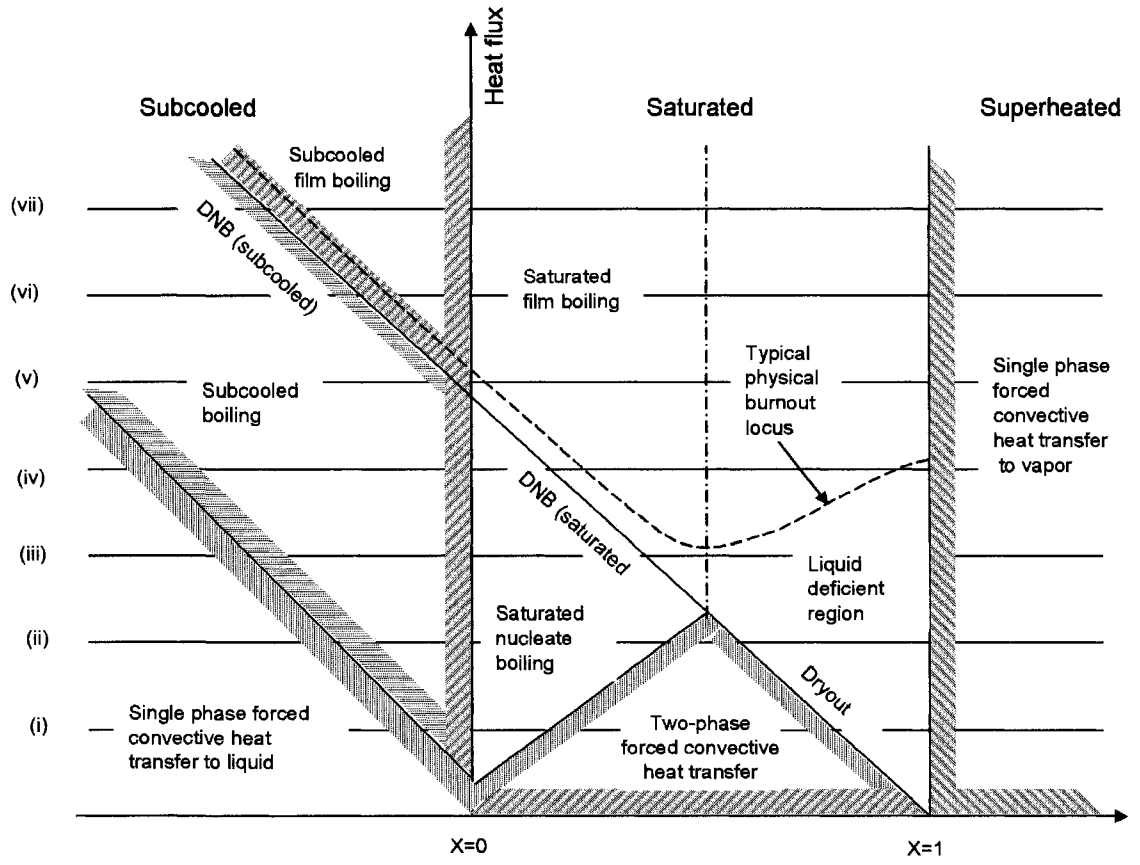

Figure 2-3 Regions of two-phase forced convective heat transfer as a function of quality with increasing heat flux as ordinate

2.4 CHF Mechanisms

Collier and Thome (1996) define critical heat flux as "sharp reduction of the local heat transfer coefficient which results from the replacement of liquid by vapour adjacent to the heat transfer surface". For heat flux controlled systems, the CHF condition will result in a sharp increase in heat transfer surface temperature, while when the temperature of the heating surface is the independent variable, a sharp decrease in heat transfer coefficient occurs.

Different researchers used various terminologies to name the critical heat flux condition. A very common term is "burnout", but it implies the physical destruction of the heating surface.

Other terms commonly used in the literature are "departure from nucleate boiling" (DNB) and "dryout", but they also imply different mechanisms of heat transfer deterioration. In this thesis the more general term "boiling crisis" or "critical heat flux condition" will be employed (Collier and Thome, 1996).

For low local thermodynamic qualities (see Figure 2-4a) and high heat fluxes the critical condition is termed "departure from nucleate boiling". This mechanism can occur at subcooled bulk fluid temperatures (negative thermodynamic qualities) and is called "departure from subcooled nucleate boiling" or at saturation (positive but relatively low thermodynamic qualities, usually below 0.05) – departure from saturated nucleate boiling.

Three distinctive mechanisms have been identified (Tong and Hewitt, 1972) that lead to initiation of CHF conditions. At high subcoolings, at the location of the growing bubbles, the liquid microlayer underneath the bubbles evaporates, leaving temporarily dry spots that are rewetted after the bubble departure (See Figure 2–4a). If the surface heat flux increases over a certain limit, the rewetting of the dry spots is no longer possible because of the high surface temperature- above the Leidenfrost temperature, consequently the CHF condition is encountered. This mechanism is also known as *nucleation induced CHF.*

At moderate subcoolings (Figure 2-4b), the increased bubble population density may lead to CHF. This mechanism is known as *bubble crowding and vapour blanketing* (Kutadeladze and Leontev, 1966, Tong, 1968). As mentioned before, in the nucleate boiling regime the vapour bubbles grow on the heating surface; the higher the heat flux, the higher the bubble population density. As the bubble boundary layer thickness increases with increased of surface heat flux, the replenishment of the liquid film close to the surface is less efficient. If the access of the liquid to the heating surface is seriously affected, overheating of the heat transfer surface occurs, leading to CHF. A continuous vapour layer is formed adjacent to the heated wall. Some researchers (Kutadeladze and Leontev., 1966) considered that the bubble crowding CHF is similar to the separation of the hydrodynamic boundary layer induced by injection of gas normal to the liquid flow direction.

There is another mechanism typical for low pressure, low flows, and narrow channels .At high heat fluxes, a slug of vapour develops in the subcooled liquid. If the channel diameter is comparable with the bubble size, then the bubble may disrupt the liquid layer between the bubble and the heated wall, leading to CHF (see Figure 2-4c). This mechanism is referred also as *vapour bridging*.

At higher thermodynamic qualities, where nucleation is suppressed, the CHF mechanism is due to *liquid film dryout*. The flow pattern at higher qualities is likely to be annular or in transition to annular (churn). In this regime heat is transferred by forced convective evaporation through the liquid film and this process is very efficient, as long as the liquid film flowing along the heated surface is not disrupted. When due to various reasons (evaporation, excessive entrainment rate, liquid film stagnation, flow instabilities, large surface waves), the liquid film breaks down, the heating surface is exposed to vapour that has a much lower thermal conductivity and heat capacity. Consequently, at the location where liquid film is disrupted, overheating of heat surface occurs. This mechanism is known as film "dryout". Although the surface overheating is less destructive than burnout, dryout can also endanger the integrity of the surface.

It is important to note that both CHF mechanisms - DNB and dryout - cause surface overheating, but DNB creates very severe temperature transients, often leading to burnout. Actually, the cause of burnout (which refers to a physical failure of the heated surface) is the combination of poor convective cooling at low vapour velocities (typical of low qualities) and high surface heat fluxes. DNB requires much higher heat fluxes than dryout, and occurs at lower thermodynamic qualities, hence more severe overheating occurs.

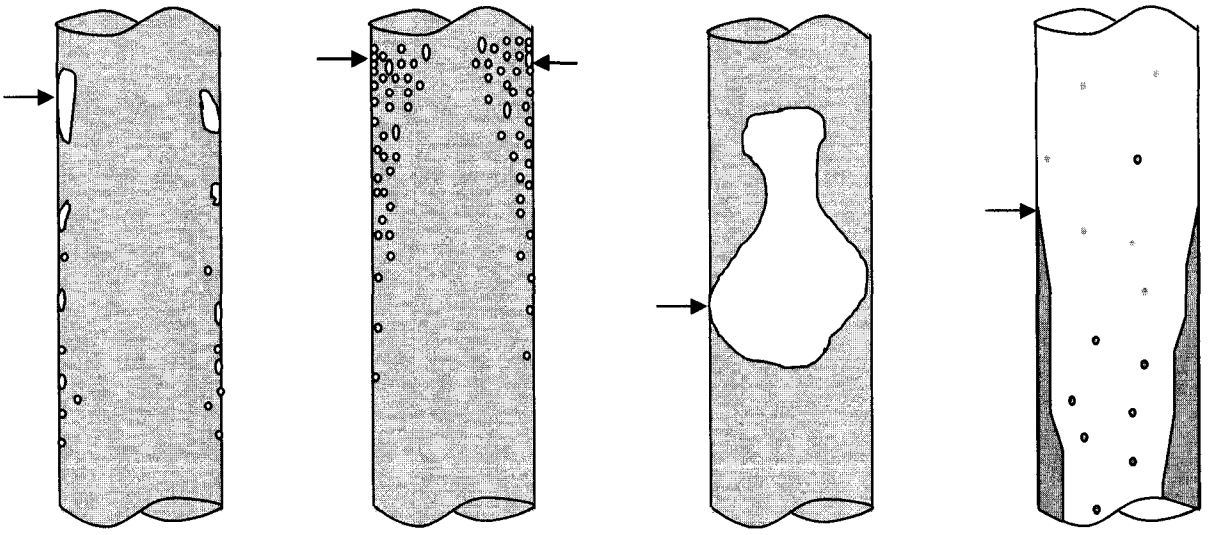

Figure 2-4 CHF mechanisms: a) nucleation induced CHF b) bubble crowding c) evaporation of liquid film surrounding a slug flow bubble (bridging) d) dryout

2.5 CHF Prediction Methods

2.5.1 General

Prediction of critical heat flux with sufficient accuracy is important in a wide variety of process equipment. It is especially important in the design and safety analysis of nuclear reactors of any type, where the CHF determines the operating and safety margins. CHF prediction methods can be classified into two major categories:

- empirical and semi-empirical correlations
- mechanistic models

Empirical correlations ignore the mechanisms and phenomena involved at the CHF condition, they just correlate the experimental data – by statistical methods or trend analysis – in functional forms between independent variables.

Unlike empirical correlations, semi-empirical correlations consider hydrodynamic and heat transfer conservation equations and/or non-dimensional criteria and relate them to critical

flux conditions. In order to fit experimental data, they use some constants, adjusted to fit the experimental data base, in order to maximize the prediction accuracy.

Many empirical and semi-empirical correlations are available in the literature, numbering over 700, and they were derived, adjusted and validated using experimental databases. In general, their extrapolation outside the original data set limits is not recommended, and can result in large errors and/or wrong asymptotic trends.

The correlations can be also classified as "local type" or "inlet type" according to the independent variables considered. Inlet-type correlations relate the CHF to flow parameters at the inlet of the heating channel. Their general form is:

$$q_c = f(P, G, h_{in}, D, z) \tag{2.1}$$

Local-type correlations relate the CHF to flow parameters and channel geometry at the location of CHF condition:

$$q_c = f(P, G, x_c, D) \tag{2.2}$$

Local-type correlations assume that CHF is not dependent on the upstream conditions or heated length, being a function only of "local conditions".

2.5.2 Empirical and semi empirical correlations

The next paragraphs briefly describe some of most common CHF correlations.

2.5.2.1 Inlet-conditions-based correlations

Bowring (1972) correlation

The correlation proposed by Bowring (1972) is similar to that proposed by Thompson and Macbeth (1964):

$$q_c = \frac{A + 1/4 DG\Delta h_{in}}{C + z}$$

$$A = \frac{2.32F_1(1/4 \cdot h_{fg} \cdot D \cdot G)}{1 + 0.0143F_2 D^{0.5} G}$$

$$C = \frac{0.077F_3 \cdot D \cdot G}{1 + 0.347F_4(7.4 \cdot 10^{-5} G)^{(2-0.0005P)}} \tag{2.3}$$

$$F_1 = \frac{Rp^{19.94} \exp(20.89(1 - Rp)) + 0.917}{1.917}$$

$$F_2 = \frac{1.309F_1}{Rp^{1.316} \exp(2.444(1 - Rp)) + 0.309}$$

$$F_3 = \frac{Rp^{17.023} \exp(16.658(1 - Rp)) + 0.667}{1.667}$$

$$F_4 = F_3 Rp^{1.649}$$

$$Rp = 2 - 0.5P$$

Katto (1982) correlation

The general form of the Katto(1982) correlation is:

$$q_c = x_c \cdot G \ (h_{fg} + K(\Delta h_{sub})_i) \tag{2.4}$$

X and K are calculated as a function of three dimensionless groups:

$$Z' = z / D$$
$$R' = \rho_g / \rho_f \tag{2.5}$$
$$W' = \frac{\sigma \rho_f}{G^2 z}$$

Five values of X and three for K need to be determined, as follows:

$$X_1 = \frac{CW'^{0.043}}{Z'}$$

$$X_2 = \frac{0.1R'^{0.133}W'^{0.333}}{1+0.0031Z'}$$

$$X_3 = \frac{0.098R'^{0.133}W'^{0.433}Z'^{0.27}}{1+0.0031Z'} \qquad (2.6)$$

$$X_4 = \frac{0.0384R'^{0.6}W'^{0.173}}{1+0.28W'^{0.233}Z'}$$

$$X_5 = \frac{0.234R'^{0.513}W'^{0.433}Z'^{0.27}}{1+0.0031Z'}$$

$$K_1 = \frac{0.261}{CW'^{0.043}}$$

$$K_2 = \frac{0.833[0.0124+(1/Z')]}{R'^{0.133}W'^{0.333}} \qquad (2.7)$$

$$K_3 = \frac{1.12[1.52W'^{0.233}+(1/Z')]}{R'^{0.6}W'^{0.173}}$$

Table 2-1 presents the criteria to calculate X and K :

Table 2-1 Parameters of Katto correlation

R`<0.15		**R`>0.15**	
condition	**X**	**condition**	**X**
X1<X2	X1	X1<X5	X1
X1>X2 and X2<X3	X2	X1>X5 and X5>X4	X5
X1>X2 and X2>X3	X3	X1>X5 and X5<X4	X4
condition	**K**	**condition**	**K**
K1>K2	K1	K1>K2	K1
K1<K2	K2	K1<K2 and K2<K3	K2
		K1<K2 and K2>K3	K3

C=0.25 for Z`<50

C=0.25+0.0009(Z`-50) for 50<Z`<150

C=0.34 for Z`>150

This correlation is valid for the following range:

0.01<z<8.8 m

0.001<D<0.038 m

5<Z`<880

0.0003<R<0.41

$3 \cdot 10^{-9} < W` < 2 \cdot 10^{-2}$

Shah (1987) correlation

The most recent version of Shah et al. (1987) correlation consists of two separate correlations: upstream conditions correlation (UCC) and local condition correlation (LCC) (more details about LCC at 2.5.2.2).

Upstream conditions correlations assume that critical heat flux depends on upstream conditions – inlet subcooling and the heated length:

$$Bo = \frac{q_c}{G \cdot h_{fg}} = 0.124 \left(\frac{D}{z_{eq}} \right)^{0.89} \left(\frac{10^4}{Y} \right)^n (1 - x_{ieq}) \qquad (2.8)$$

$$Y = \left[\frac{GDc_{pf}}{k_f} \right] \left[\frac{G^2}{\rho_f{}^2 gD} \right]^{0.4} \left[\frac{\mu_f}{\mu_g} \right]^{0.6}$$

where z_{eq} is the effective length of the tube and x_{ieq} is the effective inlet quality, and they are calculated as follows:

Condition	z_{eq}	x_{ieq}
$x_i \leq 0$	z_{CRIT}	x_i
$x_i > 0$	z_{SAT}	0

If $Y<10^4$ then n=0 for all fluids. Otherwise, for all fluids except helium:

$$n = \left(\frac{D}{z_{eq}}\right)^{0.54} \qquad \text{for Y}<10^6 \qquad (2.9)$$

$$n = \frac{0.12}{(1-x_{ieq})^{0.5}} \qquad \text{for Y}>10^6$$

2.5.2.2 Local-conditions-based correlations

Macbeth (1963) correlations

Macbeth (1963) employed the local-flow conditions hypothesis to develop two empirical correlations from experimental data to predict the CHF for high and for low flow conditions, respectively.

The starting point for Macbeth was Barnett's (1963) hypothesis – a local condition hypothesis – stating that CHF is only a function of mass quality at the CHF point. This hypothesis is supported by experimental results. Another simplifying assumption is that CHF is a linear function of inlet subcooling:

$$q_c = A + B\Delta h_{sub} \qquad (2.10)$$

where A and B are functions of flow conditions and system geometry G, p, z, and D.

Combining the heat balance equation and equation (2.10), we obtain:

$$q_c = \frac{A - B \cdot x(z) h_{fg}}{\left[1 - \frac{4Bz}{DG}\right]} \qquad (2.11)$$

For the low flow region, the final form of the Macbeth (1963) CHF correlation is expressed as:

$$\frac{q_c}{10^6} = 0.00633 \cdot h_{fg} D^{-0.1} \left(\frac{G}{10^6}\right)^{0.51} (1 - x_c) \tag{2.12}$$

For the high flow region CHF is given by:

$$q_c = y_0 d^{y1} \left(\frac{G}{10^6}\right)^{y2} - \frac{y3}{4} D^{y4} \left(\frac{G}{10^6}\right)^{y5} G \cdot x_c \cdot D \cdot h_{fg} \tag{2.13}$$

Table 2–2 gives numerical values of the constants used by the Macbeth correlations:

Table 2-2 Constants of Macbeth correlation

Pressure (psia)	y_0	y_1	y_2	y_3	y_4	y_5
15	1.12	-0.211	-0.324	0.001	-1.4	-1.05
250	1.77	-0.553	-0.26	0.0166	-1.4	-0.937
530	1.57	-0.566	-0.329	0.0127	-1.4	-0.737
1000	1.06	-0.487	-0.179	0.0085	-1.4	-0.555
1570	0.72	-0.527	0.024	0.0121	-1.4	-0.096
2000	0.627	-0.268	0.192	0.0093	-1.4	-0.343
2700	0.0124	-1.45	0.489	0.0097	-1.4	-0.529

Biasi et al. (1967) correlation

Biasi et al. (1967) derived two correlations for high and low quality regions, based on a relatively large number of experimental data. For low quality the expression for the critical heat flux is:

$$q_c = \frac{1.883 \cdot 10^3}{D^a G^{1/6}} \left(\frac{y(P)}{G^{1/6}} - x_c\right)$$

$$y(P) = 0.7249 + 0.099P \cdot \exp(-0.032P) \tag{2.14}$$

where the exponent a depends on tube diameter: $a = 0.4$ if the tube diameter is greater than 10 mm and 0.6 otherwise.

For high quality flow, the critical heat flux is:

$$q_c = \frac{3.78 \cdot 10^3 h(P)}{D^{\alpha} G^{0.6}}(1 - x_c)$$

$$h(P) = -1.159 + 0.149P \cdot \exp(-0.019P) + \frac{8.99P}{10 + P^2} \tag{2.15}$$

Doroschuck (1980) correlation

The correlation developed by Doroschuck et al. (1980) covers pressures from 5 to 19.6 MPa and mass fluxes from 0.75 to 3 $Mgm^{-2}s^{-1}$. The correlation is valid for 8 mm ID tubes:

$$q_c = \left(10.3 - 17.5\left(\frac{P}{98}\right) + 8\left(\frac{P}{98}\right)^2\right)\exp(-1.5x_c)\left(\frac{G}{1000}\right)^{0.68(P/98)-1.2x_c^{-0.3}} \tag{2.16}$$

For tube diameters between 4 and 16 mm the following expression was proposed:

$$\frac{q_{c,d}}{q_{c,8}} = \left(\frac{D}{8}\right)^{-1/2} \tag{2.17}$$

Becker (1965) correlation

For low pressure conditions, based on a large experimental database, Becker et al.(1965) developed the following CHF correlation,:

$$q_c = G^{-0.5} f_1(x(z), P) \cdot f_2(D) \tag{2.18}$$

where f_1 and f_2 are presented in graphical form.

Shah (1987) correlation

The local condition correlation (LCC) is given by:

$$Bo = F_e F_x Bo_0$$

$$F_e = 1.54 - 0.032(z_{CRIT} / D) \tag{2.19}$$

If $F_e<1$ then F_e should be set equal with one.

Bo_0 is the boiling number for $x_{CRIT}=0$. F_x is given by the authors in graphical form.

The proper choice between the UCC and the LCC is done as follows:

a) for helium, always use the UCC
b) for other fluids, if $Y<10^6$, then the UCC should be used. For $Y>10^6$, the correlation that gives the lowest Bo should be used.

Like the Katto correlations, the Shah correlation is valid not only for water but also for other fluids. It has been tested on 23 fluids, for channel diameters between 0.315 and 37.5 mm, L/D up to 940, G between 4 and 29051 kg $m^{-2}s^{-1}$, Pr between 0.0014 and 0.96, $-4<x_i<0.85$, $-2.6<x_c<1$.

A comparison between the Bowring, Katto and Shah correlations (Shah et al., (1987)) shows that the Shah correlation had the lowest Root Mean Square(RMS) error for all ranges tested, around 16%, and a maximum average error of -3%, depending on flow regime.

Hall-Mudawar (1999) correlation

Based on the hypothesis that CHF is dependent either on inlet conditions or on local conditions, Hall and Mudawar (1999) developed two nondimensional, subcoooled CHF correlations, covering a wide range of pressures, qualities and mass fluxes. Both correlations contain as few constants as possible and they were derived based on parametric trend analysis rather than statistical analysis. The heated channel diameter is implicitly taken into account.

Local condition correlations have the following general form:

$$q_c=f(D, P, L, G, h_i) \tag{2.20}$$

where D is the channel inside equivalent diameter, P –inlet pressure, L- heated length, G- mass flux and h_i – inlet enthalpy.

For the outlet conditions (local conditions) there have been made the following assumptions:

- CHF is proportional with D to a negative power
- CHF is proportional with G to a positive power
- CHF decreases linearly with increasing x_c

In non-dimensional form the dependence between CHF and other local parameters (P, G, x_c, D) has the general expression:

$$\mathrm{Bo} = \mathrm{fn}\left(\mathrm{We}_D, \frac{\rho_f}{\rho_g}, x_c\right) \tag{2.21}$$

$$Bo = \frac{q}{G \cdot h_{fg}} \quad We = \frac{G^2 D}{\rho \cdot \sigma} \tag{2.22}$$

In equation (2.21) the Weber number represents a dimensionless group for mass flux and diameter, and liquid/vapour density ratio for system pressure.

Equation (2.21) and the assumptions mentioned above would lead to a more explicit expression for *Bo*:

$$Bo = We_D^{\,c}(f_1 - f_2 x_c) \tag{2.23}$$

where constant *c* is negative and functions f_1 and f_2 are positive.
The constant and the functions mentioned above are determined based on a trend analysis. There have been selected several sets of CHF data in which all but one of the dimensionless terms appearing on the right-hand side of Eq. (2.22) were held constant. The constant ***c*** was found to be independent of pressure and is equal to -0.235. This suggests that CHF is

proportional to the square root of mass velocity for the whole pressure interval analyzed. The functions f_1 and f_2 have the following form:

$$f_1 = 0.0332 \cdot \left(\frac{\rho_f}{\rho_g}\right)^{-0.681}$$
$$f_2 = 0.0227 \cdot \left(\frac{\rho_f}{\rho_g}\right)^{0.151} \tag{2.24}$$

Unlike the inlet condition correlation, which is applicable only for uniformly heated channels, the local condition correlation may be applied even for non-uniformly heated channels. Substituting eq (2.23) in (2.22), we obtain the final form of the local condition correlation:

$$Bo = C_1 We_D^{\,c_2} \left(\frac{\rho_f}{\rho_g}\right)^{C_3} \left[1 - C_4 \left(\frac{\rho_f}{\rho_g}\right)^{C_5} x_c\right] \tag{2.25}$$

where C_1= 0.0332, C_2= -0.235, C_3= -0.681, C_4= 0.684, C_5= 0.832

Starting from local condition correlation (Eq. 2.25) and using the heat balance equation, one can obtain inlet condition correlation. The heat balance gives the outlet enthalpy as a function of inlet enthalpy, mass flux, heated length, and heat flux:

$$h_0 = h_i + 4\frac{L \cdot q''}{D \cdot G} \tag{2.26}$$

In non dimensional form, eq (2.26) can be written as:

$$x_o = x_i \left(\frac{h_{fg,i}}{h_{fg,o}}\right) + \frac{h_{f,i} - h_{f,o}}{h_{fg,o}} + 4\frac{L \cdot q''}{D \cdot G \cdot h_{fg,o}} \tag{2.27}$$

where x_i and x_o are thermodynamic equilibrium qualities at inlet and outlet of the heated channel.

Equation (2.26) can also be written as:

$$x_o = x_i^* + 4 \cdot Bo \frac{L}{D} \tag{2.28}$$

where x_i^* is the pseudo inlet quality, determined using outlet channel pressure.

Combining eq. (2.27) and (2.25) and rearranging the terms we obtain:

$$Bo = \frac{C_1 We_D^{C_2} \left(\frac{\rho_f}{\rho_g}\right)^{C_3} \left[1 - C_4 \left(\frac{\rho_f}{\rho_g}\right)^{C_5} x_i\right]}{1 + 4 C_1 C_4 We_D^{C_2} \left(\frac{\rho_f}{\rho_g}\right)^{C_3+C_5} (L/D)} \tag{2.29}$$

The parametric ranges for both correlations recommended by the authors are summarized in the Table 2-3.

Table 2-3 Parametric ranges of Hall-Mudawar(1999) correlations

Correlation	D (mm)	L/D	G (kg $m^{-2}s^{-1}$)	P (bar)	x_i	x_o
Outlet	0.25-15	n/a	300-30000	1-200	n/a	-1.00 to -0.05
Inlet	0.25-15	2-200	300-30000	1-200	-2.00-0.00	-1.00 to 0.00

2.5.3 Mechanistic Models

Mechanistic models use basic general equations for conservation of mass, momentum, and energy applied for a particular flow pattern associated with a certain type of CHF

mechanism. In principle, the CHF models can be applied for various fluids, but because the vast majority of mechanistic models still use different empirical equations and constants, their capability to be applied for many types of fluids may be limited. Although many mechanistic models are widely accepted, none of them is general and able to cover the whole range of flow conditions for practical interest. According to CHF mechanism involved, there are basically two types of CHF mechanistic models: DNB models and dryout models.

2.5.3.1 DNB models

Several DNB models are based on the critical bubbly layer mechanism. The model proposed by Weisman and Pei (1983) for subcooled and low quality flow in tubes is a typical example of this approach. The model assumes that a bubbly layer is developed between the heated wall and the core flow and the CHF is initiated when the volumetric fraction of vapour in the bubbly layer exceeds a certain critical value. The critical value is computed through the balance between the outward flow of vapour bubbles and the inward flow of subcooled liquid. The Weisman-Pei (1983) model is valid for void fractions in the core not exceeding 0.6.

Ying and Weisman (1986) improved the Weisman and Pei model (1983), extended the validity for core volumetric qualities up to 0.8 and obtained a better accuracy for the highly subcooled region. Subsequently Weisman and Pei (1988) extended also the thermodynamic quality range from 0.12 down to -0.7.

Lim and Weisman (1990) modified the original Weisman-Pei model(1983) in order to apply it to annular geometries with a heated inner rod and unheated external tube.

Chang and Lee (1991) proposed another modified version of Weisman et al (1983) using a modified hypothesis. Their assessment showed that their model was able to predict well data for water in the range of pressure from 0.1 to 20 MPa, and mass flux from 345 to 8,000 kg $m^{-2}s^{-1}$.

DNB models based on the liquid sublayer dryout mechanism hypothesis have also been proposed. These models assume that the CHF occurs when the thin liquid sublayer that

exists beneath the intermittent vapour blanket evaporates due to Helmholtz instability at the sublayer vapour interface. Lee and Mudawar (1988), Lin (1989) developed mechanistic models based on liquid sublayer dryout, valid for pressure ranges from 4.9 to 17.6 MPa, mass flux ranges from 1000 to 5000 kg $m^{-2}s^{-1}$, subcooling <50K, and void fraction <0.7. Katto (1990) proposed a model similar to Lee and Mudawar, but with more realistic assumptions.

2.5.3.2 Dryout models

For higher qualities (> 0.1) the most common flow regime is the annular flow (Collier and Thome, 1996). Therefore, almost all models for high quality CHF mathematically model the annular film dryout phenomena. The Whalley and Hewitt (1978) model is typical of the many annular film dryout models.

2.5.4 Look up tables (LUTs)

A CHF LUTs is a normalized CHF database valid for vertical upward flow in round tubes 8 mm ID for water; therefore they are classified as empirical methods for the prediction of CHF. They have several advantages: (i) simple to use, (ii) computationally efficient, (iii) wide range of application, (iv) may be applied to non-aqueous fluids using fluid-to-fluid modeling, (v) they are derived based on a very large database (Groeneveld et al., 2005). Because of these multiple advantages, the CHF LUT has been used in many practical applications such as reactor safety codes (CATHENA, CATHARE, RELAP5/MOD3, THERMALHYDRAULIK), calculation of fuel channel operating and safety margins, and nuclear fuel design.

The first attempt to develop a CHF LUT for water in round tubes was made by Doroshchuk et al. (1975). They used a very limited database, having around 5000 experimental points. Their LUT contained normalized values of CHF as a function of pressure, quality, and mass flux, for 8 mm ID round tubes.

Further improvement and research on CHF LUT was carried out at different research institutes or universities from various countries (CENG Grenoble, University of Ottawa, IPPE Obninsk, AECL Chalk River). Groeneveld et al. (1986) developed the first AECL-UO CHF look-up table based on about 15,000 experimental points. This table was then expanded into the 1995 CHF look-up table (Groeneveld et al., 1996) by incorporating the Russian IPPE database, the total having 22,946 data points. It covered a pressure range of 0.1 – 20 MPa, mass flux 0-8000 kg $m^{-2}s^{-1}$ and quality -0.5 to 1. The 1995 CHF look-up table uses the Katto (1992) semi-analytical model to provide the table CHF value at sub-cooled boiling conditions. Kirillov et al. (1989, 1991) also produced a series of standardized tables for tubes of 8 mm ID, for pressures between 1 and 20 MPa, mass fluxes 500 to 7500 kg $m^{-2}s^{-1}$ and qualities -0.5 to 0.9. Groeneveld et al. (2005) published an improved version of the 1995 CHF LUT, having a pressure range extended up to 21MPa, based on a larger number of LUT entries for better interpolation accuracy and better treatment of the limiting quality region (LQR). The experimental database for the 2005 LUT derivation was increased to more than 33,000 data points.

2.5.5 Comparison of CHF LUT with other prediction methods

A proper choice between different available prediction correlations is based on the following criteria:

- accuracy
- validity range
- easy implementation in a software application
- versatility

Look-up tables are a very practical approach in predicting CHF, satisfying all the above criteria, therefore they are preferred for most engineering applications.

Numerous studies have been carried out assessing the accuracy of the CHF LUT versus other alternative methods, namely CHF models and empirical or semi-empirical correlations.

A comparison of 1995 CHF LUT with various LUT (Doroshchuk ,1975, Groeneveld ,1986, Kirillov ,1989, 1991) and empirical correlations (Becker,1965, Biasi,1967, Bowring,1972) was performed by Groeneveld et al. (1996). The error assessment was based on a heat balance method. The number of experimental data tested was selected accordingly to LUT and correlation validity range. Their findings are summarized in Table 2-4:

Table 2-4 Comparison between CHF LUT and some empirical CHF correlations

	Diameter range (mm)	# of data	Error (%)	
			Avg	RMS
Doroshchuk et al. Table (1975b)	4-16	7 419	-0.63	11.02
The 1995 CHF Table	4-16	7 419	0.20	5.33
USSR Academy of Science Table (1977)	4-16	8 848	-0.26	9.51
The 1995 CHF Table	4-16	8 848	0.46	5.13
Groeneveld et al. Table (1986a)	4-32	22 452	1.59	9.49
The 1995 CHF Table	4-32	22 452	0.48	7.38
Kirillov et al. Table (1989a)	4-20	17 299	2.01	10.93
The 1995 CHF Table	4-20	17 299	0.75	7.08
Kirillov et al. Table (1989b)	4-20	18 094	0.13	9.60
The 1995 CHF Table	4-20	18 094	0.69	7.13
Kirillov et al. Table (1991a)	4-20	19 295	1.41	8.87
The 1995 CHF Table	4-20	19 295	0.77	7.11
Kirillov et al. Table (1991b)	4-20	18 818	1.39	8.94
The 1995 CHF Table	4-20	18 818	0.89	7.13
Biasi et al. correlation (1967)	3-37	14 977	6.48	14.38
The 1995 CHF Table	3-37	14 977	0.38	8.17
Becker correlation (1965)	4-25	11 221	5.24	12.48
The 1995 CHF Table	4-25	11 221	-1.14	7.19
Bowring correlation (1972)	2-45	13 129	37.61	49.05
The 1995 CHF Table	2-45	13 129	-0.23	6.80

As shown in Table 2-4, the CHF LUT 1995 was the best CHF prediction method at the time of its publication. Since then, both empirical correlations and the LUT improved, but the LUT kept their superiority.

An independent assessment of the CHF LUT 1995 was performed by Baek et al. (1997). Baek used the KAIST experimental database, containing 10,820 data points. In general, Baek assessment closely agrees with the results reported by the authors of CHF LUT 1995. The HBM gave a RMS error of 8%, very close to 7.82%, reported by Groeneveld et al.

(1995). Furthermore, claiming that CHF LUT is a local type prediction method, Baek computed average and RMS error using the direct substitution method (DSM), finding 4.2% and 36.7 %, respectively.

Chun et al. (1997), after a comparison of the CHF LUT 1995 with both tube-based prediction methods (Lin, Lee and Pei (1989), Weisman and Yin(1983), Katto(1984), Biasi(1967)) and bundle prediction methods (W-3R and EPRI-1), concluded that overall the CHF LUT shows the most promising results. The comparison was made for constant inlet conditions (HBM) and constant local conditions (DSM) approach. The experimental database consists of 479 CHF points obtained on Westinghouse type bundles. For comparison with experimental data, the CHF for round tubes computed using various methods mentioned above, was corrected by employing different bundle specific factors: diameter, geometry, spacer, heated length, axial flux distribution, cold wall. The authors defined:

$$R = \frac{q_{predicted}}{q_{measured}}$$

$$\overline{R} = \frac{1}{n}\sum_{i=1}^{n} R_i \qquad (2.30)$$

$$s = \sqrt{\frac{1}{n-1}\sum_{i=1}^{n}(R_i - \overline{R})^2}$$

Their results are summarized in Table 2-5. Note that the CHF LUT has the lowest standard deviations, for both HBM and DSM.

Table 2-5 Comparison between accuracy of LUT 1995 and some CHF correlations (Chun , 1997)

	HBM			DSM		
	# of data	**R**	**s**	**# of data**	**R**	**s**
CHF LUT 1995	479	0.971	0.066	479	0.931	0.171
Biasi	240	0.969	0.071	240	1.000	0.189
Katto	479	0.904	0.099	n/a		
Lin et al	445	0.968	0.073	339	0.918	0.341
Weisman& Ting	407	1.206	0.161	471	1.624	0.416

Chun also compared the CHF LUT 1995 with "ad hoc" correlations for fuel bundles, namely W-3 and EPRI-1, for rectangular and triangular arrays. The analysis reveals the superiority

of the CHF LUT versus W-3 and its agreement with EPRI-1. Table 2-6 summarizes the statistics for this comparison and shows the superiority of the 1995 CHF LUT over the W-3 equation.

Table 2-6 Comparison between accuracy of LUT 1995 and W-3 and EPRI-1 for fuel bundles (Chun , 1997)

	DSM			HBM		
	# of data	**R**	**s**	**# of data**	**R**	**s**
CHF LUT	1958	0.903	0.156	1958	0.951	0.063
W-3	1958	1.175	0.332	n/a		
EPRI-1	n/a				0.975	0.065

A more recent assessment of the subcooled region of CHF LUT 1995 by Hall et Mudawar (2000) used the PU-BTPFL database, containing around 5400 data points for the subcooled region ($x<0$), and compared the accuracy of the Hall-Mudawar CHF correlations (See 2.25) and the CHF LUT 1995. They concluded that the CHF LUT 1995 was less accurate than Hall-Mudawar subcooled CHF correlations and had a smaller flow conditions range. The LUT average absolute error was 37.5% and the RMS error 72.5% for subcooling region, much higher than the Local Condition Correlation (20% and 15%, respectively) Note that the diameter range for LUT is between 3 and 25 mm ID, while for the Hall-Mudawar it is between 0.25 -15 mm, so the error might be enlarged by the diameter correction factor. The CHF LUT 1995 relies in the subcooled region on the Katto (1992) correlation, which is less accurate than the Hall-Mudawar (1999) correlation.

Groeneveld et al. (2001) derived an improved version of the CHF LUT based on the Hall-Mudawar correlation for the low quality area and this approach has been used since then for the most recent versions of the CHF LUT.

Chandrakar et al. (2000) compared the CHF LUT 1995 with some well known empirical CHF correlations, namely Janssen-Levy, Hench-Levy, Biasi, Bowring, Zenkevitch, Macbeth (low flow, high flow), and W-3. The comparison was performed using both DSM and HBM. Their results are summarized in the Table 2–7.

Table 2-7 Comparison of CHF correlations/CHF LUT

Correlation	Method	# of data	Average error/ average absolute error	RMS error
look-up table	DSM	5953	-5.5/21.0	27.57
	HBM	5232	-4.4/8.5	13.8
Janssen-Levy	DSM	220	-28.3/37.1	35.9
	HBM	216	-6.2/16.6	19.2
Hench-Levy	DSM	88	24.5/44.1	35.8
	HBM	85	-9.1/19.1	21.7
Biasi	DSM	5280	-7.0/20.9	28.2
	HBM	3748	-0.22/5.3	6.9
Bowring	DSM	4783	18.0/27.7	36.7
	HBM	2558	1.88/5.52	7.23
Zenkevitch	DSM	402	22.1/27.2	29
	HBM	402	-7.3/13	17.1
Macbeth (low mass flux)	DSM	364	35.2/45.4	52.2
	HBM	32	12.1/1.56	2.16
Macbeth (high mass flux)	DSM	3763	15.3/24.1	33.6
	HBM	2401	-1.75/4.9	6.52
W-3	DSM	286	21.2/32.4	25.2
	HBM	174	-6.7/9.12	11.45

3. DERIVATION OF THE CHF LOOK-UP TABLE

The starting point for the derivation of the CHF look-up table is usually another CHF table, called the skeleton table (see Figure 3-1). The skeleton table can be based on a combination of empirical correlations, models or a previous CHF LUT.

The main steps for deriving an updated look-up table are illustrated in Figure 3-1. The smoothing process as well as the use of the LQR will be described in further Chapters. In the regions where a lot of experimental data are available, the updating process is more efficient and noticeable. Where no data are available, the updated table is similar to the skeleton table. Because of the scattering of experimental data, there are regions where the updated LUT shows oscillations and irregular trends, without any physical reason. Steep slopes and irregular trends are bad features, because they contribute to numerical instabilities when the LUT is used in computer codes. Consequently, the updated table is then subjected toa smoothing process, based on a 3D mathematical filter.

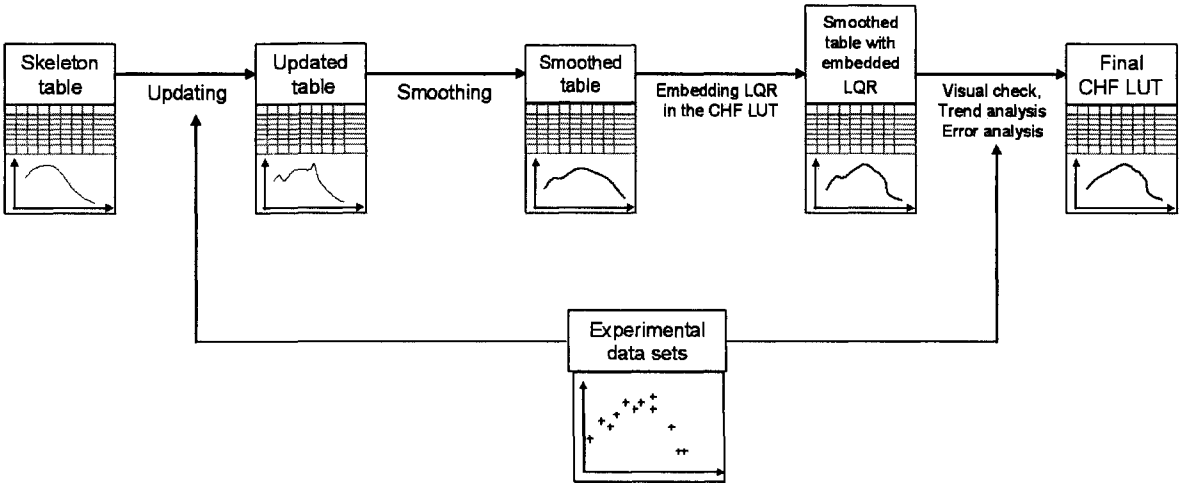

Figure 3-1 Main steps of CHF LUT derivation

Following the smoothing process, a final visual check is performed, to ensure that the table is smooth and there are no abnormal trends. If needed, manual adjustment is performed

3.1 CHF Data Screening

Data screening is the most important step in ensuring a reliable experimental CHF data base. Because the experimental data are used for the LUT derivation and assessment, the features of all new derived LUTs strongly depend on this step. Many improvements have been made to the latest version of the CHF experimental database, therefore the CHF data screening process is described in detail in Chapter 4.

3.2 LUT Updating

As previously mentioned, deriving a look-up table usually starts from a skeleton table, which is subsequently upgraded by comparing it with the experimental database.

Using the known trends of CHF with pressure, mass flux and local critical quality from the skeleton table, the experimental CHF values were extrapolated to the surrounding matrix conditions as follows:

$$CHF(8, x_i, G_j, P_k) = CHF(8, x_0, G_0, P_0) + \Delta CHF \tag{3.1}$$

where

$$\Delta CHF = \frac{\partial CHF}{\partial x}(x_i - x_0) + \frac{\partial CHF}{\partial G}(G_j - G_0) + \frac{\partial CHF}{\partial P}(P_k - P_0) \tag{3.2}$$

The extrapolated CHF values were evaluated for each of the table matrix conditions surrounding x_0, G_0, and P_0. "8" refers that the values of CHF are normalized at 8 mm tube.

Figure 3-2 illustrates the conditions of an experimental CHF value x_0, G_0 and P_0 enclosed in a box whose corner points represent the surrounding CHF LUT conditions, such that $x_i<x_0<x_{i+1}$, $G_j<G_0<G_{j+1}$, $P_k<P_0<P_{k+1}$. Weighting factors were assigned to each

experimental CHF value, extrapolated to each of the surrounding eight points. The table point closest to the experimental conditions should receive more weight than the more distant ones.

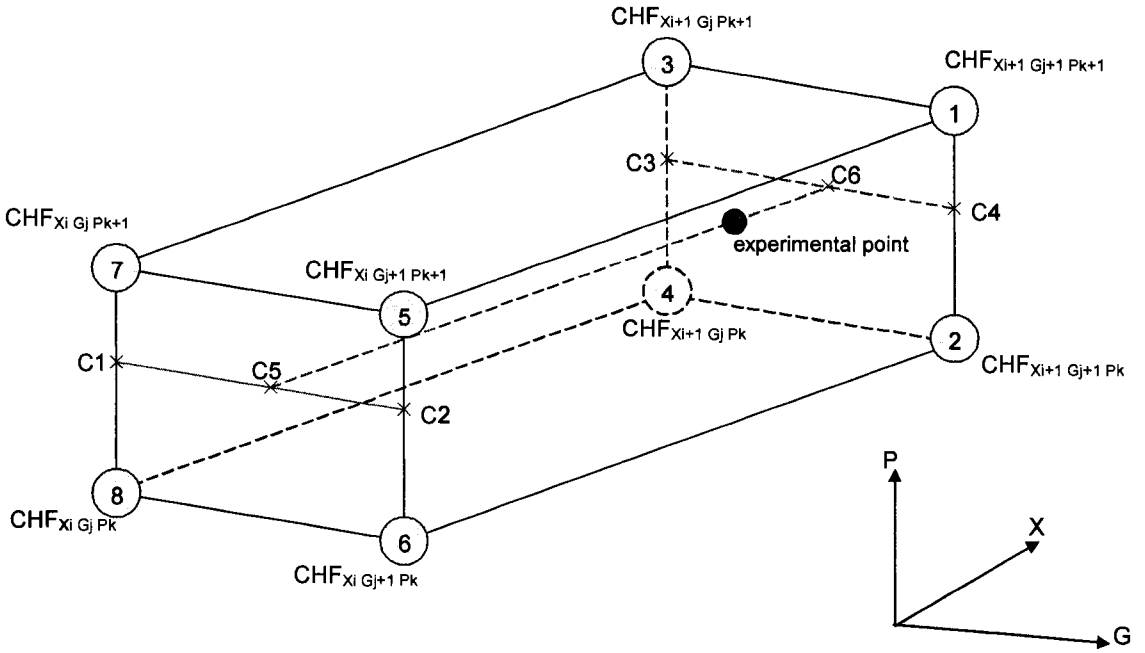

Figure 3-2 Matrix conditions surrounding the experimental point (p_0,G_0,x_0)

Using the extrapolated experimental CHF values and the weighting factors, the new CHF table values were found from:

$$CHF_{\text{table value at (xi,Gj,Pk)}} = \frac{\sum_{n=1}^{n=m}\left(w_{i,j,k}\right)_n CHF\left(x_i, G_j, P_k\right)_n}{\sum_{n=1}^{m}\left(w_{i,j,k}\right)_n} \qquad (3.3)$$

The weighted averaged CHF value thus calculated replaced the old table CHF value at matrix conditions adjacent to experimental CHF values. In regions of the CHF table where matrix conditions did not have adjacent data points, the original CHF table value was maintained.

Several weighting function have been proposed and investigated. They are defined as follows:

$$1:\ w = \left[(x_0 - x_i)(G_{j+1} - G_0)(P_{k+1} - P_0)\right]^{1/3} \tag{3.4}$$

$$2:\ w = \left[(x_0 - x_i)(G_{j+1} - G_0)(P_{k+1} - P_0)\right]^{0.5} \tag{3.5}$$

$$3:\ w = \left[(x_0 - x_i)(G_{j+1} - G_0)(P_{k+1} - P_0)\right] \tag{3.6}$$

$$4:\ w = \left[(x_0 - x_i)(G_{j+1} - G_0)(P_{k+1} - P_0)^{0.5}\right] \tag{3.7}$$

$$5:\ w = \left[(x_0 - x_i)^2 + (G_{j+1} - G_0)^2 + (P_{k+1} - P_0)^2\right]^{0.5} \tag{3.8}$$

$$6:\ w = 0.125 \tag{3.9}$$

According to results from Table 3-1, $w = \left[(x_0 - x_i)(G_{j+1} - G_0)(P_{k+1} - P_0)\right]$ seems to get the lowest RMS error, so it is recommended.

Table 3-1 Comparison of different weight factors for updating

Weigh factor	# of data	HBM		DSM		Smoothness index	
		Avg	RMS	Avg	RMS	Avg	RMS
1	26231	0.62	7.85	5.79	35.67	0.129	0.158
2	26231	0.62	7.81	5.76	35.39	0.131	0.159
3	26231	0.65	7.78	5.82	35.1	0.137	0.167
4	26231	0.64	7.8	5.81	35.18	0.135	0.165
5	26231	0.61	8	6	36.51	0.125	0.156
6	26231	0.63	8.06	6.21	37.12	0.125	0.158

A similar analysis was performed by Shan et al. (2005), and it provided the same conclusions.

3.3 Smoothness of the LUT

Applications that use the CHF LUT, especially computer-based applications, rely on relatively smooth trends of the LUT, otherwise numerical instabilities can occur. Smoothing is a mathematical filtering technique aimed to eliminate spikes, unexpected maxima and minima, and any data trends that have no physical basis. There are several factors that cause strange trends and data scattering such as: compilation of experimental

data from different authors, different experimental facilities and instrumentation accuracy, and second order parameters- heated length, surface roughness. The basis for smoothing is that, in general, natural phenomena are smooth with respect to all independent parameters. However, there may be encountered some "natural" sudden trend modification, particularly in the limiting quality region (LQR), where CHF varies significantly with a small modification of critical quality/pressure/mass flux (See Chapter 7).

The existing smoothing methods could be divided into four major categories (Huang and Cheng, 1994):

- semi-empirical physical models
- correlations
- spline functions
- mathematical filters

Note that semi-empirical models and correlations are not developed for data smoothing, but usually they display a smooth trend, hence they can be considered as smoothing techniques. Although plenty of physical models and correlations can be found in the literature, most of them are applied to a narrow range of parameters. In order to cover the whole parameter range of the CHF LUT a lot of correlations and models should be employed. Moreover, due to overlapping of applicable ranges in some of the correlations and the differences in predicted values, it would be difficult to select the most appropriate one.

The spline function is a combination of a large number of polynomials with continuous transition from one to the other. A polynomial is fitted to a specific number of data points surrounding a table entry of interest. Then the table entry is recalculated using the polynomial. The filter consists of several polynomial functions fitted to some selected data points on each parametric direction (i.e. P, G and x). The polynomials intersect at a table entry.

The filter has some adjustable parameters like the degree of the polynomials, the number of data points involved in the regression and the weighting coefficient. The difficulty of

smoothing multi-dimensional tabulated data like the CHF LUT lies in the fact that parameter trends for all independent variables must be simultaneously taken into account when a table entry is to be adjusted.

For the CHF LUT, three polynomials of degree N are fitted to M points in each parameter direction. The main constraint for those polynomials is that they intersect each other at the table entry (x_{ii}, P_{jj}, G_{kk}).
The general expression of these polynomials is:

$$\begin{aligned} q_i &= q_{ii,jj,kk} + \sum_{l=0}^{N-1} a_{l+1}(x_i - x_{ii})^l \\ q_j &= q_{ii,jj,kk} + \sum_{l=0}^{N-1} b_{l+1}(P_i - P_{ii})^l \\ q_k &= q_{ii,jj,kk} + \sum_{l=0}^{N-1} c_{l+1}(G_k - G_{kk})^l \end{aligned} \tag{3.10}$$

where i, j and k are the indices which vary according to the number of table entries M in each parametric direction.
The intersection condition is expressed as:

$$q_i(x_{ii}) = q_i(P_{jj}) = q_k(G_{kk}) = q_{ii,jj,kk} \tag{3.11}$$

The fitting criterion for polynomials to data points is to minimize the sum of squares of deviation of the prediction of the polynomial from the original tabulated data:

$$\varepsilon = \sum_{i=1}^{M} w_i(q_i - Q_i)^2 + \sum_{i=1}^{M} w_j(q_j - Q_j)^2 + \sum_{i=1}^{M} w_k(q_k - Q_k)^2 \tag{3.12}$$

The minimum condition is that the partial derivatives with respect to the coefficients a_1, b_1, c_1 and $q_{ii,jj,kk}$ are equal to zero:

$$\frac{\partial \varepsilon}{\partial a_1} = \frac{\partial \varepsilon}{\partial b_1} = \frac{\partial \varepsilon}{\partial c_1} = \frac{\partial \varepsilon}{\partial q_{ii,jj,kk}} \tag{3.13}$$

Q_i, Q_j, Q_k are the original tabulated values and w_i, w_j and w_k are the weighting coefficients.

The matrix form of the equation (3-13) can be written as:

$$Axq=S \tag{3.14}$$

where

$$A=\begin{vmatrix} A_{1,1} & \cdots & A_{1,N} & 0 & \cdots & 0 & 0 & \cdots & 0 & A_{1,3N+1} \\ \cdots & \cdots & \cdots & \cdots & \cdots & \cdots & \cdots & \cdots & \cdots & \cdots \\ A_{N,1} & \cdots & A_{N,N} & 0 & \cdots & 0 & 0 & \cdots & 0 & A_{N,3N+1} \\ 0 & \cdots & 0 & A_{N+1,N+1} & \cdots & A_{N+1,2N} & 0 & \cdots & 0 & A_{N+1,3N+1} \\ \cdots & \cdots & \cdots & \cdots & \cdots & \cdots & \cdots & \cdots & \cdots & \cdots \\ 0 & \cdots & 0 & A_{2N,N+1} & \cdots & A_{2N,2N} & 0 & \cdots & 0 & A_{2N,3N+1} \\ 0 & \cdots & 0 & 0 & \cdots & 0 & A_{2N+1,2N+1} & \cdots & A_{2N+1,3N} & A_{2N+1,3N+1} \\ \cdots & \cdots & \cdots & \cdots & \cdots & \cdots & \cdots & \cdots & \cdots & \cdots \\ 0 & \cdots & 0 & 0 & \cdots & 0 & A_{3N,2N+1} & \cdots & A_{3N,3N} & A_{3N,3N+1} \\ A_{3N+1,1} & \cdots & A_{3N+1,N} & A_{3N+1,N+1} & \cdots & A_{3N+1,2N} & A_{3N+1,2N+1} & \cdots & A_{3N+1,3N} & A_{3N+1,3N+1} \end{vmatrix}$$

$$q=|\, a_1,\ldots,a_N,\ b_1,\ldots,\ b_N,\ c_1,\ldots,\ c_N,\ q_{ii,jj,kk}|^T \tag{3.15}$$

$$S=|S_1,\ \ldots,\ S_N,\ S_{N+1},\ \ldots,S_{2N},\ S_{2N+1},\ \ldots,\ S_{3N},\ S_{3N+1}|^T$$

Three adjustable parameters influence the smoothening characteristic of the filter:

1) The degree of the polynomial, N
2) The number of LUT entries involved in each parameter direction for each smoothing step, M
3) The definition of the weighting coefficients, w

The degree of the polynomial shapes the function that "passes" through the LUT entries, describing its flexibility to adapt to the varying trend of CHF LUT. A low degree will

introduce a strong interference with the data to be smoothed or even dump out real physical trends. A too high degree will be able to adapt itself to data variation, reducing the effectiveness in filtering of unwanted noise. Visual examination of the CHF LUT trends suggests that a 2^{nd} or 3^{rd} degree polynomial is a reasonable choice. However, for comparison purposes, 1^{st} degree polynomial were considered, too.

The minimum number of LUT entries involved in each parameter direction for each smoothing step is equal to the degree of the polynomial. In this case there is no smoothing, since the polynomial goes through each LUT entry. On the other hand, a high number of LUT entries combined with low order polynomial makes it more difficult for the polynomial to follow the physical LUT trends, e.g. steep changes in CHF trends such as those in the limiting quality region will be smoothed out. The M table entries in each parameter direction are divided to both sides of the table entry being considered, i.e. (M-1)/2 on each side of table entry being smoothed. A perfect symmetry is when M is an odd number and is far enough from the boundaries of the parameter range. When the table entry being smoothed is close to the boundary, the data symmetry is broken. For the table points located on the boundary, the smoothing is based on extrapolation

Table 3-2 shows the results of a sensitivity analysis with respect to the degree of the smoothing polynomial, N, and the number of table entries taken in each parametric direction. As expected, a polynomial of 1^{st} degree gives smoother tables than 2^{nd} or 3^{rd} degree polynomials. The lowest errors are obtained by higher degree polynomials with the least number of table entries, a combination that makes the polynomial pass almost through all points. Therefore, the error is minimal but smoothing is very weak. A reasonable compromise is considered the 1^{st} degree polynomials with 4 table entries (M=4). This result is explained, on one side by the strong smoothing given by first degree polynomials and on the other side by the relatively small number of table entries (1-2) considered on each side of entry being smoothed, which allows the polynomial to fit better the LUT values, reducing the error.

The smoothness index quantifies the overall smoothness of the LUT. Assuming that the look-up table has P_k, G_j, and x_i as its grid points, with $k = 1, 2, \ldots, K$; $j = 1, 2, \ldots, J$; and $i = 1, 2, \ldots, I$, the local smoothness of the look-up tables is simply presented by the

average of the absolute value of the relative slope differences in each direction of a local grid point.

Table 3-2 Influence of the degree of the smoothing polynomial and the number of the table entries used for smoothing on CHF LUT error statistics

Degree of smoothening polynomial	# of LUT entries	HBM			DSM			Smoothness index	
N		No. data	Avg (%)	RMS (%)	No. data	Avg (%)	RMS (%)	Avg (-)	RMS (%)
1	3	26231	0.14	7.81	26231	2.91	35.90	0.094	10.8
	4	26231	0.03	7.65	26231	2.51	36.00	0.092	11.0
	6	26231	-0.15	7.84	26231	2.03	36.80	0.090	11.8
	10	26231	-0.21	8.24	26231	2.07	38.95	0.085	11.9
2	4	26231	0.62	7.85	26231	5.75	36.66	0.109	12.4
	6	26231	0.38	7.65	26231	4.58	36.96	0.097	11.1
	10	26231	0.26	7.69	26231	4.15	37.98	0.095	11.5
3	4	26231	0.64	7.78	26231	5.78	35.08	0.137	16.7
	6	26231	0.65	7.80	26231	6.29	36.89	0.104	11.9
	10	26231	0.40	8.13	26231	5.99	38.17	0.094	11.1

$$\omega_{q_c}(P_k,G_j,x_i)=\frac{1}{3}\left[\left|\left(\frac{1}{\bar{q}_c}\frac{\partial q_c}{\partial k}\right)_+-\left(\frac{1}{\bar{q}_c}\frac{\partial q_c}{\partial k}\right)_-\right|+\left|\left(\frac{1}{\bar{q}_c}\frac{\partial q_c}{\partial j}\right)_+-\left(\frac{1}{\bar{q}_c}\frac{\partial q_c}{\partial j}\right)_-\right|+\left|\left(\frac{1}{\bar{q}_c}\frac{\partial q_c}{\partial i}\right)_+-\left(\frac{1}{\bar{q}_c}\frac{\partial q_c}{\partial i}\right)_-\right|\right]_{P_k,G_j,X_i} \tag{3.16}$$

where "+" refers to the forward slope, and "-" refers to the backward slope, q_c is the CHF, and $\bar{q}_c$ is the average CHF at its corresponding interval. The smoothness index for the entire LUT is defined as the overall average of the local smoothness at all internal grid points.

$$\Omega_{q_c} = \frac{\sum_{k=2}^{K-1}\sum_{j=2}^{J-1}\sum_{i=2}^{I-1}\omega_{q_c}(P_k, G_j, x_i)}{(K-2)(J-2)(I-2)} \tag{3.17}$$

The RMS of the smoothness is calculated in a similar manner:

$$RMS_{\omega_{qc}} = \sqrt{\frac{\sum_{k=2}^{K-1}\sum_{j=2}^{J-1}\sum_{i=2}^{I-1}\left[\omega_{q_c}(P_k, G_j, x_i) - \Omega_{q_c}\right]^2}{(K-2)(J-2)(I-2)}} \tag{3.18}$$

Figure 3-3 shows the smoothness index of the CHF LUT 2005 as a function of local quality, pressure and mass flux. It can be noticed that smoothness index is higher (i.e. steeper trends) within the limiting quality region (pressures from 1 to 3 MPa and 13 to 16 MPa, mass fluxes from 750 to 2500 kg $m^{-2}s^{-1}$, and qualities from 0.3 to 0.6). A large variation in local smoothness appears at very high qualities and it is caused by very low average CHF values at high qualities. Examination of the CHF LUT at high qualities show relatively smooth trends, therefore the current way how smoothness index is defined can be improved to be less dependent on the flow conditions.

3.4 Limiting Quality Region (LQR)

The LQR is characterized by a sharp decrease of CHF with a small increase in local quality (e.g. a steep change in slope in CHF versus x). It was observed for pressures from 3 to 16 MPa (Galin and Kirilov, 1987) and mass fluxes from 500 to 2500 kg $m^{-2}s^{-1}$ and pressures below 16 MPa and mass fluxes from 500 to 2500 kg $m^{-2}s^{-1}$ (Tolubinskiy et al., 1980). The LQR usually occurs in the intermediate quality region, for water typically between x=0.3 and x = 0.6. CHF LUT 2005 is the first LUT that embedded the LQR. A detailed presentation of the LQR and the embedding in the CHF LUT can be found in Chapter 7.

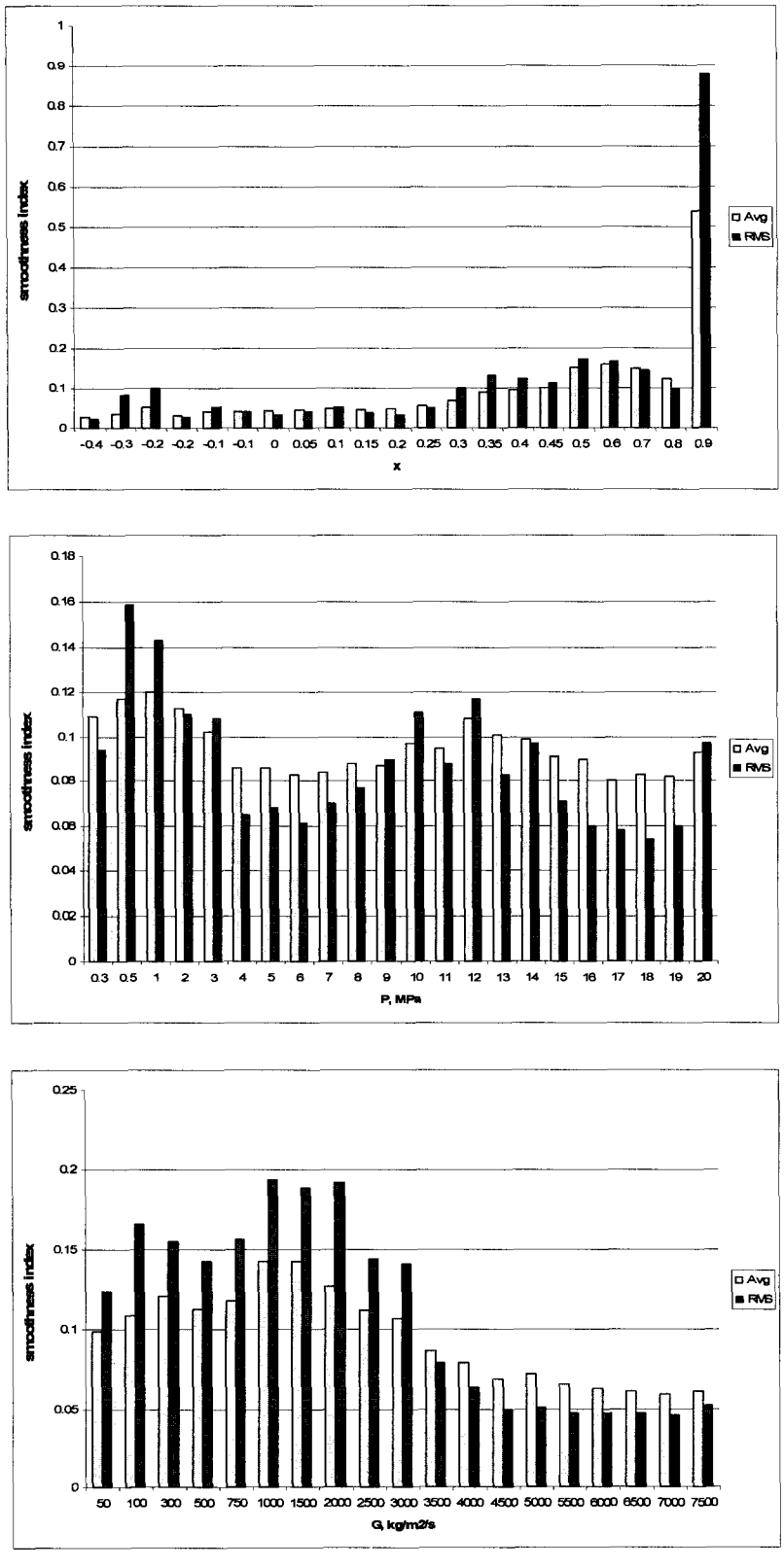

Figure 3-3 Variation of smoothness of CHF LUT 2005 with quality, pressure and mass flux

3.5 CHF Look-Up Table Prediction Accuracy

Measurement errors and uncertainties

The approach on uncertainty described below follows the approach described by Tavoularis (2005). It is assumed that a measurable property (such as CHF) has a *true value* which is unknown; therefore, in order to obtain an estimate of the true value one may need a measurement system which provides a *measured value*. The measured value is generally different from the true value. The *absolute measurement error* represents the difference between the measured value and the true value, both values being expressed in the same units. The ratio between the absolute error and the true value, expressed as percentage or fraction is called the *relative measurement error*.

The errors can be classified as bias (or systematic) and precision (or random). Bias errors are either positive or negative and they are constant through the experiment. If an estimate of the bias errors can be obtained (e.g. by comparing the measurements with more accurate ones), they can be eliminated, but usually they are unknown, especially if they are relatively small. Because, the true value of the quantity to be predicted is generally unknown, both the absolute and the relative errors are unknown.

The uncertainty of a measurement is the interval within the true value is assumed with a certain probability. It is generally accepted that if x is the measured value of a property, the uncertainty of the measurement (u) is such as the true value is contained with 95% confidence in the interval [x-u, x+u]. All types of errors contribute to measurement uncertainty. If b is the bias error and p is the random error, the uncertainty is defined as:

$$u = \sqrt{b^2 + p^2} \tag{3.19}$$

If the CHF LUT is assumed the closest to true CHF values, then absolute and relative errors of experimental data (measurement errors) may be calculated. However, the above mentioned assumption cannot be demonstrated rigorously. The calculated "errors" are rather "uncertainties" in determining the true value of the CHF. To be consistent with previous analysis, the term "error" will be used in this thesis for the CHF LUT accuracy assessment.

The accuracy of the CHF LUT is characterized by an average error (Avg) and Root Mean Square (Standard Deviation or RMS) of the errors. They are defined as follows:

$$Avg = \frac{1}{N}\sum_{i=1}^{N}(Error)_i$$

$$RMS = \sqrt{\frac{1}{N}\sum_{i=1}^{N}(Error)^2{}_i} \tag{3.20}$$

$$Error = \frac{q_{Predicted}}{q_{Measured}} - 1$$

Heat balance method versus direct substitution method

The assessment of CHF correlations, CHF experimental data or CHF operating margins for nuclear reactors can be performed using different methods. There are two major types of CHF correlations for the subcooled or low quality region (Hezjlar and Toderas., 1996).

The Type 1 correlation has the general form:

$$q_c = f(G, x_c, P, D) \tag{3.21}$$

Sometimes the heated length is taken into account and the equation takes the form:

$$q_c = f(G, x_c, P, D, L) \tag{3.22}$$

If the local quality is eliminated using a heat balance equation up to the point "z" of interest, then the CHF correlation takes the following form (Type 2)

$$q_c = f(G, x_{in}, P, D, z) \tag{3.23}$$

The CHF LUT is a typical example of a Type 1 general correlation, because it presents the CHF based on four local independent parameters: pressure, mass flux, local quality and diameter. This approach assumes that CHF is a "local" phenomenon, and the upstream conditions (such as inlet temperature, inlet quality, heated length, flow history) do not affect the CHF. Note that in general the CHF occurs at the exit of the heated length for uniformly heated channels.

Experimental data sets used for LUT derivation and assessment contain the following flow parameters: diameter (D), heated length (L), pressure (P), mass flux (G), critical quality (x_c), inlet temperature (T_{in}), inlet subcooling (Δh_{in}). Not all experimenters report all of these parameters, therefore some of these parameters were evaluated during the data compilation process at the University of Ottawa by employing the heat balance equation.

Using the local conditions approach (or direct substitution method - DSM), any experimental point characterized by a certain pressure (P), mass flux (G) , dryout quality (x_{exp}), and critical heat flux (q_{exp}) is compared directly with the CHF LUT table at the specific local conditions mentioned above. In Figure 3-4 the experimental point is plotted by its q-x coordinates, q_{exp} and x_{exp} respectively. The negative slope curve represents a typical trend of CHF LUT (and any local condition correlation in general) in surface heat flux vs. local quality coordinates. The critical heat flux predicted by the CHF LUT is calculated by substituting directly (hence the name of Direct Substitution Method) P, G, x_{exp} in the CHF LUT and obtaining q_{DSM}. The absolute error is the distance between q_{DSM} and q_{exp}:

$$\varepsilon_{DSM} = q_{DSM} - q_{exp}. \tag{3.24}$$

This method is very straightforward and it is widely used in practical applications of the CHF LUT (CHFR, DNBR calculation, computer codes).

For the heat balance method (HBM) or constant inlet condition approach, CHF depends on inlet conditions, rather than local conditions. The exit quality (x_o) is expressed using the heat balance equation:

$$x_o = \frac{1}{h_{fg}}\left(\frac{4L \cdot q_c}{D \cdot G} - h_f + h_{in}\right) \tag{3.25}$$

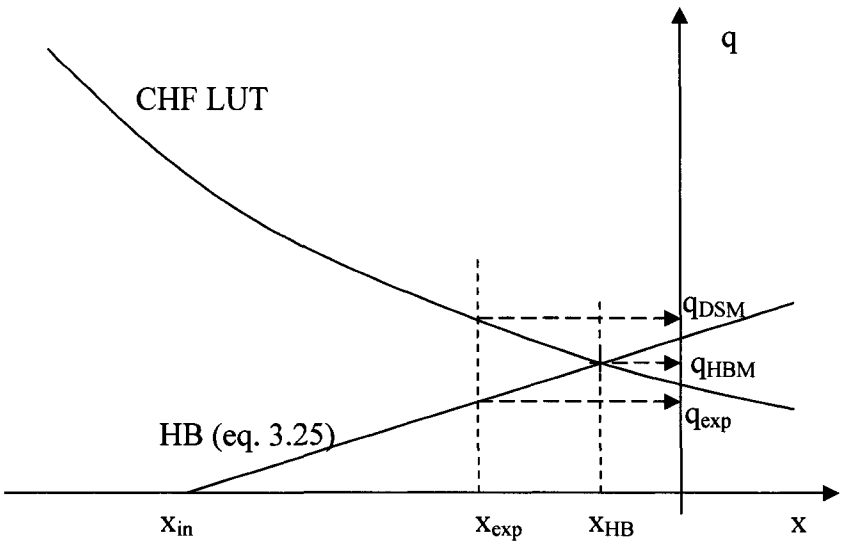

Figure 3-4 Schematic representation of the DSM and the HBM

The curve representing this equation is the positive slope of the heat balance (HB) line in Figure 3-4. The equation (3.24) correlates q as a function of x_o. The CHF LUT also correlates q as a function of x_o. Note that in the heat balance approach the exit quality at the predicted CHF value as well as the predicted CHF value are the unknowns. The intersection between the HB curve and the CHF LUT curve occurs at the predicted CHF value obtained by the HBM, q_{HBM} in Figure 3-3. The corresponding quality is x_{HB}. The absolute error is the distance between q_{HBM} and q_{exp}:

$$\varepsilon_{HBM} = q_{HBM} - q_{exp}. \tag{3.26}$$

In summary, when applying DSM in order to predict CHF, one uses P, G, x_{ex} and D as input parameters, substitutes them in the CHF LUT and calculate the predicted value, q_{DSM}.

For the HBM, H_{in}(or T_{in}, or x_{in}), L, G, P, and D are the input parameters, and the predicted CHF value, q_{HBM} is calculated (graphically or iteratively) as the solution of the CHF LUT and HB equations. Note that the HBM requires iterations, so it is computationally less efficient than the DSM.

In this thesis, CHF LUT errors (average and RMS) are expressed both in DSM (referred to as "constant local conditions") and HBM (referred to as "constant inlet conditions").

Figure 3-4 shows that the errors calculated by DSM method are higher than these calculated by HBM. Indeed, the analysis showed that RMS errors calculated using DSM are typically 2-5 times higher than HBM errors, depending on the CHF versus x slope. At low quality these slopes are very steep, increasing the difference between the experimental value and the corresponding predicted value, at the same local quality. That is, a steep slope acts as an "error amplifier", when the local conditions approach is used.

Many papers available in the literature (Groeneveld et al. 1986, 1996, Lahey and Moody, 1993, Inasaka and Nariai, 1996, Hezjlar and Toderas, 1996, Celata,1996) have compared both approaches, and have discussed the differences in errors and its implications in thermal analysis.

Over the years, the accuracy of the CHF LUT has improved continuously. However, a direct comparison between the early and the latest versions of the CHF LUT is not easy to make, because of (i) the increase in the experimental database, (ii) the expansion of LUT coverage and (iii) the changes in CHF LUT screening criteria. Therefore, the values in Table 3-3 should be judged cautiously, since they are intended to give an indication of the evolution of LUT accuracy.

A more systematic and comprehensive study by Groeneveld et al. (2005) compares the CHF LUT 1995 and the CHF LUT 2005 against the same experimental database (25217 points), for the whole parametric range and for different regions of interest, as well (i.e. subcooling, LQR, x< LQR, x>LQR).

Table 3-3 Comparison between Doroshchuck, Groeneveld (1986), Kirilov (1991) and Groeneveld(1995) CHF LUT

Table	# of exp data	HBM	
		Avg[%]	RMS[%]
Doroshchuk(1975)	~5000	-0.63	11.2
Groeneveld(1986)	22452	1.59	9.49
Kirilov (1991)	18 818	1.39	8.94
Groeneveld(1995)	22452	0.48	7.38

The conclusion of their analysis is the CHF LUT 2005 outperforms the CHF LUT 1995 from all points of view, (see Table 3-4):

Table 3-4 Comparison between CHF LUT 1995 and CHF LUT 2005

Table	# of exp data	HBM		DSM	
		Avg	RMS	Avg	RMS
CHF LUT 1995	25217	0.75	9.18	7.63	42.96
CHF LUT 2005	25217	0.08	7.10	4.09	38.92

3.6 CHF for Non Aqueous Fluids

The CHF LUT is a normalized CHF data base valid for vertical upward flow in 8 mm ID tubes for water. The CHF values for water can be successfully used to predict CHF for other fluids, if proper scaling factors are used (Groeneveld 1967, 1969, 1970).

The most common fluids involved in CHF experimental work are water and several types of refrigerants (i.e. R-11, R-12, R-22, R-134a). The conversion of CHF data from one fluid to another is based on the hypothesis that the dimensionless CHF is a unique function of certain dimensionless parameters.

Using dimensional analysis, Ahmad (1973) proposed three dimensionless groups to relate the CHF between two different fluids: $\Delta h_{sub}/h_{fg}$, ρ_f/ρ_g, L/D. He combined all above mentioned groups as follows:

$$\Psi crit = \left[\frac{GD}{\mu_f}\right]\left[\frac{\mu_f^{\,2}}{\sigma D \rho_f}\right]^{2/3}\left[\frac{\mu_f}{\mu_g}\right]^{-1/5} \tag{3.27}$$

where Ψcrit is a non-dimensional modeling parameter. Ψcrit is then related graphically to boiling number ($Bo=q_c/(h_{fg}G)$), hence to q_c.

A more recent study by Groeneveld et al. (1997) revealed that fluid to fluid modeling involves equivalence of three criteria: geometric, hydrodynamic and thermodynamic similarities.

Geometric similarity is satisfied if the(L/D) ratio is equal for both fluids:

$$\left(\frac{L}{D}\right)_W = \left(\frac{L}{D}\right)_F \tag{3.28a}$$

where W denotes water and F the modeling fluid.

Thermodynamic similarity requires that thermodynamic properties be equivalent for both fluids. This is achieved when thermodynamic qualities are the same at any axial position:

$$x(z)_W = x(z)_F \tag{3.29}$$

From the heat balance equation, quality can be expressed as:

$$x(z) = 4\left(\frac{q_c}{h_{fg}G}\right)\left(\frac{z}{D}\right) - \left(\frac{\Delta h}{h_{fg}}\right) \tag{3.30}$$

From the above equation, equality of x(z) implies equality of boiling numbers ($Bo=q_c/(h_{fg}G)$) and inlet qualities($x_i=\Delta h_i/h_{fg}$) for both fluids:

$$\left(\frac{q_c}{h_{fg}G}\right)_W = \left(\frac{q_c}{h_{fg}G}\right)_F \tag{3.28b}$$

$$\left(\frac{\Delta h}{h_{fg}}\right)_W = \left(\frac{\Delta h}{h_{fg}}\right)_F \tag{3.28c}$$

Hydrodynamic similarity requires that the vapour/liquid density ratios and non-dimensional mass fluxes be equal. Therefore:

$$\left(\frac{\rho_f}{\rho_g}\right)_W = \left(\frac{\rho_f}{\rho_g}\right)_F \tag{3.28d}$$

$$\Psi_W = \Psi_F$$

where Ψ represents the non-dimensional mass flux. For CHF modeling, Groeneveld et al. (1997) found that the best prediction is given by:

$$\Psi = \frac{GD^{0.5}}{(\rho\sigma)_f} \tag{3.31}$$

The parameters mentioned above are summarized in the Table 3–5 .

Table 3-5 Fluid-to-fluid modeling criteria

Geometric similarity	$(L)_R = (L)_W$, $D_R = D_W$
Hydrodynamic similarity	$(G^2 D / (\rho_f \sigma))_R = (G^2 D / (\rho_f \sigma))_W$ $(\rho_f / \rho_g)_R = (\rho_f / \rho_g)_W$
Thermodynamic similarity	$(x_z)_R = (x_z)_W$

Although fluid-to-fluid modeling is generally an accurate method for relating the CHF in two fluids, there are some particular phenomena such as flashing, frictional heat, critical flow, and stratification (Tain et al., 1995) where the fluid-to-fluid modeling is less accurate. The vast majority of CHF experiments are done with water and refrigerants, so most modeling parameters were derived based on these results. Note that for specific flow conditions (horizontal with flow stratification, high flow with M>0.4) fluid to fluid modeling of CHF may not be valid.

3.7 CHF Prediction for Flow in Other Geometries

Many practical applications of CHF analysis are for heated channels that are not circular. Furthermore, channels may be equipped with appendages and flow obstacles to prevent excessive vibrations and/or to enhance the CHF or the heat transfer coefficient. Typical examples are fuel bundles in nuclear reactors. For such situations the prediction of CHF raise some additional issues, such as:

a) equivalent diameter approach
b) obstacle effect
c) shape effect
d) cross flow
e) mixing
f) axial flux distribution
g) radial flux distribution
h) horizontal/inclined flow
i) downward flow

As previously mentioned, the CHF LUT is normalized for circular, 8 mm ID tubes, fully developed, vertical, upward flow, with uniform surface heat flux. CHF predictions for any geometry or flow conditions that do not match the normalized values and the reference configuration, for which the LUT was derived, should be specifically addressed.

There is plenty of experimental evidence that the shape of the heated channel (round, rectangular, annular, dumbbell-shaped, etc) influences the value of CHF, especially for the low quality range (Pioro et al., 2000) for given P, G, x_c. and D_{hy}. Comprehensive literature reviews on the geometry effects of CHF have been performed by Groeneveld (1992), Doerfer (1997), Pioro (2000), Chen(2001). In general, for the same local flow conditions (P,G, x) and equivalent hydraulic diameter, the highest CHF values are obtained in tubes. Any other geometry usually gives lower CHF values (Chen, 2001). One simple reason is that though the CHF mechanisms are the same for any geometry, the best flow symmetry occurs in circular tubes.

Sharp corners, as found in triangular or rectangular channels, slow down the local flow rate, thus preventing good flow mixing and bubble removal. Therefore, the CHF is initiated preferentially at corners at lower heat flux values than those for round channels. Obviously, the corner effect strongly depends on the flow conditions. Supporting experimental evidence come from various sources. De Bortoli (1958) found that CHF in rectangular ducts with two heated sides is as much as 45% lower than in tubes for the same inlet conditions.

Numerous experiments were conducted using annular test sections with possible different combinations: internal and/or external wall heating, eccentric/concentric geometry. Chen et al., (2001) found that at similar flow conditions and hydraulic diameter CHF in annular geometries is lower than in tubes, especially for narrow gaps.

The gap effect was explained by Moek et al. (1966). He proposed two possible mechanisms to explain the lowering of CHF with decreasing gap size. First refers to increase of interfacial shear stress on the heated wall with decreasing gap size. An increase in shear stress results in a decrease of liquid flow rate in the narrow gap region and increases the entrainment rate, thus reducing the CHF. The other mechanism implies that for narrow gaps, the waves from the unheated wall came in contact with the liquid film from the heated wall and entrain it toward the unheated wall (thermo-capillarity effect), which also lowers the CHF. Dryout CHF in annular geometries is also influenced by the unheated wall, acting as a sink for the entrained liquid. On the contrary, for DNB CHF it seems that the unheated surface does not have a significant impact.
For annular geometries important geometric parameters are the minimum gap size and the difference in radii between the heated and unheated surfaces. For this particular geometry all the researchers agreed that CHF decreases with increasing eccentricity for the same local conditions. Some researchers noticed that higher the flow, the higher the effect of gap. For very small gaps (less than 0.5mm) the dependence of CHF on local conditions (pressure, quality, mass flux) is not significant. Furthermore, for high qualities, the CHF in eccentric and concentric geometries tend to be the same. For bilaterally heated annuli, CHF occurs always on the inner heating surface if the heat flux ratio

outer/inner surface is below 1.2. If the heat flux ratio is greater than 2.2 , then CHF occurs always on the outer surface (Becker et al., 1965).

A particular type of geometry is the dumbbell-shape. This shape is the closest to a CANDU fuel bundle subchannel. Systematic studies –theoretical and experimental - on CHF in a dumbbell-shape have been carried out by Green (1969) and Chen (2001). Both studies revealed that the gap size considerably influences CHF.

A complex flow geometry is the fuel bundle. Many experiments have been carried out in fuel bundles and the influence of different bundle-specific parameters, have been studied as well. There have successful attempts to use the round tube CHF correlations or the CHF LUT for predicting CHF for various geometrical configurations.

Although the CHF mechanism in round tubes and fuel bundles (or other noncircular geometries) are similar, there are several specific factors that may strongly influence the CHF and they should be considered. According to Groeneveld et al. (1992), prediction of CHF in fuel bundle using the CHF LUT (or other similar round tube correlation) is given by the following equation:

$$CHF_{bundle} = CHF_{LUT} \cdot K_1 \cdot K_2 \cdot K_3 \cdot K_4 \cdot K_5 \cdot K_6 \tag{3.32}$$

where K_n (n=1..6) are bundle specific factors, as described below.

K_1 is the subchannel or tube diameter cross section geometry factor and quantifies the variation of CHF with channel diameter. The diameter effect on CHF is described in detail in Chapter 5.

K_2 is the bundle factor and predicts the gap effect and local quality:

$$K_2 = \min\left(1, \left(\frac{1}{2} + \frac{2\delta}{D}\right) \cdot \exp\left(-\frac{x_c^{1/3}}{2}\right)\right) \tag{3.33}$$

K_3 takes into account the CHF enhancement produced by flow obstacles such as grids, spacers, or appendages. It was observed that flow obstacles enhance downstream turbulence and cross flow mixing, thus enhancing the CHF. In subcooled CHF better bubble removal and better mixing between the heated liquid microlayer and the subcooled core are the main mechanisms for increasing the CHF. In the saturated region the supplementary turbulence induced within vapour the phase increases the droplet deposition rate, and hence the CHF. There may be situations when obstacles may disrupt the liquid film or cause an increase of entrainment rate that decrease CHF, but in general flow obstacles enhance CHF. Due to flow obstacles, the location of CHF may change, according to flow regime and system geometry, from the end of heated channel to just upstream from a flow obstacle. The effect of a flow obstacle is maximum just downstream of it and diminishes with increasing distance downstream. For CANDU fuel bundles (37 fuel elements), an approximate expression of obstacle effect is given by:

$$\begin{aligned} K_3 &= 1 + A \cdot \exp(-BL_{sp} / D_{hy}) \\ A &= 1.5K^{0.5}(G/1000)^{0.2} \\ B &= 0.1 \end{aligned} \tag{3.34}$$

where K is the pressure loss coefficient (Groeneveld et al. 1992) .

Experiments have shown that the CHF in short channels is higher compared with long channels, at the same flow conditions. This was explained by the turbulence induced by channel entry and the development of the flow inside channels. The expression for L/D factor, valid for L/D>5, is:

$$\begin{aligned} K_4 &= \exp(D_{hy} / L)\exp(2\alpha_h) \\ \alpha_h &= x\rho_f / (x\rho_f + (1-x)\rho_g) \end{aligned} \tag{3.35}$$

More details about L/D mechanisms can be found in Chapter 6.

Because the neutron flux in nuclear reactors is not uniformly distributed, the surface heat flux within fuel bundles is not uniform, but varies axially and circumferentially. To account for these effects, additional two factors K_5 and K_6 have been introduced.

K_5 is the axial flux distribution factor and is calculated as:

$$\begin{aligned} K_5 &= 1 && \text{if } x \leq 0 \\ K_5 &= \frac{q_{loc}}{q_{BLA}} && \text{if } x > 0 \end{aligned} \tag{3.36}$$

where q_{loc} denotes the local heat flux and q_{BLA} is the averaged value of heat flux over the boiling length:

$$q_{BLA} = \frac{1}{L_B} \int_{L_{x=0}}^{L_{x=xc}} q_{loc} \cdot dL \tag{3.37}$$

The radial flux distribution factor (K6) is calculated in a similar way:

$$\begin{aligned} K_6 &= 1 && \text{if } x \leq 0 \\ K_6 &= \frac{q(z)_{avg}}{q(z)_{\max}} && \text{if } x > 0 \end{aligned} \tag{5.38}$$

where $q(z)_{avg}$ is the averaged surface heat flux at axial location z, and $q(z)_{max}$ is the maximum heat flux at the same axial location.

CHF LUT is not the only tube prediction method that can be used for complex geometries. Many correlations or CHF models for tubes (e.g. Biasi, W-3, Lee and Mudawar) have been modified to predict the CHF for fuel bundles. There are other CHF correlations (Omega-1, CU-EPRI, CE-1) that were specifically developed for fuel bundles. They have been incorporated in subchannel codes (e.g. ASSERT, COBRA, FIDAS, MENUET, FLICA) used for core and fuel design, verification and safety analysis. A literature review of the most common CHF correlations for fuel bundles can be found in Appendix 1.

4. CHF DATA SCREENING

The size of the experimental CHF data base has been increasing continuously during the past 30 years. As mentioned by Shan et al. (2005), 82 datasets, comprising 33,175 datapoints have been used to derive the CHF LUT 2005. A number of 33 new data sets have been added since then, and the current database contains more than 36,500 data points, from 116 datasets. Details regarding the experimental database structure (Authors, References, No of data, flow range, geometry, etc) is provided in Appendix 2.
To quantify the effect of introducing additional datasets on the CHF LUT 2005, an error assessment has been performed. The results are shown in Table 4 -1.

Table 4-1 Influence of database size on prediction accuracy of CHF LUT 2005

# of datasets	# of exp. data	HBM		DSM	
		Avg	RMS	Avg	RMS
82	24174	-0.08	7.26	3.7	38.06
108	26231	-0.19	7.26	3.37	37.91

The RMS local error based on DSM decreases slightly when the experimental database is increased with 33 new datasets, therefore it can be concluded that the additional experimental data agree better with the CHF LUT 2005. However, the impact on the errors is not significant.

Obviously, the accuracy and the reliability of the CHF LUT strongly depends on the accuracy and reliability of the experimental data base, so screening of the CHF data is one of the most important steps of LUT derivation. This process involves identification of all data that are unreliable or duplicate. Unreliable data are considered those that are either far from the bulk data, or that do not satisfy the heat balance, or data having a local dryout quality > 1. In Table 4-2, all the screening criteria used for CHF LUT 1995, 2005 and 2006 are listed:

Table 4-2 Screening criteria for the CHF LUT 1995 and 2005

Parameter	1995 Selection Criteria	2005 Selection Criteria	2006 Selection Criteria	Number of data removed due to 2006 selection criteria
No. of data in database	25630	33175	36510	
No. of data sets in database	49	82	116	
D, mm	3 < D < 25	2<D<16	3<D<45	1909
P, kPa	100 < P < 20 000	100<P<21000	100<P<21000	39
G, kg m^{-2} s^{-1}	0<G < 8000	Same	Same	392
X	X_e < 1.0	Same	Same	412
Inlet temperature	Tin>0.01	Same	Same	9
L/D, X_{in}<0	L/D > 80	L/D>50 for X_{cr}>0, L/D>25 for X_{cr}<0	L/D>50 for X_{cr}>0, L/D>25 for X_{cr}<0	2505
L/D, X_{in}>0	not accepted, X_{in} <0	L/D>100	L/D>100	417
Heat balance	Out by >5%	out by >5%	out by >5%	1156
Other data removal criteria	Duplicates	Duplicates	Duplicates	2121
		Outliers as identified by "slice" method	Outliers as identified by "slice" method	229
"Bad" data sets removed	Mayinger et al., 1967; Era et al., 1967; Bertoletti et al., 1964	Bertoletti et al., 1964 ; Ladislau 1978		1090
No. of data accepted for LUT derivation	23114	24781	26231	(total of above: 10279)

4.1 Slice Method

The slice method, described by Durmayaz et al. (2004), has been used extensively for outlier and duplicate data identification and for LUT trend visualization. This method assigns all the experimental data to an appropriate slice and permits us to obtain helpful information about the experimental data (e.g. identification of outliers, duplicate data and "bad" data sets) from the slice through visual inspection and observation. For example for a slice of CHF vs. x for a nominal $G=G_j$ and $P=P_i$ all data falling between $\frac{P_{i-1}+P_i}{2} < P < \frac{P_{i+1}+P_i}{2}$ and $\frac{G_{j-1}+G_j}{2} < G < \frac{G_{j+1}+G_j}{2}$ are extrapolated to a value of CHF $(P_i\, G_j.\, x)$ using the equation to as follows:

$$CHF(P_i, G_j, x) = CHF(P_0, G_0, x) + \Delta CHF_{i,j} \tag{4.1}$$

where $CHF(X_0, G_0, P_0)$ is the experimental CHF value and

$$\Delta CHF_{i,j} = \frac{\partial CHF}{\partial P}(P_i - P_0) + \frac{\partial CHF}{\partial G}(G_j - G_0) \tag{4.2}$$

This allows us to generate the 2-dimensional graphics for $CHF = CHF(x)$ slice at P=P_i and G= G_j.

A similar approach is applied to generate the graphics for $CHF = CHF(G)$ at x_k, P_i and for $CHF = CHF(P)$ at G_j, x_k . An example of a slice is shown in Figure 4-1

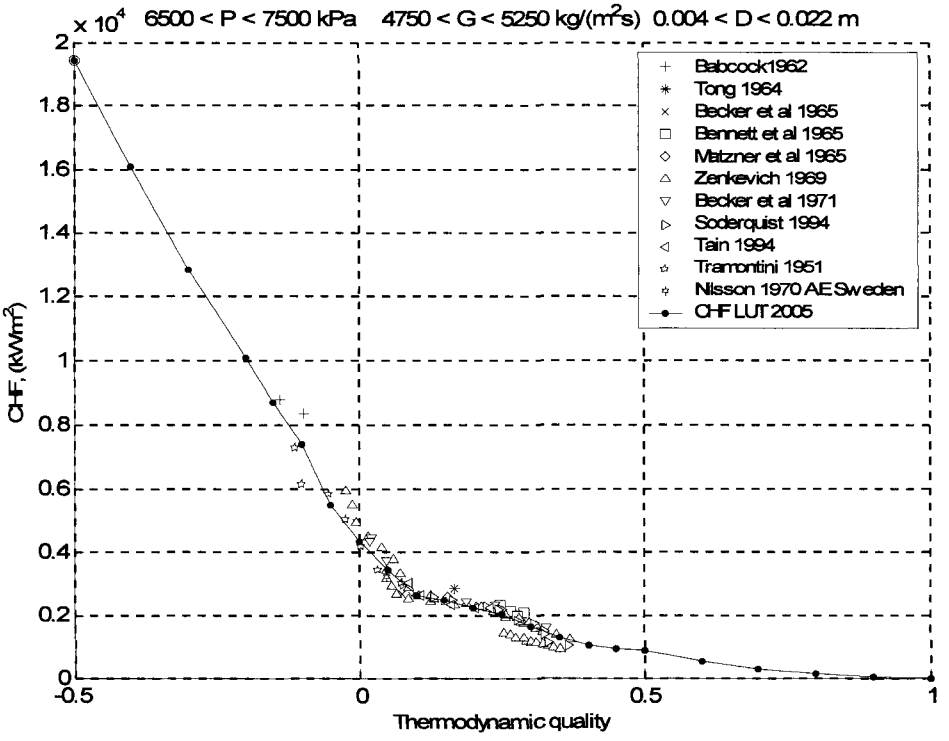

Figure 4-1 Slice at nominal P =7000 kPa, G=5000 kg $m^{-2}s^{-1}$

4.2 Identification of Outliers

Outliers are data points located relatively far from the majority of the data. They have significant impact for all steps of the LUT table derivation. Therefore, removal of outliers is an important step in data processing, since it can dramatically improve the accuracy of the CHF LUT (such as RMS error) , and also curve fitting for the smoothing operation and the general LUT trends.

Normality tests

Experimental systems may be subject to *systematic influences* of measured data (e.g. variations of powerline voltage, permanent electromagnetic perturbations signals) and/or *random influences* (e.g. random electromagnetic perturbations). In general, random effects are difficult to detect and they contribute to data scatter. However significant systematic influences can be detected and removed.

One common way of assessing randomness of a data set is the normality test, which compares the statistical properties of repeated measurements with a Gaussian (or normal) random variable properties. The basis of this approach is central limit theorem which states that the probability distribution function (pdf) of the sum of a large number of repeat measurements should approach Gaussian pdf if the experiment is under statistical control. The statistical control gives some reassurance that an experiment is not subject to significant systematic influences.

In practical applications the normality test is performed by plotting the histogram of repeat measurements on the same graph with Gaussian pdf and visually compare them. Alternatively, a more elaborate, quantitative test, χ^2 (chi-square) may be applied. (Tavoularis, 2005).

Statistical methods for identification of outlier data

As previously mentioned, outlier data are spurious experimental data that contain errors significantly higher than usual uncertainty. They can be identified by Chauvenet's criterion, which state that a value z_i is an outlier if

$$\tau\sigma \leq |z_i - \mu_x| \qquad (4.3)$$

where σ is the variance and μ is the mean of the sample.

The parameter τ is defined as follows:

N	3	4	5	6	8	10	15	20	25	50	100
τ	1.38	1.54	1.65	1.73	1.87	1.96	2.13	2.24	2.44	2.57	2.81

Application of Chauvenet's criterion for CHF database would require caution for the following reasons:

- experimental data have different sources and even at similar local conditions the CHF they can not be treated as repeated data.
- there are specific flow regions (e.g. limiting quality region, data at high thermodynamic qualities) where physical phenomena show high scatter and outlier identification can not be performed.

For this study, two types of outliers were considered: unreliable data sets and "isolated" outliers.

Unreliable data sets are data sets that, for different reasons (unstable experimental conditions, wrong data processing), are obviously far from the "bulk" data. If so, the "outlier" data sets are excluded from the LUT derivation process. Some examples of "outliers" data sets are Bertholeti (1964), Ladislau (1978), Mihaila (1970). Figure 4-2 shows a slice with the two outlier data sets, Mihaila (1970) and Ladislau (1978).

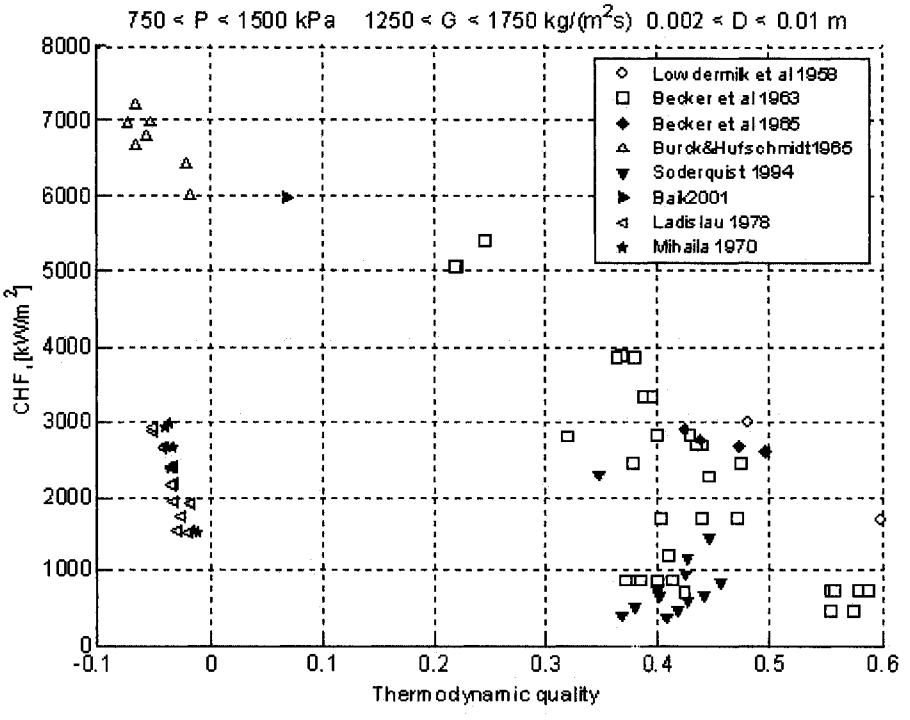

Figure 4-2 Slice at nominal P=1000 kPa , G=1500 kg $m^{-2}s^{-1}$, with two outlier data sets, Mihaila(1970) and Ladislau(1978)

Direct data visualization through the slicing method has been used to identify the unreliable data sets. Only data sets showing obvious outliers were considered for removal. Based on this approach the following unreliable data sets were identified (see Table 4-3):

Table 4-3 Outlier data sets

Data set	# of data	HBM		DSM	
		Avg (%)	RMS (%)	Avg (%)	RMS (%)
Longo et al. 1957	20	52.5	66.6	75.5	94.92
Umekawa et al., 2005	84	1.75	22.4	19.9	122
Bertholetti et al., 1964	386	55	115	260	569
Ladislau , 1968	136	132	142	225	239
Lowdermilk and Weiland, 1951	155	77.7	156	516	887
Mihaila , 1970	149	125	135	208	223
Weatherland and Lottes, 1954	92	3	17.6	13.8	60.2
Lee, 1969	68	15.2	21.6	53.5	62.1
Total	**1,090**	**68.5**	**114.8**	**218**	**463**

Note that the high errors provide extra proof that these outlier data set did not agree with the bulk of the data

Isolated outliers: After identification of outlier data sets, there are still a small percentage of the remaining data that are far from the "bulk" experimental points. These "outliers" came from different data sets and could be generated by random instrumentation errors, instability of experimental conditions, data processing errors, etc.. Those isolated outliers are removed during the error analysis process, by ranking the absolute errors of all experimental data points and eliminating the first 1%, 2%, 3% and 5% of data having the highest errors. This process significantly improves average and RMS error, for both inlet and local conditions, as presented in Table 4-4.

Table 4-4 Influence of outlier data on CHF LUT error

% of data removed	# of data removed	Outlier data				Remaining data			
		HBM		DSM		HBM		DSM	
		Avg	RMS	Avg	RMS	Avg	RMS	Avg	RMS
	0	-	-	-	-	-0.19	7.26	3.37	37.91
1%	263	8.05	37.9	233	254	-0.27	6.22	1.06	28.18
2%	526	2.88	31.7	179	200.7	-0.25	5.77	-0.2	25.36
3%	789	2.61	28.3	134	172	-0.28	5.44	-0.66	23.65
5%	1315	1.74	24.2	92.8	141.7	-0.29	4.97	-1.32	21.29

4.3 Identification of Duplicates

Identification of duplicate data is the next step of data screening. Duplicate data usually came from large experimental data compilations that contain data already included in the AECL-UO CHF database. One attempt for duplicate data identification was made by checking the references of all papers that published experimental CHF data. This way proved to be helpful up to a certain extent, but was not complete. In general, in data compilations, although the sources of data are referenced, the compiled data are often mixed together, making it very difficult to identify their original source. Hence there is a need for a "duplicate data filter".

4.3.1 Dissimilarity measure

Shan et al. (2004) proposed a method called "dissimilarity measure". He used the "Euclidean Distance" to assess dissimilarity (distance) measure:

$$Dis(\boldsymbol{x}_1, \boldsymbol{x}_2) = \sqrt{\sum_{j=1}^{p} (x_{1j} - x_{2j})^2} \tag{4.4}$$

where x is a normalized vector that includes p variables.

The parameters listed in the CHF database are diameter, length, pressure, mass flux, dryout quality, inlet sub-cooling and CHF. According to their "reliability", directly measured such as P, D, Lh or very simply calculated parameters (q_c, G) receive a higher weight then the calculated parameters (x_c or inlet subcooling). Different weights are assigned to different parameters, as shown in Table 4-5, so the distance definition is modified to:

$$Dis(\boldsymbol{x}_1, \boldsymbol{x}_2) = \sqrt{\sum_{j=1}^{p} w_j (x_{1j} - x_{2j})^2} \tag{4.5}$$

Shan et al. (2004) proposed that two data can be treated as duplicate if Dis<0.01.

Equation 4-4 implies that if one parameter gives a much larger distance and the others are nearly identical (which may indicate a duplicate), the dissimilarity measure may give a false result.

Table 4-5 Weight for dissimilarity measure calculation

Index (j)	Parameter	Weight
1	Diameter	0.15
2	Length	0.15
3	Pressure	0.145
4	Mass flux	0.145
5	Dryout quality	0.2
6	Inlet sub-cooling	0.01
7	CHF	0.2

To overcome this weakness, a modified methodology was used for 2006 duplicate screening.

The experimental data were screened for duplicates as follows:

a) Duplicates inside each data set

b) Duplicates between different data sets

4.3.2 Identification of duplicates inside each data set

Duplicates inside each data set are the data for which all screening parameters: diameter, heated length, pressure, mass flux, dryout quality, inlet temperature, and q_c are virtually identical. The method is based on the assumption that even for the same author and the same experimental conditions (system geometry, pressure, mass flux, inlet temperature, measuring devices) it is very unlikely that all recorded parameters are identical. Consequently, most data having all screening parameters identical are considered duplicates. The inner duplicates are not removed completely from the database; they are labeled "duplicate" and one of the duplicates will be ignored during the subsequent LUT development steps.

Each data set has been checked for internal duplicates. The results of screening are presented in the Table 4-6.

Table 4-6 Inner duplicate data

No	Author	# of data in the dataset	# of identical CHF points
1	Ornatskii&Kichigin1961	222	2
2	Becker at al 1963	2659	32
3	Peterlongo et al 1964	349	6
4	Becker et al 1965	1326	38
5	Hewitt et al 1965	442	6
6	Lee 1966	435	150
7	Babarin et al 1969	163	40
8	Bailey&Lee 1969	158	6
9	Zenkevich 1969	5595	14
10	Becker et al 1970	116	2
11	Zenkevich 1971	392	6
12	Smolin et al 1979	2987	12
13	Groeneveld 1985	118	2
14	Borodin 1993	494	204
15	Vandervort etal 1994	210	18
16	Soderquist 1994	1463	4
17	Mudawar&Bowers 1999	174	2
18	Stein 2004	383	4
19	Jens&Lottes 1952	34	2
20	Weatherhead 1963 June	62	2
21	Weatherhead 1963 March	232	2
22	Lee 1963	625	76
Total: 630 identical lines (315 duplicates)			

4.3.3 Identification of duplicates between different data sets

The basis for this method is the proper choice of limits for each parameter considered, in order to properly distinguish between real duplicates and independent points. Directly measured parameters such as q_c, diameter, heated length, pressure, and inlet temperature are unaffected by fluid property subroutines and are less likely to be affected by conversion errors, so they were considered to be the key parameters for the investigation. The calculated parameters inlet subcooling, mass flux and critical quality which can be influenced by conversion subroutines and/or fluid properties are considered auxiliary parameters. In general, the conversion errors for key parameters (including conversion ratio, round/truncation errors) should be less than 0.1%, for the 4-5 significant digit

numbers. For the auxiliary parameters the error margin was set to 1-2%. The ranges for each parameter are presented in Table 4-7.

Table 4-7 Tolerances for duplicate data

Parameter	**Screening criteria: less than:**	**Criterion No.**
Diameter	0.1 mm	1
Length	5 mm	2
Pressure	1%	3
Mass flux	2%	4
Dryout quality	0.02	5
Inlet temperature	0.5 ^{0}C	6
Inlet subcooling	2%	7
CHF	1.5 %	8

Logic criterion: 1 AND 2 AND 3 AND 4 AND 5 AND (6 OR 7) AND 8

Data that satisfy the above mentioned logic criterion are considered as suspect duplicates. In such cases the slicing method is used as an additional check to confirm the suspected duplicates. The duplicate data are not removed completely from the database, they are labeled "duplicate" and only the earlier one of the duplicate data is used during subsequent LUT development steps.

The following identifiers are placed at the beginning of each line (for each experimental data point):

N- for normal data point

I- for internal duplicate

D- for duplicate between two different data sets

O- for outlier data

An example of a section of a data set from Ornatski et al. (1962) before and after the screening process is given below. The duplicates are between the data sets Ornatskii and Kichigin(1961) and Ornatskii and Kichigin(1962). As previously mentioned, the duplicates (D) are labeled in the most recent data set (1962), while for the earlier set the same data are labeled as normal (N):

File Orna1962.txt before screening

Run	D	Lh	P	G	Xdo	dHin	qcr	Tin
No.	m	m	kPa	kg m-2s-1	-	kJkg-1	kWm-2	øC
.001.	0.00200	0.040	7599.38	5000.00	-0.0368	273.432	13714.220	237.11
.002.	0.00200	0.040	7599.38	5000.00	-0.0476	270.604	12552.000	237.72
.003.	0.00200	0.040	7599.38	5000.00	-0.0791	342.949	14179.110	222.14
.004.	0.00200	0.040	7599.38	5000.00	-0.1132	400.372	14644.000	209.52
.005.	0.00200	0.040	7599.38	5000.00	-0.1233	390.936	13133.110	211.61
.006.	0.00200	0.040	7599.38	5000.00	-0.1725	411.068	9878.890	207.14
.007.	0.00200	0.040	7599.38	5000.00	-0.2360	550.706	12784.440	175.58
.008.	0.00200	0.040	7599.38	5000.00	-0.3038	687.301	15108.890	143.91
.009.	0.00200	0.040	7599.38	5000.00	-0.4816	1096.846	24406.670	46.43
.010.	0.00200	0.040	7599.38	5000.00	-0.5481	1175.743	23244.440	27.46
.011.	0.00200	0.040	10132.50	5000.00	-0.0453	198.836	8716.670	276.12
.012.	0.00200	0.040	10132.50	5000.00	-0.1367	364.935	11622.220	242.23

File Orna1962.txt after screening

Run	D	Lh	P	G	Xdo	dHin	qcr	Tin
No.	m	m	kPa	kg m-2s-1	-	kJkg-1	kWm-2	øC
D_.001.	0.00200	0.040	7599.38	5000.00	-0.0368	273.432	13714.220	237.11
D_.002.	0.00200	0.040	7599.38	5000.00	-0.0476	270.604	12552.000	237.72
D_.003.	0.00200	0.040	7599.38	5000.00	-0.0791	342.949	14179.110	222.14
D_.004.	0.00200	0.040	7599.38	5000.00	-0.1132	400.372	14644.000	209.52
N_.005.	0.00200	0.040	7599.38	5000.00	-0.1233	390.936	13133.110	211.61
D_.006.	0.00200	0.040	7599.38	5000.00	-0.1725	411.068	9878.890	207.14
D_.007.	0.00200	0.040	7599.38	5000.00	-0.2360	550.706	12784.440	175.58
D_.008.	0.00200	0.040	7599.38	5000.00	-0.3038	687.301	15108.890	143.91
D_.009.	0.00200	0.040	7599.38	5000.00	-0.4816	1096.846	24406.670	46.43
N_.010.	0.00200	0.040	7599.38	5000.00	-0.5481	1175.743	23244.440	27.46
N_.011.	0.00200	0.040	10132.50	5000.00	-0.0453	198.836	8716.670	276.12
N_.012.	0.00200	0.040	10132.50	5000.00	-0.1367	364.935	11622.220	242.23

For LUT derivation and error assessment purposes only the experimental data flagged with "N" are considered. This approach has the advantage of excluding duplicates from the LUT derivation process, while preserving intact the original structure of the data sets.

As mentioned, the logical parametrical screening, implemented in a short MATLAB application, identifies only the *suspect* duplicate data. Confirmation that a suspect point is a duplicate data point is made by visualization, using the slice method. An example of a slice containing suspect duplicates is presented in Figure 4-3, while the identified duplicate data sources are summarized in Table 4-8. For further LUT derivation and assessment data by Eicheldinger(1962) and Griffel(1964) are preserved (labeled "N") and the data by Tong(1965) are marked as duplicate :

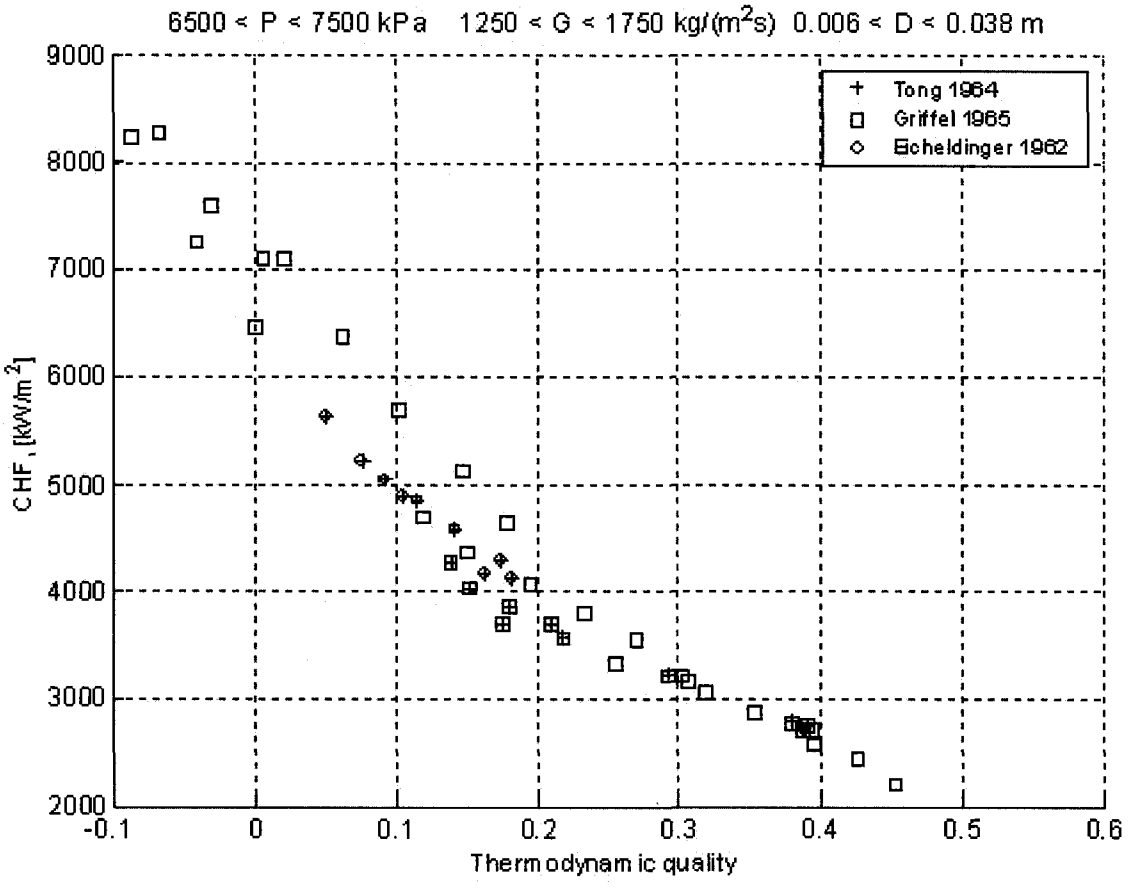

Figure 4-3 Slice at P=7MPa, G=1500 kg $m^{-2}s^{-1}$, containing duplicate data

Table 4-8 Duplicate data

No	Author	# of data in the dataset	# of duplicates
1	Ornatskii&Kichigin 1961	222	59
2	Ornatskii&Kichigin 1962	169	
3	Babcock 1962	39	39
4	Hood 1962a	61	
5	Swenson et al 1962	25	25
6	Tong 1964	266	
7	Smolin 1962	369	311
8	Smolin 1979	2987	
9	Hood 1962b	24	14
10	Hood&Isakoff 1962	28	
11	Isakoff&Measley 1962	10	10
12	Hood 1962b	24	
13	Tong 1964	266	159
14	Griffel 1965	397	
15	Tong 1964	266	73
16	Becker 1965	1326	
17	Becker 1965	1326	173
18	Griffel 1965	397	
19	Waters et al 1965	37	14
20	Tong 1964	266	
21	Becker 1965	1326	242
22	Lee&Obertelli 1963	625	
23	Zenkevich 1969	5595	38
24	Hunt et al 1955	93	
25	Tong 1964	266	26
26	Eicheldinger 1962	26	
27	Lee 1965	38	38
28	Bennett et al 1965	201	
29	Lee 1965	38	38
30	Zenkevich 1974	823	
31	Becker 1971	1457	118
32	Groeneveld 1985	118	
33	Zenkevich 1974	823	141
34	Bennett et al 1965	201	
35	Zenkevich_1969	5595	14
36	DeBortoli&Masnovi_1957	33	
37	Zenkevich 1969	5595	70
38	Perskov 1961	264	
39	Becker et al 1971	1455	103
40	Nilsson 1970	588	
41	Rudzinski 1993	106	55
42	Tain 1994	55	
43	Hunt et al 1955	93	93
44	Weatherhead&Lottes 1954	93	
45	Alessandrini 1964	753	23
46	Hassid 1968	191	
	Total		**1806**

4.4 Visual Checking and Trend Analysis

Visual checking and trend analysis is the last step of the CHF LUT table derivation. It ensures that LUT is reasonably smooth, accurate and shows the correct trends with respect to all parametric directions. Visual checking is based on the slice method, as described in 4.1.

A MATLAB application with a user friendly interface has been developed and used to check the CHF LUT 2005. The application allows simultaneous visualization of the CHF LUT in three parametric directions, P, G and x. A typical interface is showed in Figure 4-4

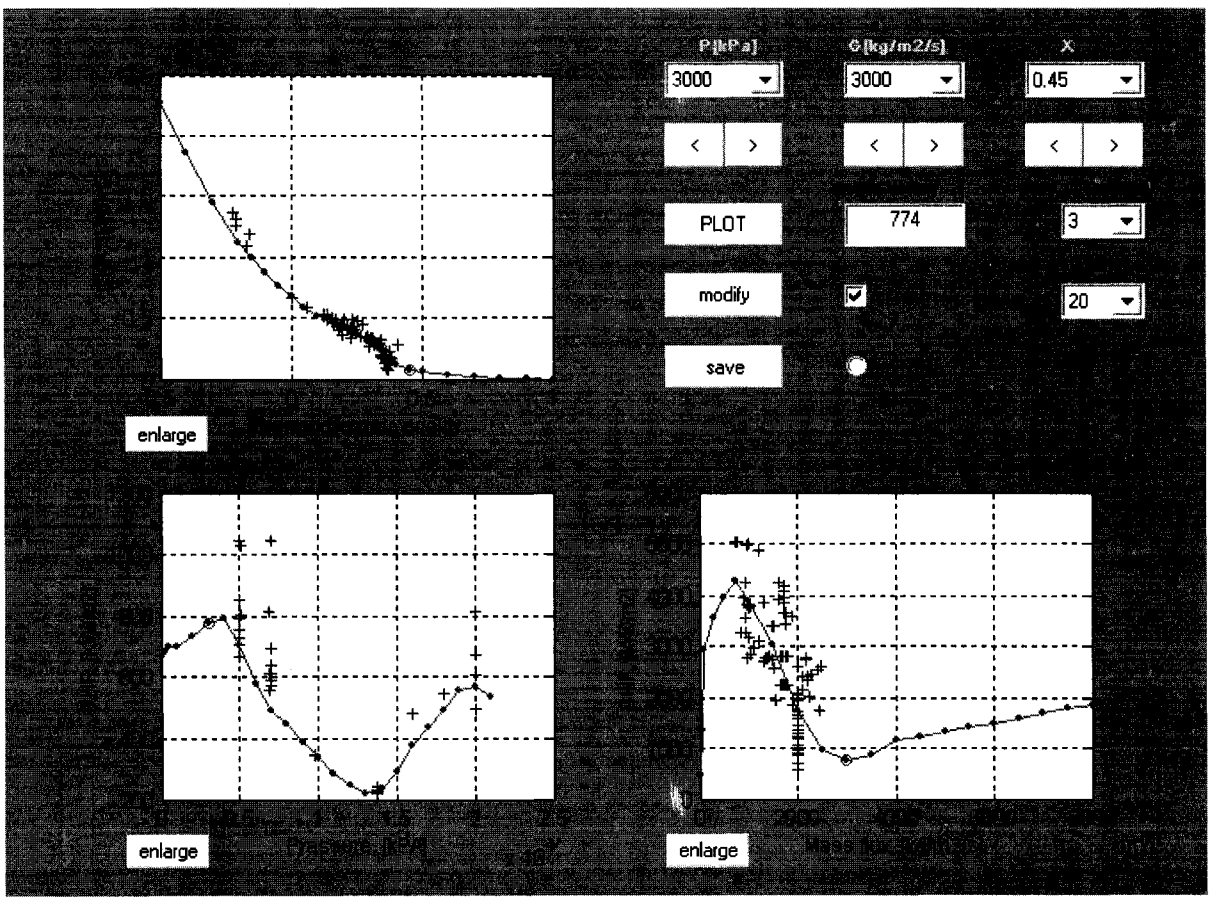

Figure 4-4 Screen of main user interface of CHF LUT trend checking program

Three subplots display simultaneously slices of CHF with respect to x, P and G. Because of the small size of sub plots, the experimental data are plotted in one color, regardless of the author. The user may use a zoom to obtain a more detailed part of any subplot. The button

"enlarge" will open a new window containing a more detailed plot of the CHF LUT and the experimental data, as well as a legend. An example of an "enlargement" of the subplot CHF versus x , is shown in Figure 4-5:

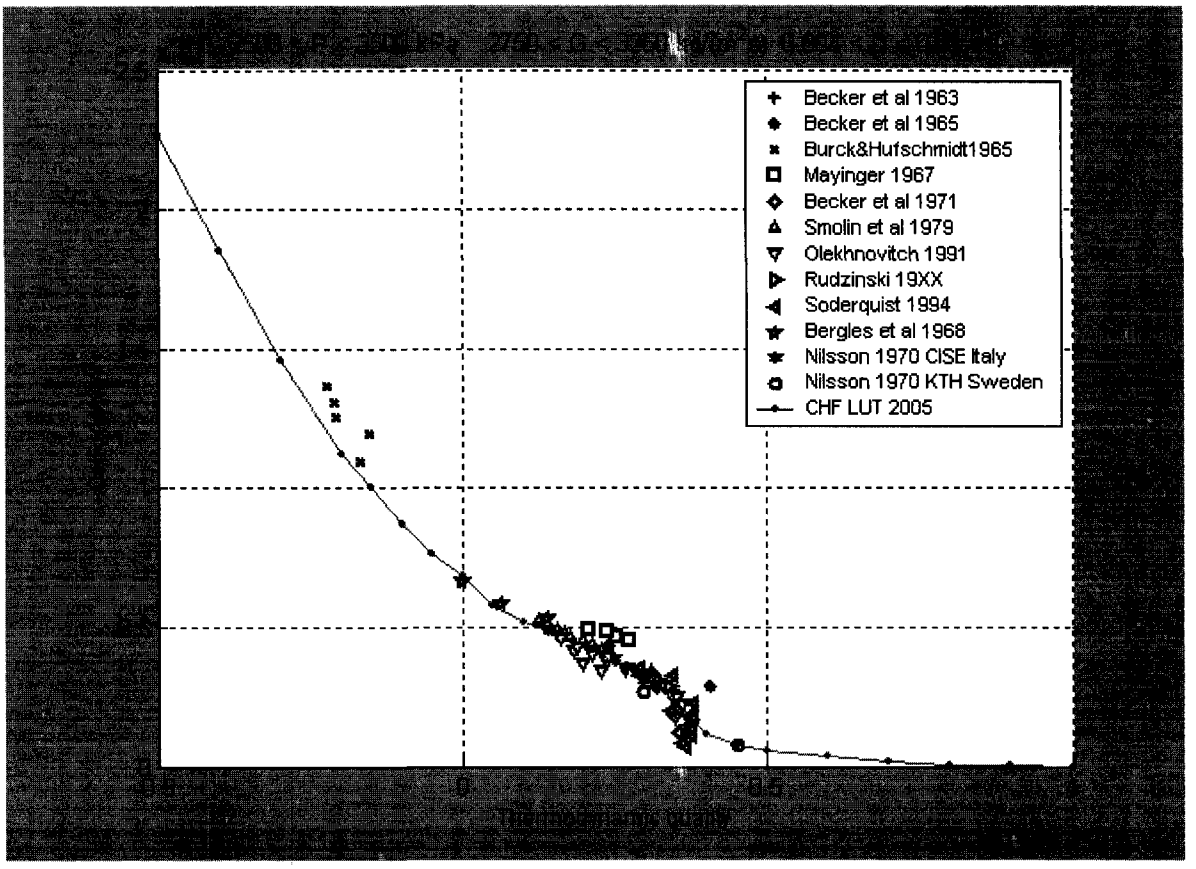

Figure 4-5 Example of an "enlarged" q versus X slice

The user can select the desired slices through popup menus containing the choices for pressure, mass flux and quality. The diameter range for experimental data can be selected, as well. The "table entry" text box is editable, allowing manual modification of the CHF LUT. The effect of any modification can be assessed for all parameters simultaneously. If the modification is going to be "permanent", the button "save" would perform this task.

Two or three CHF LUT's can be compared simultaneously, with or without displaying the experimental data, by checking the box labeled "experim". The above mentioned methodology facilitates the final verification of the CHF LUT in terms of efficiency, LUT accuracy and trends.

4.5 Summary

Between 2005 and 2006, 33 new datasets, having in total 4171 data points, have been added to the AECL-OU CHF experimental database. The error analysis performed has shown that the new data sets added are reliable.

A new data set labeling methodology that allows the selection of reliable data for LUT derivation while preserving the unaltered datasets has been introduced and successfully used. Eight outlier datasets (1090 data points) and 229 isolated outliers have been identified through the slice method and labeled. A significant reduction in the LUT errors resulted from removing the outliers. An improved methodology for duplicate data identification has been applied; this method detected 315 duplicate data within individual data sets and 1806 duplicates different between datasets. The duplicates were confirmed by the slice method.

A MATLAB application that displays simultaneously slices of CHF in respect to x, P and G has been developed. It facilitates the final verification of the CHF LUT in terms of efficiency, accuracy and trends.

5. DIAMETER EFFECT ON CHF

The values of the CHF LUT are "normalized" for an 8 mm ID tube. Prediction of CHF for various diameters involves "conversion" from one diameter to another. Despite a great amount of CHF experimental data and numerous analytical studies, the effect of diameter on CHF is still not well understood. The main obstacle for a comprehensive description of this effect is that CHF data for different tube diameters were not obtained at comparable conditions. The effect of tube diameter on critical heat flux has been examined by: (1) analyzing existing experimental data; (2) reviewing existing correlations and semi-analytical models; and (3) phenomenological models.

The vast majority of experiments performed with heated test sections of different diameters revealed that the CHF in smaller diameter tubes is higher than in tubes with larger diameters at similar local flow conditions (Wong, 1996). Wong's conclusions are based on an investigation over many data sets different authors. There are a few exceptions, e.g. Boltienko et al.(1988) reported reverse trends (higher diameters produce higher CHF) at subcooled flow conditions.

5.1 Mechanistic Description of the Diameter Effect

This section describes several mechanisms thought to be responsible for the observed diameter effect on CHF

Subcooled CHF:

The higher CHF at smaller diameters for subcooled flow could be due to the reduced distance between the bubbly boundary layer and subcooled core for small diameter tubes; this reduced distance enhances the rate of vapour condensation within the boundary layer, thus increasing CHF. At similar flow conditions (P, G and x) the average flow velocity is similar, regardless tube diameter, but smaller tubes result in larger radial velocity gradients. A higher velocity gradient enhances the rate of detachment of the growing bubbles, increasing the CHF.

Furthermore, higher temperature gradients in smaller tubes enhance the heat transfer between bubbles and liquid, reducing bubble generation and increasing CHF.

Film dryout: At higher critical qualities, the annular flow regime is encountered and the observed experimental trends are explained through the annular flow model by considering the variation of entrainment, evaporation and deposition rates with diameter. In general the entrainment rate strongly depends on liquid film thickness, a thicker film producing higher amplitude surface waves, thus enhancing the entrainment rate. At a similar local quality, pressure and mass flux, smaller tubes have a thinner film and a smoother liquid film interface, thus reducing entrainment rate. Furthermore, for the same L/D ratio and the same local conditions (P,G and x) a small diameter channel would have a shorter length, hence there will be less time available for entrainment.

Another effect that enhances CHF in small diameter tubes is the higher temperature gradient that decreases the liquid film superheat, reducing the evaporation rate. Table 5.1 summarizes the main phenomena and mechanisms for CHF enhancement in small diameter tubes (Wong, 1996).

Low flow or zero-flow CHF: The CHF mechanism at zero and very low flows usually corresponds to the countercurrent flow limitation (CCFL) or flooding, except for very large diameters when a pool type CHF occurs. For these flow conditions, experimental data suggest that higher CHF is obtained at higher diameters.

Large diameters allow better development of the counter-current flow due to lower velocity gradients and shear stress, therefore the liquid flow limitation occurs at higher surface heat fluxes.

At zero/very low flows, larger channel diameters result in a bigger volume of subcooled liquid, therefore better bubble dissipation and condensation, hence it is less likely that vapour slugs are formed that could otherwise bridge the heated channels and initiate the CHF condition. A more detailed description of this mechanism is provided on Chapter 8, Section 8.1.

Table 5-1 Diameter effect and mechanisms according to Wong (1996)

	Phenomenon in small diameter tubes	**Mechanisms for CHF increase**
Subcooled and low quality flow	Smaller vapour bubble size Thinner vapour bubble boundary layer	Better heat transfer because of core flow close to the wall
	Void fraction within bubble layer decreases	Re-entry of liquid replenishment easier
	Velocity gradient of 2-phase boundary layer increases	Growing vapour bubble detaches easier before forming vapour patches at wall
	Temperature gradient of wall layer higher	Bubble generation slower due to high condensation rate at the tip of the bubble
	Interfacial friction inversely proportional with Re number	Increase friction at two phase boundary and increase heat transfer
High quality, annular flow	Flow of liquid layer at wall thinner	Boiling suppressed in the liquid film
	Lower entrainment rate	Higher liquid film thickness
	Temperature gradient of liquid film at wall increases	Reduced liquid superheat in the film, lower evaporation rate
	Rate of liquid deposition increases	Higher liquid film thickness
Zero flow/low flow	Smaller subcooled liquid volume Higher liquid/vapour velocity gradients	Lower bubble dissipation rate Higher shear stress at interface liquid/vapour

5.2 Prediction Methods for Diameter Effect

To account for the diameter conversion for the CHF LUT Doroschuk, (1975) and Groeneveld, (1986, 1996) proposed correlations of the following form:

$$\frac{CHF_D}{CHF_{D=8}} = \left(\frac{8}{D}\right)^n \tag{5.1}$$

Different values of the exponent n have been recommended: 1/2 (Doroschuk, 1975, Groeneveld, 1996) and 1/3 (Groeneveld, 1986). These exponents are optimized from large

data bases and represent average values. Analysis of the available experimental data suggests that the exponent n can also be a function of pressure, mass flux, dryout quality, and diameter itself. For example, the exponent for the diameter term in the Biasi correlation is 0.4 for a tube of diameter less than 10mm, and 0.6 otherwise.

The diameter effect in tubes was also investigated by other researchers (Lee, 1966, Stevens et al., 1964). They found that the diameter has a strong effect on CHF especially at small diameters, but this result is not conclusive since their data weren't obtained at the same dryout conditions.

At low pressures, Bergles (1963) reported that the CHF was lower for larger diameter tubes based on a constant outlet quality. The diameter effect on CHF is strongest for small diameters.

In a separate study at a pressure of 2500 kPa, Ornatskiy (1969) found a similar trend. He also reported that for large diameters, CHF approaches constant values, depending on the mass flux. Groeneveld (1986) suggested that the ratio between CHF at diameters larger than 16 mm and CHF at 8 mm is approximately constant at 0.6.

For the high pressure CHF data, Becker (1967) presented ratios of CHF for various values of tube diameter to CHF for a 10mm tube. These ratios varied from 1.18 for a 4-mm tube to 0.90 for a 25-mm tube.

Based on the experimental database of the Institute of Physics and Energy, Obninsk and his own experiments using Freon, Boltienko et al. (1988) proposed a correlation which takes into account the flow regimes and the CHF mechanisms. He used three different tubes of 8, 16 and 20 mm ID and observed that for the low quality region (x_c<0.2) the CHF increases with tube ID, while high qualities showed a reverse trend. To quantitatively assess the diameter effect, he used the general correlation (5.1), where the exponent n varies according to the flow regimes as presented in Table 5-2:

Table 5-2 Exponent n as a function of flow regime and pressure

P(MPa)	Region 1 (bubbly flow)	Region 3 (annular dispersed flow – entrainment controlled dryout)	Region 5 (annular dispersed flow – deposition controlled dryout)
1 - 6	-0.188	0.068	0.266
6 -14	-0.263	0.164	0.197
14 -20	-0.418	-	0.163

Regions 2 and 4 denote transition from bubbly to annular – entrained controlled CHF and annular entrained controlled CHF to deposition controlled CHF, respectively.

The onset of annular dispersed flow (Region 3) is given by:

$$X_1 = 2.7\left(\frac{\rho_g \sigma}{G^2 D}\right)^{0.25}\left(\frac{\rho_g}{\rho_f}\right)^{0.333} \tag{5.2}$$

The upper limit of Region 3 can be calculated as:

$$X_2 = 1.05\left(\frac{\rho_g \sigma \cdot 10^3}{G^2 D}\right)^{0.204}\left(\frac{\rho_g}{\rho_f}\right)^{0.214} \quad 1<P<6 \text{ MPa} \tag{5.3a}$$

$$X_2 = 0.52\left(\frac{\rho_g \sigma \cdot 10^3}{G^2 D}\right)^{0.280}\left(\frac{\rho_g}{\rho_f}\right)^{0.0119} \quad 6<P<20 \text{ MPa} \tag{5.3b}$$

The lower boundary of Region 5 is given as:

$$X_3 = 1.18\left(\frac{\rho_g \sigma \cdot 10^3}{G^2 D}\right)^{0.238}\left(\frac{\rho_g}{\rho_f}\right)^{0.204} \quad 1<P<6 \text{ MPa} \tag{5.4a}$$

$$X_3 = 0.57\left(\frac{\rho_g \sigma \cdot 10^3}{G^2 D}\right)^{0.3}\left(\frac{\rho_g}{\rho_f}\right)^{-0.0367} \quad 6<P<20 \text{ MPa} \tag{5.4b}$$

If the dryout quality falls in the transition regions (Regions 2 or 4), then n is calculated through linear interpolation between adjacent regions.

Fortini et al. (2002) proposed a correlation for diameter correction, very similar to Boltienko.

Table 5-3 shows the most common diameter correction correlations from literature and their range of applicability.

Table 5-3 Summary of the diameter correction correlations

<table>
<tr><th>Prediction Method</th><th>Reference:</th><th>Comments</th></tr>
<tr><td>$\frac{CHF_D}{CHF_{D=8mm}} = \left(\frac{8}{D}\right)^{1/3}$</td><td>Groeneveld et al [1986]</td><td>For 4 <D <16 mm
For D>16 mm the correction factor is equal to 0.6</td></tr>
<tr><td>$\frac{CHF_D}{CHF_{D=8mm}} = \left(\frac{8}{D}\right)^{1/2}$</td><td>Groeneveld et al [1995]</td><td></td></tr>
<tr><td>$\frac{CHF_D}{CHF_{D=8mm}} = \left(\frac{8}{D}\right)^{1/2}$</td><td>Doroschuck et al [1975]</td><td>Valid for 4<D<16 mm for ΔTsub <75 C and not very high qualities</td></tr>
<tr><td>$\frac{CHF_D}{CHF_{D=10mm}} = \left(\frac{10}{D}\right)^{n}$

$CHF_D=CHF_8(8/10)^{0.6}(10/D)^n$

n=0.4 if D>10mm
n=0.6 if D<10mm</td><td>Biasi et al [1967]</td><td>Ranges :
D=3-37.5 mm
P=270 -1400 kPa
G=100 – 6000 kg m^{-2} s^{-1}</td></tr>
<tr><td>$\frac{CHF_D}{CHF_{D=10mm}} = f(D)$

<table><tr><td>D</td><td>4</td><td>6</td><td>8</td><td>10</td><td>12</td><td>14</td><td>18</td><td>24</td><td>25</td></tr><tr><td>f</td><td>1.18</td><td>1.76</td><td>1.085</td><td>1.00</td><td>0.973</td><td>0.962</td><td>0.94</td><td>0.917</td><td>0.9</td></tr></table></td><td>Becker [1967]</td><td>Ranges:
D=4-25mm
P=270-10000 kPa
G=120 – 5400 kg m^{-2} s^{-1}</td></tr>
</table>

Modified Becker correlation for ID=8 mm tubes D: 4, 6, 8, 10, 12, 14, 18, 24, 25 f: 1.09, 1.62, 1.00, 0.92, 0.9, 0.89, 0.86, 0.84, 0.83		X=0-0.5
$\frac{CHF_D}{CHF_{D=8mm}} = \left(\frac{8}{D}\right)^{0.1}$	Macbeth [1963]	Valid for low flow ($G<300$ kg m^{-2} s^{-1})
$\frac{CHF_D}{CHF_{D=8mm}} = \left(\frac{8}{D}\right)^{0.235}$	Mudawar [1999]	$100<p<20000$ kPa $300<G<30000$ kg m^{-2} s^{-1} $x<-0.05$ $0.25mm<D<15mm$
$\frac{CHF_D}{CHF_{D=8mm}} = \left(\frac{8}{D}\right)^{n}$ $n = 0.58 \cdot (1-0.25 \cdot \exp(-2 \cdot x)) \cdot (1-15 \cdot D^{-6} G)$	Wong (1996)	

Figure 5-1 shows a plot of $R=q_D/q_{8\ mm}$ versus D to compare the different constant exponents .

5.3 Diameter Effect in Analytical Models

Wong (1996) examined systematically some common CHF models and correlations and, where possible, separated the diameter effect. He found that both the Lee-Mudawar (1988) and Katto (1990) models predict a CHF proportional to $d^{-0.5}$. Tong's model (1968), valid for subcooled conditions only, predicts CHF proportional to $d^{-0.6}$.

Based on the hypothesis that CHF is affected by the rate of bubble formation and rate of bubble removal, Leviatan (1990) found that CHF in subcooled region is proportional to $d^{-0.6}$.

Similar to other models, the Celata model (1994) shows an increasing CHF with decreasing tube diamteter, $q_c \sim d^{-0.5}$.

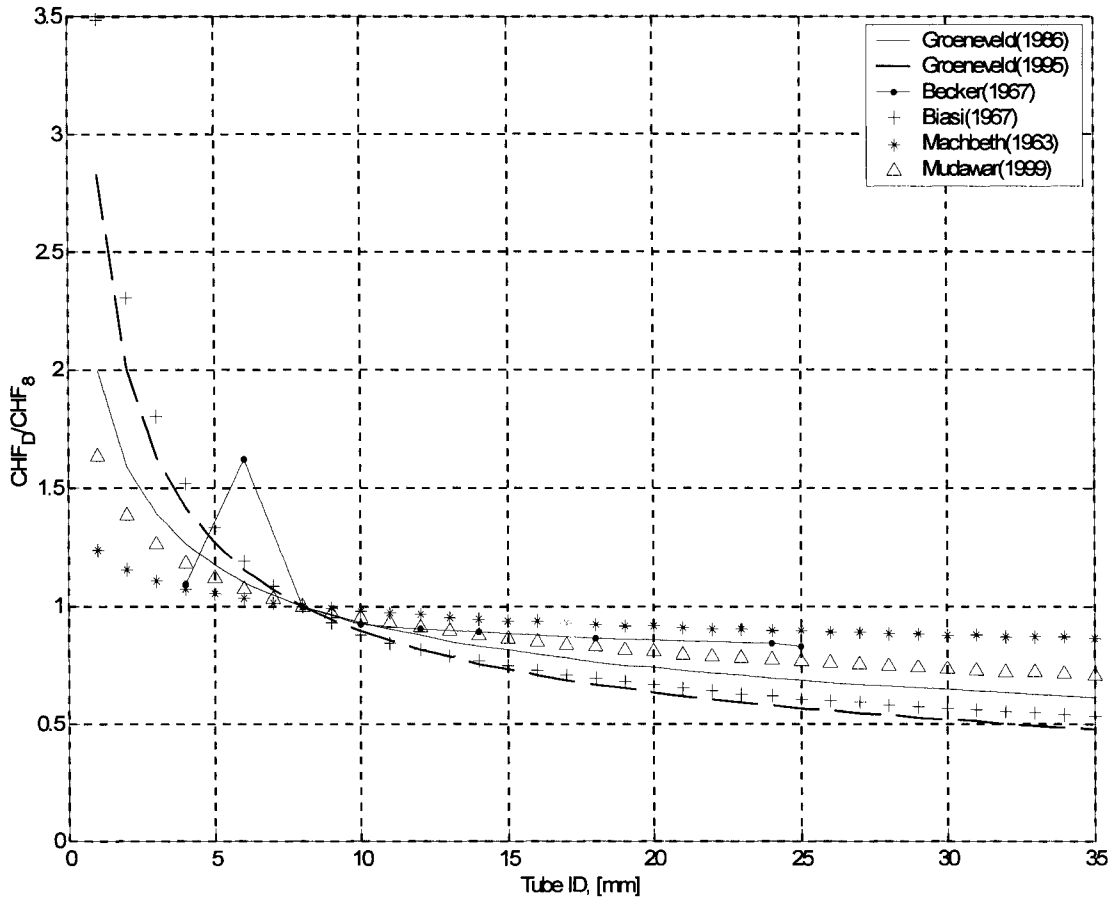

Figure 5-1 Comparison of different diameter effect correction factors

The Weisman-Pei model (1983) for low qualities predicts a diameter effect of $d^{-0.7}$ for constant dryout conditions. The model shows an increase of CHF with a decrease in diameter, since both the deposition rate is slower ($\sim d^{-0.5}$) and the entrainment rate is higher for larger diameters ($\sim d^{0.316}$).

At higher qualities, the tube diameter dependence predicted by the annular film dryout model is d^n, where n varies between -0.5 and -0.8 (Wong,1996).

5.4 Observed Experimental Trends for Diameter Effect on CHF

Methodology

The basis for the assessment is to "separate" the effect of the diameter from the effect of other parameters. For this analysis the CHF is considered a local conditions function, as follows:

$$CHF = \Phi(P, G, X, D) \tag{5.5}$$

where Φ is an unknown real function.

A slicing method was used to isolate the diameter effect: for each nominal LUT pressure $(P_{i-1}+P_i)/2 < P < (P_{i+1}+P_i)/2$, nominal mass flux $(G_{j-1}+G_j)/2 < G < (G_{j+1}+G_j)/2$ and nominal quality $(X_{k-1}+X_k)/2 < X < (X_{k+1}+X_k)/2$, a CHF versus diameter plot was created. Hence, for each slice the unknown function Φ (P, G, X) turns into Ψ(D), with P, G, X =constant. For such conditions, the study of Ψ with diameter is more straightforward.

The whole range of possible flow conditions was divided in 24 sections for pressure, 21 for mass flux and 23 for quality. For each slice, the experimental parameters are not exactly the same as the nominal values of the slices, because the experimental parameters fall in the slicing range. To be able to compare the values at the same flow conditions, a correction based on the slopes of the 2005 LUT was applied. Experimental values were modified based on their distances from the nominal value, with respect to all three directions, P, G and X, respectively:

$$q_c = q_{c_0} + \frac{\partial q_c}{\partial P}(p_0 - p_i) + \frac{\partial q_c}{\partial G}(G_0 - G_j) + \frac{\partial q_c}{\partial x}(x_0 - x_k) \tag{5.6}$$

where "0" index refers the experimental points and i, j, k refer the nominal values which characterize the slice with respect to P, G and x. The partial derivatives (slopes) were obtained from the 2005 LUT.

The main parameters characterizing the accuracy of a correlation are *average error* and *root mean square (RMS) error*. They are defined as follows:

$$Avg.\ error = \frac{1}{N}\sum_{i=1}^{N}(Error)_i \tag{5.7}$$

$$Rms\ error = \sqrt{\frac{1}{N}\sum_{i=1}^{N}(Error)_i^2} \tag{5.8}$$

$$Error = \frac{\Pr edicted\ CHF}{Measured\ CHF} - 1 \tag{5.9}$$

The prediction errors are calculated for each data point in the database. All the errors are based on local conditions.

Although it was possible to produce 11592 slices (21x23x24), only those slices that contained CHF data at different diameters were considered, thus allowing the establishment of a trend. A sample of a slice at nominal P=7000 kPa, G=4000 kg $m^{-2}s^{-1}$, x_c=0, is presented in Figure 5-2. As shown in the figure, the reference diameter is 8 mm and the reference CHF at 8 mm is calculated by averaging all the CHF values at 8 mm. The prediction of CHF at other diameters was performed using equation 5.1. The exponent n was varied until the RMS error calculated reached its minimum; for the above plot n=0.3 produced a minimum RMS error of 10.0%. If the generated slice does not contain any data at D=8 mm, then the reference diameter is taken as the closest of 8 mm, regardless of whether it is smaller or larger .

The general equation is:

$$\frac{CHF_{D1}}{CHF_{D2}} = \left(\frac{D_2}{D_1}\right)^n \quad \text{or} \quad CHF_{D1} = CHF_{D2}\cdot D_2{}^n \cdot \left(\frac{1}{D_1}\right)^n \tag{5.10}$$

To examine more closely whether n remained reasonably constant, the whole range of P, G and x was subdivided based on the observed trends and the following considerations:

- Because the pressure has the least impact on CHF and n, two subranges, low and medium pressures (<14000kPa) and high pressures (>14000kPa) have been considered; this approach is consistent with Boltienko's pressure subdivision;
- Experimental data and some papers (Mishima, 1984, Chang, 2001) revealed that at low flows (<250 kg $m^{-2}s^{-1}$) the CHF mechanisms are different compared to other flow regimes, therefore this limit was considered important.

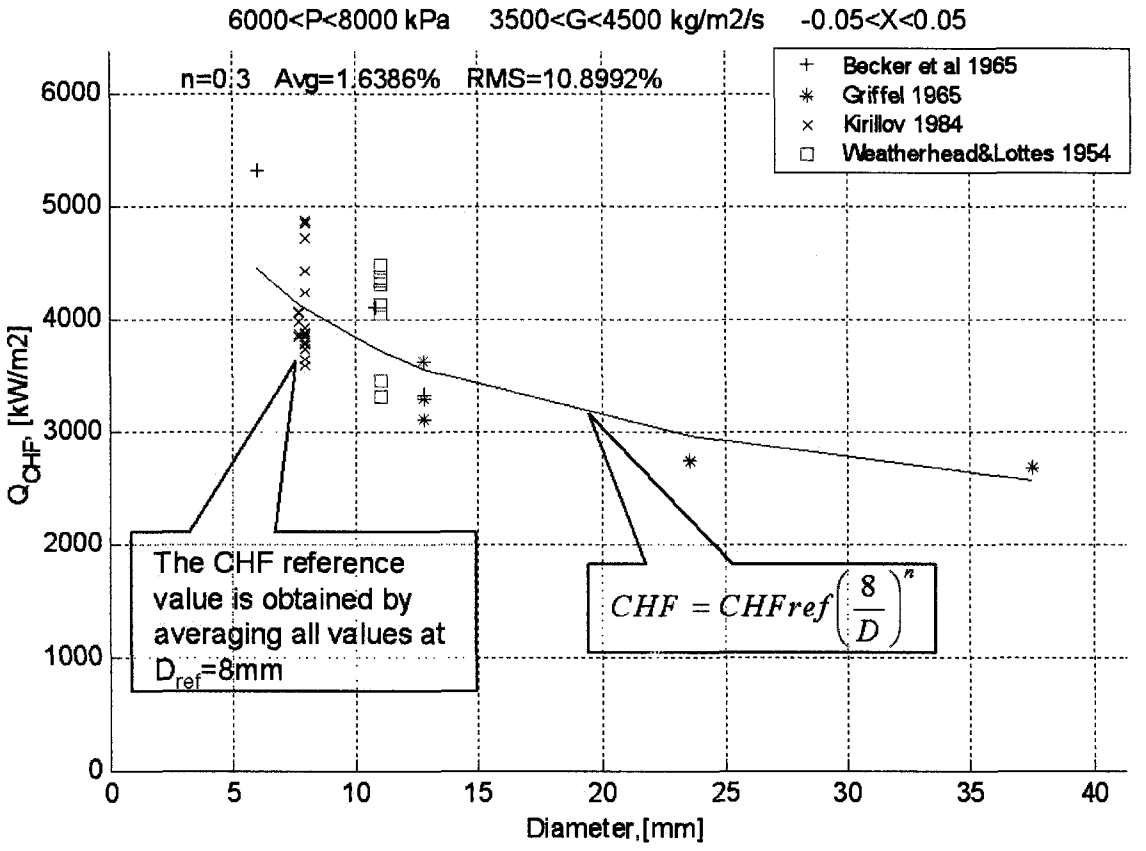

Figure 5-2 Slice showing the typical trend of CHF versus diameter and the best fitting curve

- Experimental data at flows higher than 3000 kg $m^{-2}s^{-1}$ suggested a different optimized coefficient n than medium flows, so this limit was chosen as second boundary for mass flux range.
- Different CHF mechanisms are employed in subcooled and saturated quality regions, respectively, therefore the boundary at x=0 was considered; because the quality has a

strong impact on CHF, another two boundaries that evenly divide the subcooled and saturated regions have been considered.

- Variation in the optimized coefficient n between the different subregions investigated suggested that the increase in the number of subdivisions would have a positive impact on correlation accuracy but it would make it more complicated; hence the choice of the number of subdivisions is a compromise.

Within each subregion the exponent n has been computed as a weighted average (the weight of each exponent being proportional to the number of experimental data for each slice) of all available exponents that have fallen inside the subregion:

$$n = \frac{\sum_{i=1}^{M} N_i n_i}{\sum_{i=1}^{M} N_i} \tag{5.11}$$

where N_i is the number of experimental data points within the slice i, n_i the computed exponent for the slice i, and M the number of slices considered within the subregion .

The values of optimized exponents n for each range of pressure, quality and mass flux are shown in Table 5-4:

Table 5-4 Exponent n as a function of pressure, mass flux and local quality

Quality (x)		**-0.5 to -0.25**	**-0.25 to 0**	**0 to 0.5**	**0.5 to 1**
Pressure [kPa]	**Mass flux ($kg\ m^{-2}s^{-1}$)**				
100 - 14000	**0 to 250**	-0.2	-0.2	-0.2	-0.3
	250 to 3000	0.4	0.4	0.5	0.6
	3000 to 8000	0.3	0.3	0.4	0.4
14000 – 21000	**0 to 250**	-0.2	-0.2	-0.2	-0.3
	250 to 3000	0.4	0.2	0.4	0.4
	3000 to 8000	0.3	0.2	0.2	0.2

The prediction errors for this method are given in the next section.

5.5 Assessment of Correlations for Diameter Correction

Seven correlations for diameter correction factor have been assessed against the AECL-UO CHF database and the CHF LUT 2005. The results are shown in Tables 5-5, 5-6 and Figures 5-3 and 5-4. The symbols used are as follows:

Be	Becker (1967)
Bi	Biasi (1967)
G86	Groeneveld (1986)
G95	Groeneveld (1995)
K	Kirillov (1992)
N	No correction
T	This thesis (Table 5.4)
W	Wong (1996)

:

Table 5-5 General average error and RMS errors for different diameter corrections

Correlation	# of data	HBM		DSM	
		Avg	RMS	Avg	RMS
This thesis (Table 5.4)	26231	-0.03	7.27	3.71	37.98
Kirillov(1992)	26231	1.52	9.68	8.61	42.66
Wong(1996)	26231	-0.13	7.21	3.33	37.81
Groeneveld(1986)	26231	0.55	7.26	5.56	38.75
Groeneveld(1995)	26231	-0.19	7.26	3.37	37.91
Becker (1967)	26231	2.10	9.09	11.89	44.54
Biasi(1967)	26231	0.01	7.40	3.94	38.26
No correction	26231	2.03	9.75	11.28	45.12

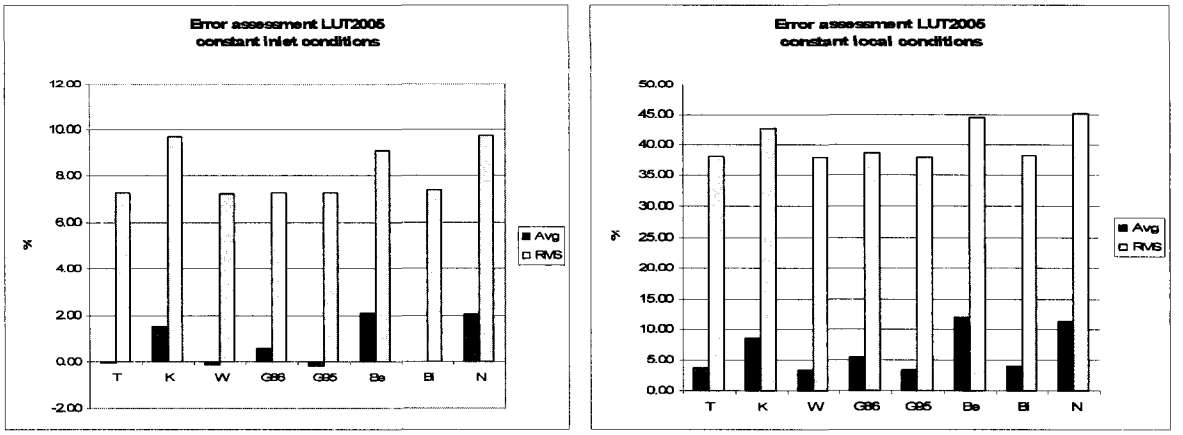

Figure 5-3 General error assessment of CHF LUT2005

Table 5-6 Average and RMS errors for different diameter corrections, subcooled region

Correlation	# of data	HBM		DSM	
		Avg	RMS	Avg	RMS
This thesis	2055	-0.45	5.74	-0.52	11.67
Kirillov(1992)	2055	3.77	16.69	8.84	34.92
Wong(1996)	2055	-0.53	5.85	-0.52	11.89
Groeneveld(1986) (n=1/3)	2055	-0.15	5.76	-0.05	11.79
Groeneveld(1995) (n=0.5)	2055	-1.13	6.67	-1.29	12.93
Becker (1967)	2055	2.31	9.03	6.90	20.13
Biasi(1967)	2055	-0.73	6.73	-0.45	13.75
No correction (n=0)	2055	2.03	10.59	4.12	20.41

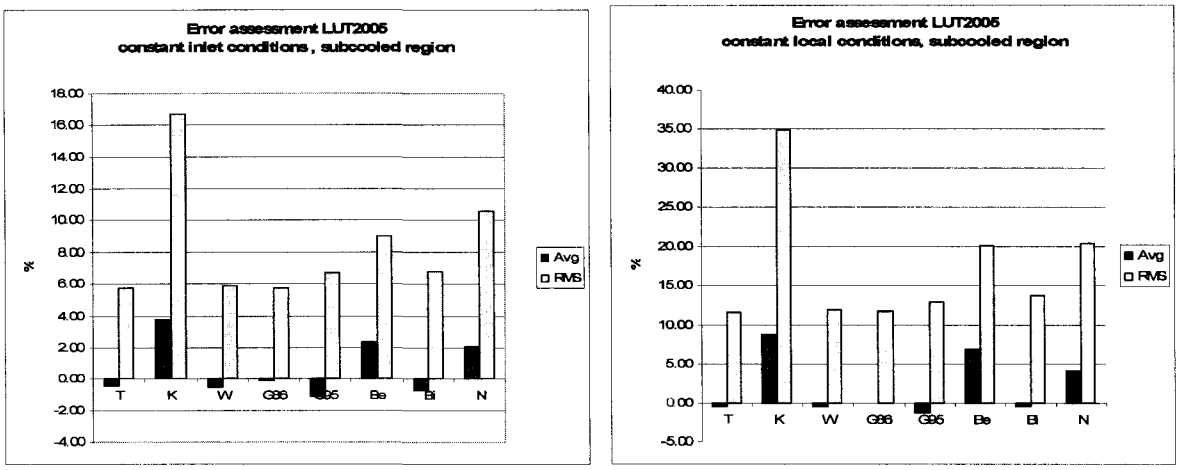

Figure 5-4 Subcooled region error assessment of CHF LUT2005

A special reference case (last row in Table 5-5 and 5-6) where no correction for diameter has been applied is considered for comparison purposes. As it can be seen in Table 5-5, all correlations except Kirillov's and Becker's provide very similar results, both at constant inlet and local conditions. However, in terms of numerical values, the Wong correlation provides the lowest RMS errors.

Applying no correction for diameter would lead to significantly higher errors than most of the analyzed correction factors. For inlet conditions the RMS error is approximately 2.5 % higher. For local conditions the increase is about 8 %. Taking into account that Tables 5-5 and 5-6 are computed based on the whole diameter ranges and that the experimental data equal or close to 8 mm represent almost 50% of the database, while the data well away from 8 mm are quite scarce (see histogram from Figure 5-5), it appears that diameter correction has a significant impact on CHF; therefore the application of the diameter correction factor is strongly recommended, especially for diameters relatively far from 8 mm.

A more detailed comparison between diameter correction correlations can be found in Appendix 3. In these plots the whole ranges of critical quality, pressure and mass flux are evenly divided in subdomains, allowing for a finer comparison between different equations. From Tables A3-1 and A3-6 one can notice that all analyzed correlations, except Kirillov and Becker, give similar results. Kirillov is the only one that assumes that at subcooled dryout conditions a higher diameter results in a higher CHF. It seems that this trend is in

contradiction with the experimental data and with the other correlations, as well. From Table 5-5, Figure 5-4, Figure A3-1 and A3-4, it can noticed that the highest errors of the Kirillov correlation came from subcooled and low quality data, being even greater than the reference case, where no diameter correction has been applied. This suggests the trends in the subcooled region predicted by the Kirillov correlation are not correct; at higher qualities, the Kirillov correlation gives results close to other correlations (See Appendix 3).

To further assess the impact of the diameter corrections selected, the CHF LUT was re-derived, using as skeleton table LUT2005. Different diameter correction equations were used for deriving a new CHF LUT. Hence eight CHF LUTs were derived, each corresponding to one diameter conversion method. Error analysis was performed using the same diameter correction method as for the derivation. The results are presented in the Table 5-7. It can be observed that the re derived tables has slightly lower errors than the skeleton table, for all cases analyzed. The Wong correlation provides the lowest RMS error for constant inlet conditions and the correlation proposed by this thesis the lowest errors for constant local conditions. The variation between most of the methods is small.

Table 5-7 Error analysis for the re derived CHF LUT

		HBM		DSM	
	Data #	Avg	RMS	Avg	RMS
T	26231	-0.43	7.21	0.29	36.43
K	26231	-0.06	8.64	1.40	38.69
W	26231	-0.43	7.00	0.65	37.15
G86	26231	-0.23	7.03	1.12	37.34
G95	26231	0.42	7.06	0.72	37.19
Be	26231	0.10	8.40	3.40	40.76
Bi	26231	-0.35	7.20	0.92	37.42
N	26231	0.29	8.57	3.14	40.32

5.6 Discussion

Table 5-7 shows that Wong (1996), Groeneveld (1986), Groeneveld (1995), Tanase (2006) and Biasi (1967) provide similar results when compared with the AECL-UO CHF experimental database and the CHF LUT2005. Although Wong's correlation gives the lowest

RMS errors, it seems that a constant exponent n = 0.4 to 0.5 satisfactorily predicts the whole range of pressure, mass flux and critical quality of the CHF LUT.

5.6.1 Effect of variation of exponent *n* (constant *n*, for the whole LUT range)

A sensitivity analysis of average and RMS errors with respect to exponent *n* has been performed. Different exponents *n* were tested and the results are shown in Table 5-8 and 5-9, and graphically in the Figure 5-6.

Table 5-8 Variation of CHF LUT errors with n, for constant inlet conditions

n	0.2	0.3	0.4	0.5	0.6
avg	1.15	0.7	0.25	0.19	-0.65
RMS	7.91	7.37	7.14	7.26	7.69

Table 5-9 Variation of CHF LUT errors with n, for constant local conditions

n	0.2	0.3	0.4	0.5	0.6	0.7
avg	7.61	6.04	4.63	3.37	2.24	1.26
RMS	40.46	39.08	38.25	37.91	37.99	38.44

Figure 5-6 shows that the minimum RMS error is obtained at n=0.4, while for constant local conditions the minimum RMS is obtained at values slightly higher than 0.5.

5.6.2 Effect of multiple CHF LUT re-derivations using different exponents *n*, (constant *n*, for the whole LUT range)

Because most of diameter correction factors give very close results, in most applications the simplest one (constant exponent n for the whole range of flow conditions) would be preferred; therefore, analysis of error statistics of the re-derived CHF LUT was considered relevant.

Starting from the same skeleton table and following the steps described in Chapter 3, the CHF LUT was derived and assessed using different exponents, 0.33, 0.4 and 0.5 respectively (see Table 5-10). Note that for a certain LUT, for consistency reasons, the same exponent was used both for derivation and assessment. The first re-derived CHF LUT shows lower errors, for HBM and DSM. Surprisingly, the second re-derived LUT, that uses as skeleton table the first re-derived CHF LUT show slightly higher errors than first re-derived LUT, but lower than LUT2005. This result may emphasize the importance of the skeleton table in further derivation of a CHF LUT.

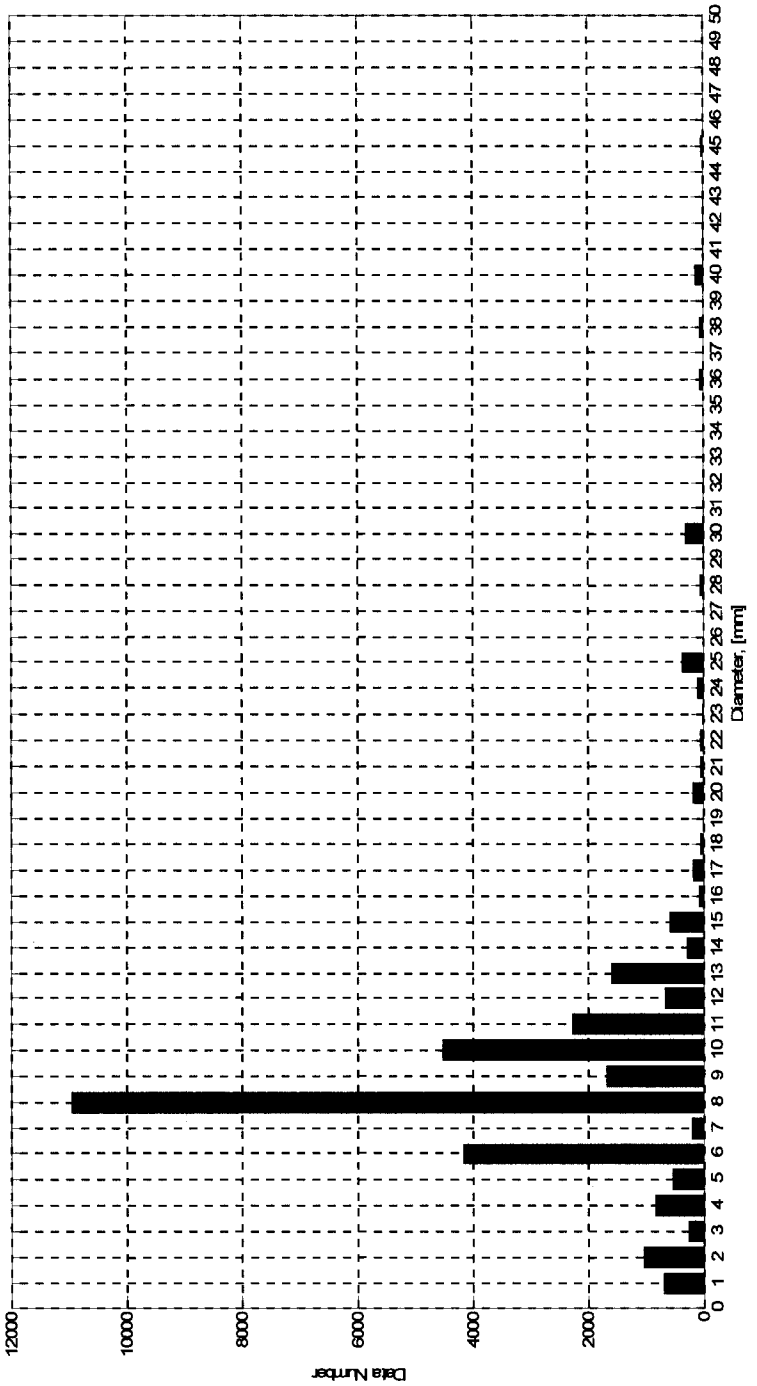

Figure 5-5 Distribution of number of experimental data with respect to inside diameter

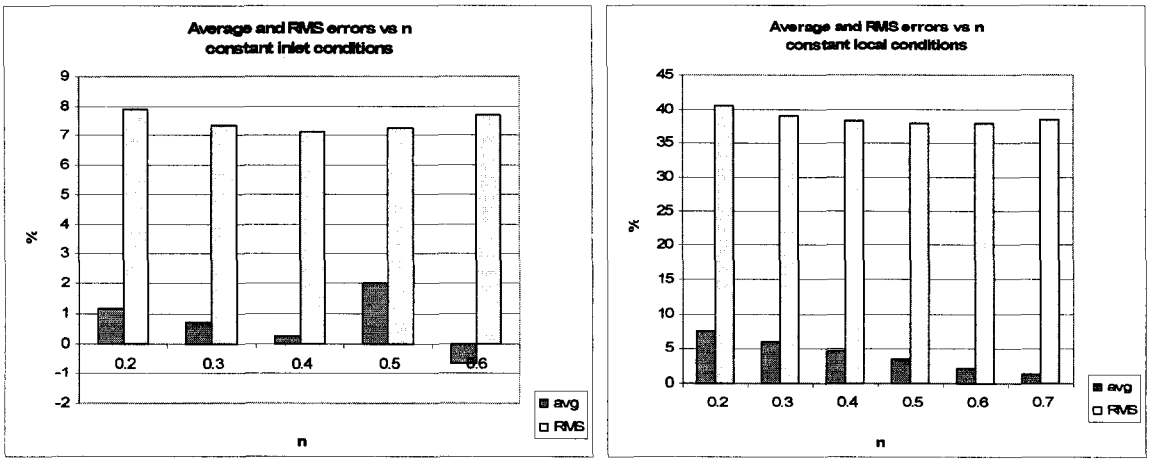

Figure 5-6 Variation of CHF LUT 2005 error in respect to n, for constant inlet and local conditions

Unlike the re-derived CHF LUTs, which were just derived by special computer programs, the CHF LUT2005 was visually checked and adjusted for correct trends. Visual checking is very time consuming, therefore it is applied only for final versions of CHF LUT. Moreover, it has some subjectivity. The results from Table 5-10 prove also that the CHF LUT is not an "iterative" process, where the error improves with every step until reaches a relatively stable value. It seems that a constant exponent 0.4-0.45 gives the best compromise in terms of HBM and DSM errors, therefore it is recommended.

Table 5-10 Effect of multiple re-derivation of CHF LUT using different exponents

Table	CHF LUT 2005				1st re-derived CHF LUT				2nd re-derived CHF LUT			
	HBM		DSM		HBM		DSM		HBM		DSM	
n	Avg	RMS	Avg	RMS	Avg	RMS	Avg	RMS	Avg	RMS	Avg	RMS
0.33	0.55	7.26	5.56	38.75	-0.23	7.03	1.12	37.34	-0.25	7.13	1.04	37.24
0.4	0.25	7.14	4.63	38.25	-0.31	6.98	0.91	37.19	-0.32	7.07	0.88	37.10
0.5	-0.19	7.26	3.37	37.91	-0.42	7.06	0.72	37.20	-0.42	7.13	0.74	37.14

5.6.3 Final recommendation for diameter correction

Tables 5-5 , 5-8, 5-9 and 5-10 have shown that most diameter corrections give significantly lower errors when compared with the reference case (no correction), hence a diameter correction is highly recommended when predicting CHF in tubes with ID far from 8 mm.

Very small differences between Groeneveld(1986), Groeneveld(1995), Wong(1996), Biasi(1967) and the correlation proposed by this thesis lead to the conclusion that any of them can be successfully applied for most applications. Obviously, a simple one (a constant exponent over the whole LUT range) may be preferred. The analysis from 5.6.2 has shown that a constant n=0.4 to 0.45 seems to give the most promising results. However, when a higher degree of accuracy for the diameter correction is required, a more complicated correlation (such Wong's) is recommended.

From the Table 5-6 and Figure 5-4 it can be noticed that, in the subcooled region, a lower exponent (Groeneveld, 1986, n=0.33) gives better results. As shown in Table 5-3, for this region Mudawar (1999) recommends an exponent 0.235. Therefore, in the subcooled range, a constant n =0.25 to 0.3 or Groeneveld(1986) correlation is recommended.

Another particular aspect is represented by the low flow region (<250 kg $m^{-2}s^{-1}$). As pointed out by Mishima et al. (1985, 1987) and shown in Figure 8-5, in the flooding type CHF (low flow low pressure conditions) the CHF increases with an increase in diameter, therefore an exponent n=-0.2 to -0.3 is recommended. More details about the phenomena and CHF mechanisms at low flow conditions can be found in Chapter 8, Subsection 8.1.

6. LENGTH-TO-DIAMETER RATIO EFFECT ON CHF

6.1 Mechanistic Approach to Length-to-Diameter Effect on CHF

Collier and Thome (1996) considered the tube length as an important second order effect on critical heat flux. The length of the heated tube can have a significant influence on CHF for two reasons:

1) it has been proven theoretically and experimentally that both thermal and hydrodynamic boundary layers need a certain developing length (Incropera and De Witt., 1996), Celata et al. (1997)

2) the turbulence introduced by the tube inlet influences the downstream flow structure and the phase distribution, and therefore the CHF.

Most researchers agree with the hypothesis that the CHF is a "local" phenomenon if the L/D ratio exceeds a certain value, determined mainly by flow conditions. Experiments have shown that the L/D effect is stronger in two phase than in single phase flow. In heated channel flow, immediately after the tube entrance the hydrodynamic and thermal boundary layers start to develop. The flow becomes "fully developed" when the velocity (or temperature) profile doesn't change in the axial direction. In single phase flow, the development of the boundary layer is governed mainly by the fluid velocity, properties and system geometry. According to Incropera and De Witt. (1996) the hydrodynamic entry length lasts between 10 and 60 length-to-diameter ratios, a typical value being 30. The same reference recommends a thermal entry length equal to 10 L/D. It appears that subcooled flow is the closest to single phase flow and the observed L/D trends for subcooled flow are in close agreement with single phase hydrodynamic boundary layer development (Celata et al., (1997), recommend L/D~30 for fully developed subcooled flow CHF).

Two phase flows have different flow patterns, the most common being bubbly flow, slug flow and annular flow.

In bubbly or slug flow, the existence or formation of vapour bubbles that may grow, collapse and coalesce creates supplementary turbulence that disturbs and delays the establishment of boundary layers. This phenomenon is stronger when at the inlet of the heated test section there is a two phase mixture, because the turbulence induced by the tube entrance increases both entrainment and droplet deposition rates, modifying the droplet concentration in the vapour core, hence the phase distribution. The interaction between phases and the phenomena associated with full development of each phase are very complicated and not well understood yet. It may be assumed that the relative length required for the droplet concentration and the annular film to fully develop (to be restored to the values in the absence of tube entry effects) is combined to a relative length required for each phase to develop, therefore the developing length for a two phase inlet is higher than a single phase inlet.

A closer look at the mechanisms that govern CHF suggests that for DNB-type CHF the heated length may not have a strong influence. Neither mechanism of DNB – nucleation-induced or the bubble crowding resulting in vapour blanketing, is influenced significantly by the upstream distance and the flow history. As previously mentioned, the hydrodynamic entry length is between 10 and 60 L/D, and for DNB type CHF one can expect the heated length effect to be within this interval. An examination of Figure 6-1 reveals that for DNB-type CHF ($X<0.05$) the L/D has a weak influence on the CHF value. Note that at L/D greater than 30-40, the heated length influence became negligible. This value is also in agreement with the hydrodynamic entry length.

For the CHF LUT 1995 a unique screening criterion for L/D, 80 regardless of the flow conditions, was applied. This criterion seems too tight for subcooled data and may discard some useful experimental data. Consequently, the screening criteria for L/D were refined for the CHF LUT 2005 for $Xc<0$ (subcooled dryout). An $L/D > 25$, while rather permissive, is still close to 30, the limit above which the length effect became negligible for subcooled flow conditions.

The influence of the heated length is far more important in the dryout type CHF; Figure 6-1 suggests the limit for heated length influence is 60-70 L/D.

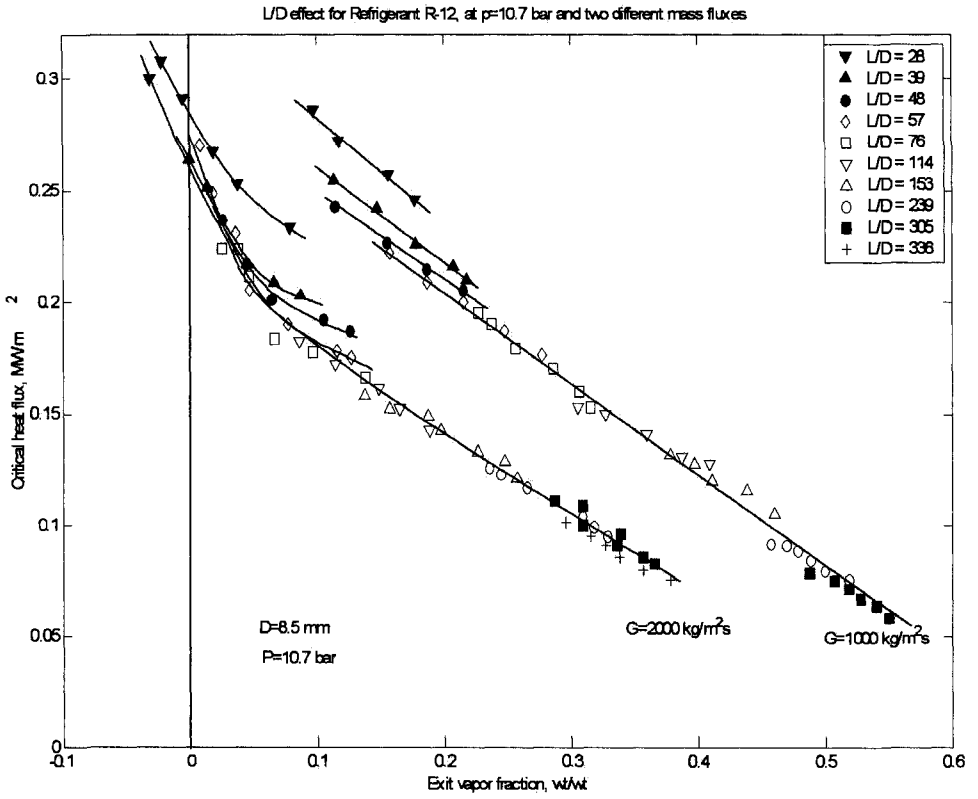

Figure 6-1 L/D effect for refrigerant R-12 at p=10.7 bar and G= 1000 respectively 2000 $kgm^{-2}s^{-1}$

6.2 Experimental Observations

The experiments carried out by Stevens (1964) with refrigerant R-12 suggest that for an L/D ratio greater than 75, the effect of the L/D ratio becomes negligible. Figure 6-1 shows the effect of L/D at a pressure of 10.7 bars and two mass fluxes, 1000 and 2000 kg $m^{-2}s^{-1}$, respectively.

The mass flux does not seem to have a strong influence on the L/D effect: at low mass fluxes, the local condition hypothesis is valid at L/D values starting from 55 (at G=1000 kg $m^{-2}s^{-1}$) while for G=2000 kg $m^{-2}s^{-1}$ this ratio increases to 75.

The L/D ratios inferred from Figure 6-1 are in agreement with the hydrodynamic entry length suggested for single-phase viscous flow.

Lee et al. (2000) suggested that the threshold value above which the length effect for the local conditions is negligible may be a more complex function of pressure, local quality and mass flux rather than a constant value, therefore he carried out an extensive investigation on the heated length effect, using the KAIST experimental database, which contains approximately 15000 CHF data points.

The influence of L/D is presented in Figure 6-2. One can notice that at low local qualities (most likely the CHF mechanism being DNB) the trend steeply decreases for low L/D and becomes more stable at L/D over 100. At higher local qualities (transition to annular flow and annular flow) the CHF versus L/D trend decreases continuously, which implies that at high local qualities, there is no threshold value beyond which L/D can be neglected.

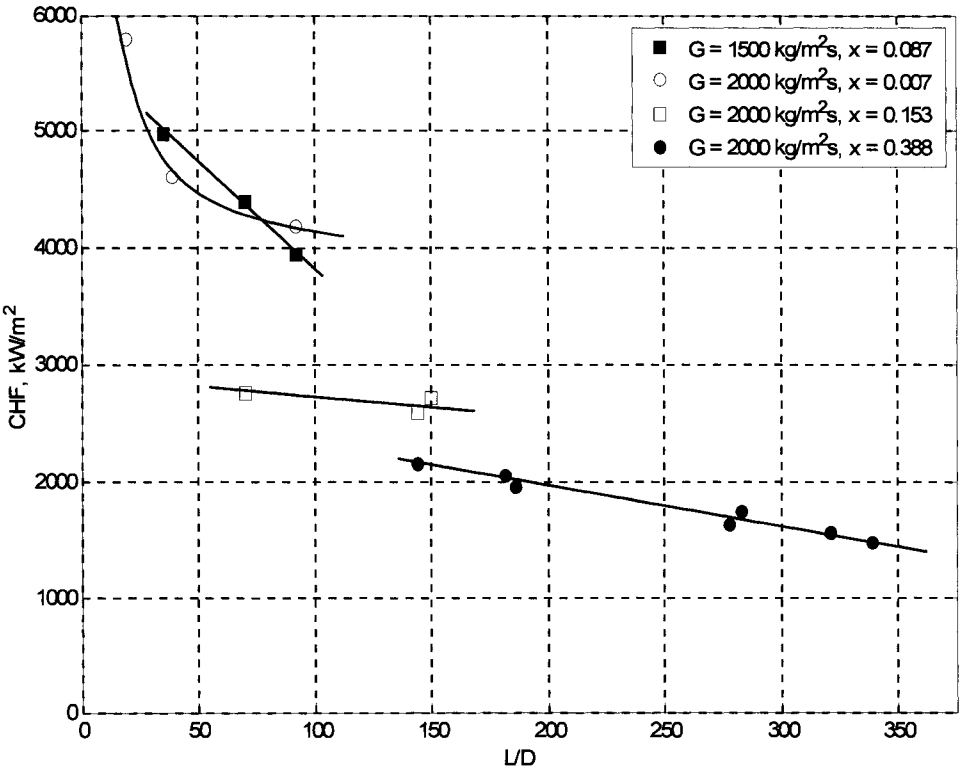

Figure 6-2 Exit quality effect on L/D

Figure 6-3 shows the trend of CHF versus L/D for pressure between 68.7 – 69.5 bar, mass flux 2000 – 2200 kg $m^{-2}s^{-1}$, and x =0.39 – 0.47 for different diameters. The regression curves suggest that even at L/D greater than 800, the length-to-diameter effect seems not to disappear completely. Because this refers to the specific flow conditions mentioned above, there is no evidence to extend this conclusion at other flow conditions, but it is a very interesting subject for further studies.

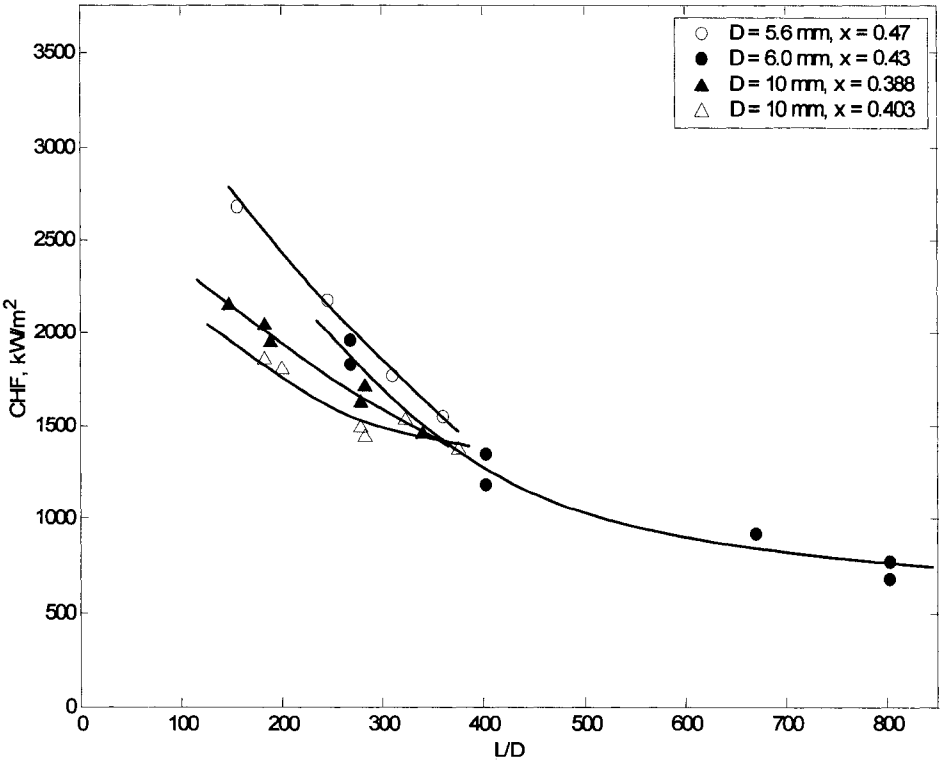

Figure 6- 3 Diameter effect on L/D for P=68.7-69.5 bar and G=2000-2200 kg $m^{-2}s^{-1}$

6.3 Prediction Methods for Length-to-Diameter Effect

The L/D ratio versus CHF trend suggests that at medium and presumably at high dryout qualities, there is no threshold for the L/D effect. Consequently, according to Lee et al. (2000), it seems that for medium and high quality data, the local condition hypothesis is uncertain and a correction factor for L/D effect is recommended. Lee et al. used artificial neural networks (ANN) and conventional regression techniques to derive a correction factor

for the L/D effect. They assumed that the boiling number is a function of several flow parameters and fluid properties as follows:

$$\frac{q_c}{Gh_{fg}} = f\left(\frac{\rho_g}{\rho_f}, \frac{\sigma\rho_f}{G^2 L}, \frac{L}{D}, x\right) \tag{6.1}$$

Using the KAIST experimental database, they were able to tune the coefficients of their model and the final expression for correction factor as:

$$C.F. = -0.2945\left[(1+x)^{1.237}\left(\frac{\sigma\rho_f}{G^2 D}\right)^{0.01155} + 0.312\left(\frac{\rho_f}{\rho_g}\right)^{-0.0617}\right]\ln\left(\frac{L/D}{L/D|_{th}}\right)+1 \tag{6.2}$$

If the L/D ratio for a given system is greater than a calculated threshold value, then the correction factor is set to 1. Otherwise, the correction factor is calculated with equation (6.2). A plot of correction factor at P=2500 kPa and G=3000 kg $m^{-2}s^{-1}$ is shown in Figure 6-4.

The threshold value varies between 15 and 300 and depends mainly on exit quality. The correlation for threshold L/D has the following form:

$$L/D|_{th} = 252.86\left(\frac{\sigma\rho_f}{G^2 D}\right)^{0.135}\left(x + 0.25\left(\frac{\rho_f}{\rho_g}\right)^{-0.189}\right)+10 \tag{6.3}$$

The lower threshold values are typical for high flow and low exit qualities (x<0.1) and higher values for high qualities and low flow conditions.

6.4 Assessment of Length-to-Diameter Criteria for the CHF LUT

The L/D threshold value of 300-400 suggested by Lee at al. (2000), beyond which the length effect is no longer significant, is much higher then values suggested by others (Stevens, 1964, Incropera and De Witt, 2004, Groeneveld et al., 2005).

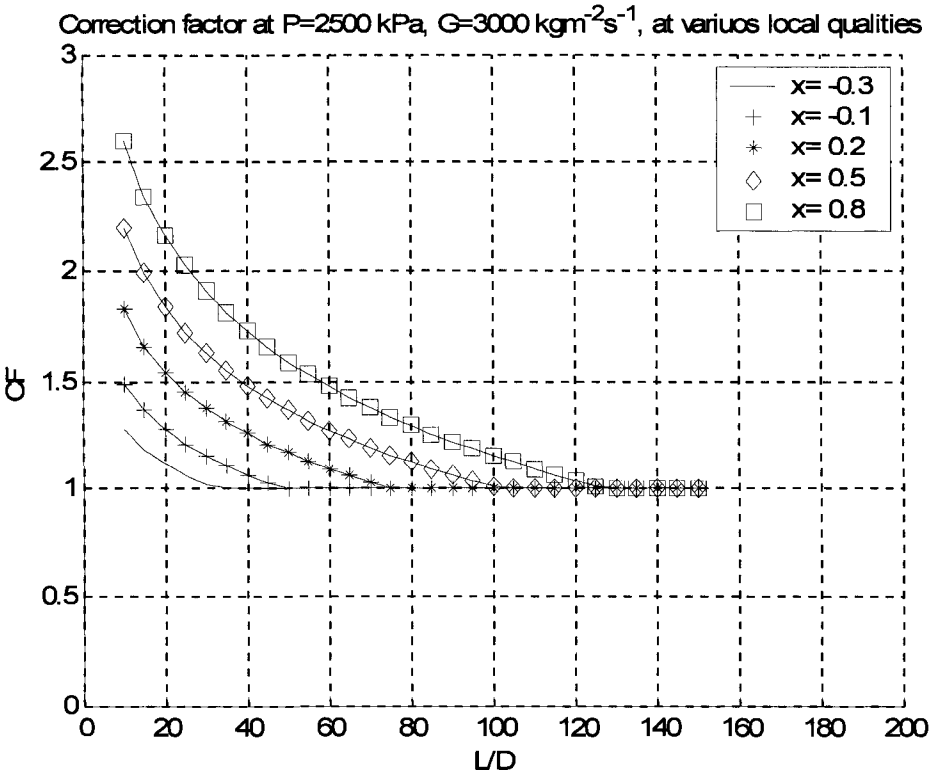

Figure 6-4 Correction factor at P=2500 kPa, G=3000 kg $m^{-2}s^{-1}$, at various local qualities

Therefore an assessment of the Lee correlation against the AECL-UO data base and the CHF LUT2005 has been performed. Figure 6-6 presents the distribution of the AECL-UO CHF experimental data base with respect to L/D ratio. Table 6-1 shows a comparison of average and RMS errors of the CHF LUT 2005, assessed with and without the L/D correction factor proposed by Lee. The result shows that both average and RMS errors increase significantly. These results are due to the decrease of experimental CHF values by the correction factor predicted by Eq. 6-2.

Table 6-1 Effect of L/D correction factor on CHF LUT 2005 error analysis

HBM			
	Data #	**Avg**	**RMS**
With L/D	26231	-3.64	13.50
No L/D	26231	-0.19	7.26
DSM			
	Data #	**Avg**	**RMS**
With L/D	26231	10.28	46.02
No L/D	26231	3.37	37.91

Because the CHF LUT 2005 has been derived using the screening criteria mentioned in Table 4-2 and no other correction for L/D has been applied, a more relevant analysis would consider a re-derivation of the CHF LUT, taking into account the L/D correction factor. The error analysis revealed that the re-derived CHF LUT has slightly lower RMS errors, as shown in Table 6-2. The L/D correction factor (Eq. 6-2) was used for the derivation process and for the error assessment, as well.

Table 6-2 Effect of L/D correction factor on LUT accuracy for re-derived CHF LUT

HBM			
L/D Screening criteria	Data #	Avg	RMS
2005 screening criteria, no L/D correction, original LUT	26231	-0.19	7.26
2005 screening criteria	26231	0.47	7.25
L/D>5	28761	0.42	10.18
DSM			
Screening criteria	Data #	Avg	RMS
2005 screening criteria, no L/D correction, original LUT	26231	3.37	37.91
2005 screening criteria	26231	4.52	36.84
L/D>5	28761	4.25	37.84

From the lower RMS error of the re-derived CHF LUT 2005 one could conclude that the L/D correction factor proposed by Lee et al. (2000) may be successfully used for different applications, such as CHF LUT derivation and assessment or prediction of CHF in relatively short heated channels.(see Table 6-3). In Table 6-3, all the errors for the re-derived CHF LUT are much smaller, except the RMS error for DSM. For this comparison, the difference in average errors is more significant because, at very low L/D ratios, the correction factor very high and the corrected experimental value is lower, which increases the relative error.

Table 6-3 Comparison between CHF LUT2005 and the re-derived CHF LUT for data with L/D ratios between 5 and 50

		HBM		**DSM**	
	#	Avg	RMS	Avg	RMS
CHF LUT2005	3384	-17.1	28.1	-25.02	40.1
Re-derived LUT	3384	0.53	22.09	3.05	42.7

Note that the errors of the CHF LUT 2005 (calculated without L/D correction factor) and the re-derived CHF LUT are very close, which suggests that L/D screening criteria for CHF LUT 2005 are properly selected.

Further analysis using the slice method revealed that Lee's L/D correction factor has a significant impact on experimental data at high qualities, which are typically associated with low pressure and low flow conditions. Figure 6-5 shows a comparison of two slices containing data not corrected for L/D (a) and corrected for L/D using Eq. 6-2 (b). In general, the corrected data show significantly lower CHF values and scatter, which explains the results from Tables 6-1 and 6-2.

Table 6-4 presents the errors of the CHF LUT2005 and the re-derived LUT in the saturation quality range. In the 0.5 to 1.0 quality range HBM errors decrease significantly by 1.3% and DSM by almost 1%. Within the 0 to 0.5 quality range the HBM error for the re-derived LUT is slightly higher, but the DSM error is lower by more than 1.3%.

Table 6-4 Comparison between CHF LUT 2005 and re-derived LUT with L/D correction, in the saturated quality region

Quality range	**0 to 0.5**					**0.5 to 1**				
Table	**Data #**	**HBM**		**DSM**		**Data #**	**HBM**		**DSM**	
		Avg	RMS	Avg	RMS		Avg	RMS	Avg	RMS
CHF LUT 2005, no L/D correction	16397	0.56	6.85	6.36	36.77	7897	-0.51	8.18	-1.64	43.94
Re-derived LUT, with L/D correction	16397	0.69	7.34	5.89	35.46	7897	-0.05	6.89	2.48	42.99

The relatively small difference in errors is explained by the reduction in the experimental CHF value with the L/D correction factor. The error is calculated as $(q_{exp}-q_{pred})/q_{exp}$, and by applying Lee's correction factor the absolute error $q_{exp}-q_{pred}$ for the re-derived LUT decreases, but the denominator q_{exp} also decreases, hence the general effect on error is not as strong as visualization suggests. Also, the vast majority of experimental data (more than 90%) are within the saturation region. There is no doubt that, in general, the application of a correction

factor for length-to-diameter effect improves both errors and a trend of the CHF LUT and Lee's correction factor is a promising start. It is expected that the inclusion of a properly-derived L/D correction factor in the future will lead to a reduced experimental data scatter and lower CHF LUT errors.

A sensitivity analysis of CHF LUT 2005 error versus L/D has been performed, in order to determine whether the L/D screening criteria for the CHF LUT 2005 are suitably selected or can be further improved. The results presented in Table 6-1 and 6-2 respectively and the visual analysis using the slice method suggest that in general L/D criteria for the CHF LUT 2005 derivation are satisfactory. However, some differences between uncorrected and corrected data are significant at high qualities (0.5 to 1) and low flows (0 to 750 kg $m^{-2}s^{-1}$), as exemplified in Table 6-4 and Figure 6-2.

As mentioned in Chapter 4 , the following criteria have been used for L/D:

Table 6-5 CHF LUT 2005 screening criteria for L/D

L/D, X_{in}<0	L/D>50 for X_{cr}>0, L/D>25 for X_{cr}<0	L/D>50 for X_{cr}>0, L/D>25 for X_{cr}<0
L/D, X_{in}>0	L/D>100	L/D>100

The L/D threshold for all mentioned three criteria has been varied and the results are presented in Table 6-6 and graphically in Figure 6-7. Figure 6-7 a) and b) show that errors are sensitive to variation of L/D for subcooled experimental data. A variation of L/D from 20-25 to 30-40 decreased the RMS error (HBM) from 17.4 to 7.5%,. For the same range of L/D, RMS error (DSM) decreased from 22.8% to10.8%. These trends and the relatively small variation of RMS and average errors at L/D greater than 30 suggest that this should be the L/D ratio screening limit for subcooled data; therefore in the future the current value of 25 should be replaced with 30 .

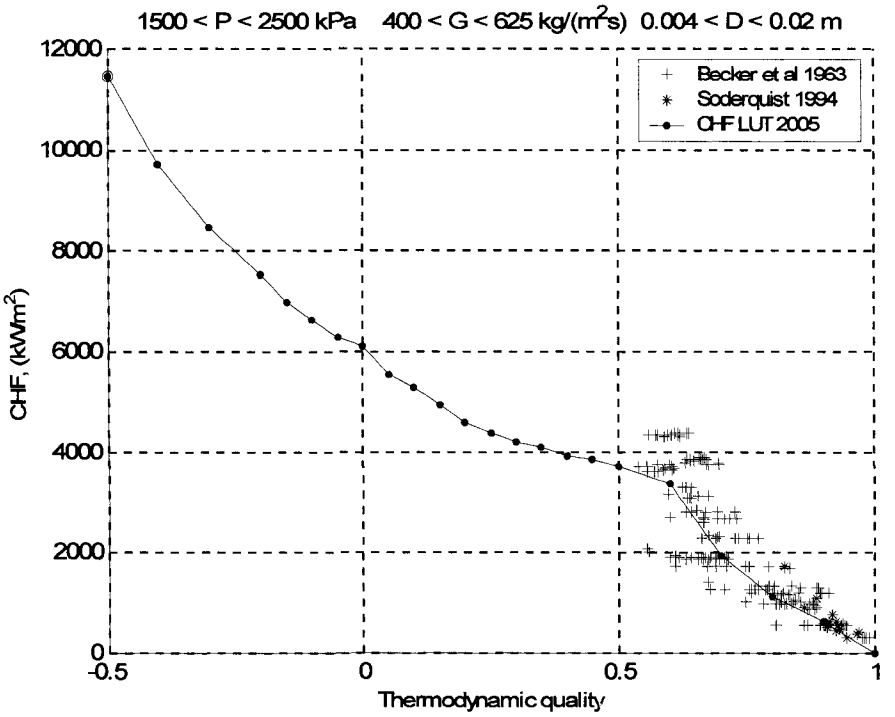

a)

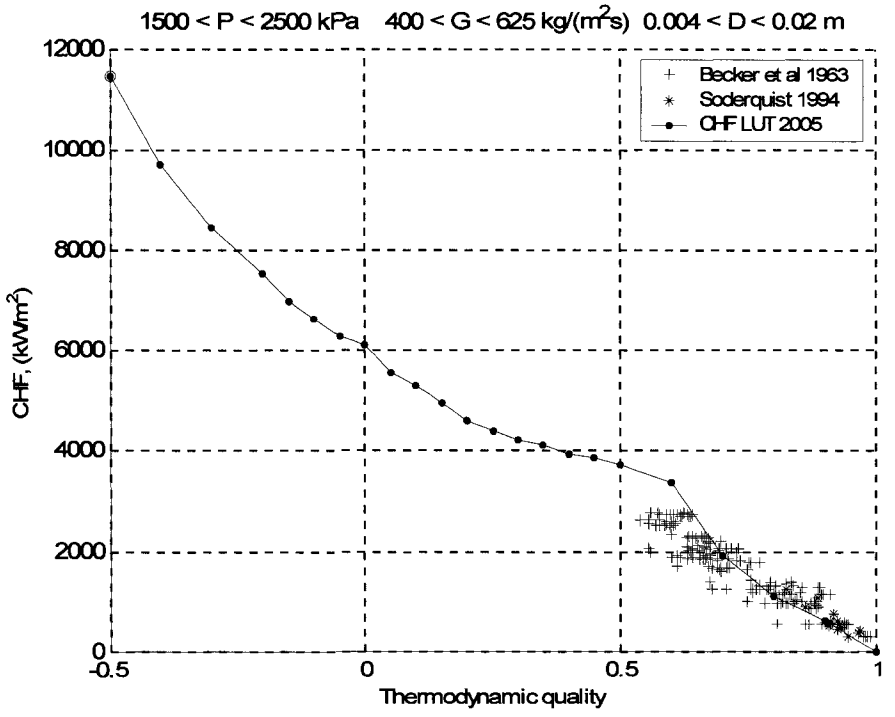

b)

Figure 6-5 Slices at P_{nom} = 2000 kPa and G_{nom} = 500 $kgm^{-2}s^{-1}$ comparing the CHF LUT 2005 and experimental data without L/D correction (a) and with L/D correction (b)

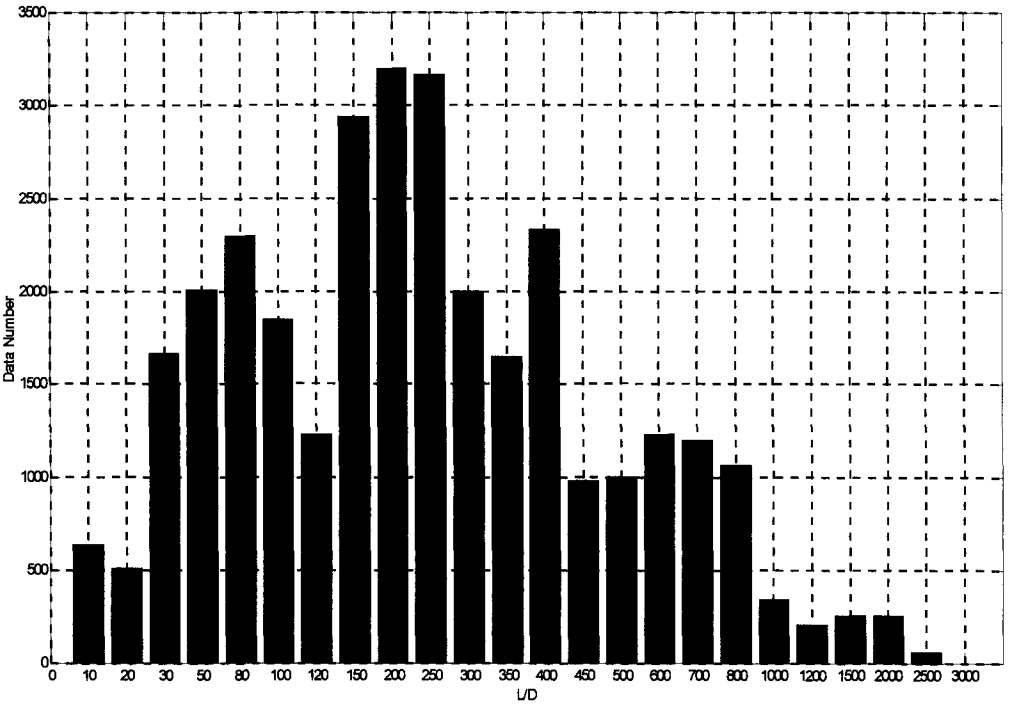

Figure 6-6 Distribution of number of AECL-UO experimental data with respect to L/D ratio

Table 6-6 Sensitivity of CHF LUT 2005 error with respect to L/D screening criteria

HBM							
Xcr<0							
L/D	**20-25**	**25-30**	**30-40**	**40-50**	**50-70**	**70-100**	**>100**
Avg	-3.24	-5.8	-2.9	-1.75	-1.4	-0.69	0.42
RMS	17.4	16.1	7.56	5.09	8.3	5.14	4.73
No	13	81	516	209	131	337	751
Xcr>0							
L/D	**20-30**	**30-50**	**50-70**	**70-100**	**100-150**	**150-200**	**>200**
Avg	-32.99	-14.59	-7.72	-1.78	-2.28	-0.22	1.15
RMS	36.65	22.66	14.34	10.92	7.02	5.31	5.95
No	572	943	1181	1914	3297	2888	14643
Xin>0							
L/D	**50-70**	**70-100**	**100-150**	**150-200**	**200-300**	**>300**	
Avg	-8.18	-1.99	-0.37	9.55	11.09	2.21	
RMS	13.59	16.28	12.18	14.9	12.36	15.28	
No	158	139	138	66	36	88	

DSM							
Xcr<0							
L/D	**20-25**	**25-30**	**30-40**	**40-50**	**50-70**	**70-100**	**>100**
Avg	-2.86	-6.1	-4.15	-2.47	-0.82	-0.94	0.71
RMS	22.85	20.39	10.83	8.08	13.87	12.28	14.16
No	13	81	516	209	131	337	751
Xcr>0							
L/D	**20-30**	**30-50**	**50-70**	**70-100**	**100-150**	**150-200**	**>200**
Avg	-44.42	-22.8	-16.13	-6.08	-8.12	-1.38	10.14
RMS	48.55	35.41	37.48	22.34	24.59	23.01	45.84
No	572	943	1181	1914	3297	2888	14643
Xin>0							
L/D	**50-70**	**70-100**	**100-150**	**150-200**	**200-300**	**>300**	
Avg	-11.75	-0.84	-0.02	25.06	41.28	16.64	
RMS	19.03	27.32	31.55	40.28	48.22	43.00	
No	158	139	138	66	36	88	

The L/D screening for saturated dryout data (Figures 6-7 c,d) has a larger impact on error, especially for constant inlet conditions (HBM method). In general, average and RMS errors decrease with increasing L/D for both constant inlet and local conditions. At low L/D ratios (20-30) the RMS errors are quite large, 36% for HBM and 48% for DSM. A significant decrease occurs at L/D larger than 70 for both methods, hence this value can be recommended as the L/D screening limit for saturated region. It can be noticed that the errors still continue to decrease at L/D higher than 70, but less significantly, on the order of few percent. The choice of this limit is usually a compromise because the vast majority of experimental data are in the saturation quality region, therefore a higher limit for screening criterion would slightly decrease the errors, but it would discard an important amount – thousands - of experimental data, too. The screening limit for CHF LUT 2005 - 50 may be too liberal without the use of a L/D correction factor. It is expected that the relevance of the L/D screening criterion will become less important for the future versions of the CHF LUT, if Lee's or other similar correlation were used to correct the experimental data for the L/D effect.

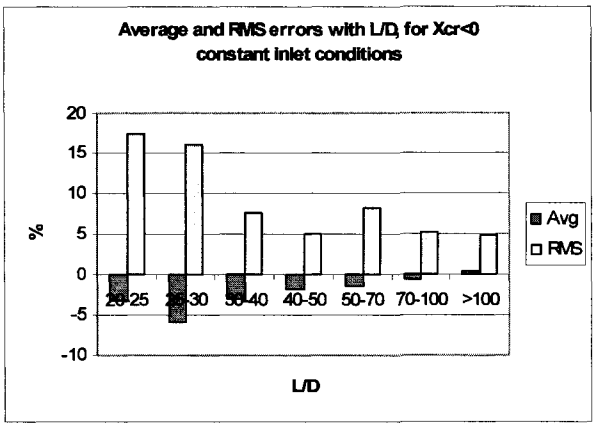

a)

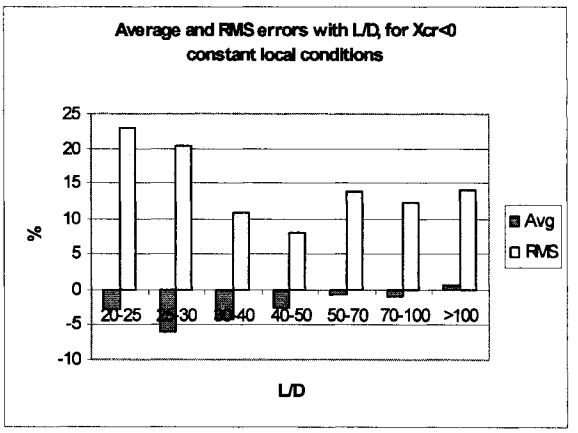

b)

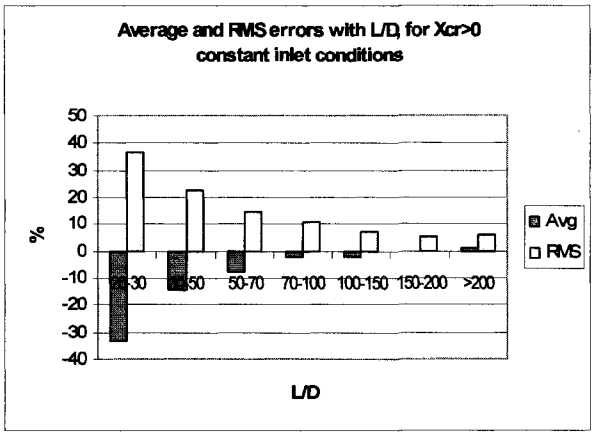

c)

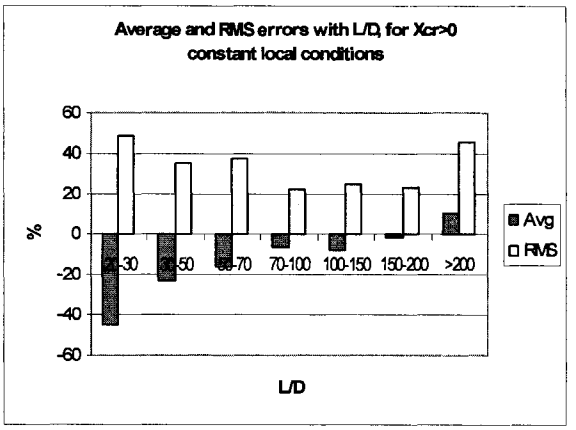

d)

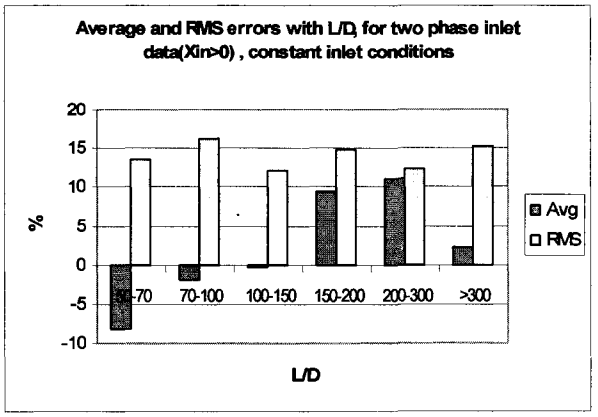

e)

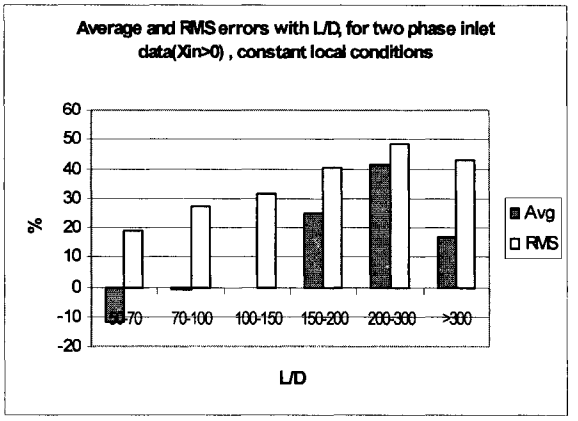

f)

Figure 6-7 Sensitivity of CHF LUT 2005 error with respect to L/D screening criteria

Data having an inlet thermodynamic quality greater than zero (two phase inlet), generally have a stronger entrance effect than single phase subcooled data (e.g. see discussion in Section 6.1); therefore a screening criterion for L/D was chosen as 100. Figure 6-7 e) shows very little variation of errors with L/D varying from 50 to 300. Unlike the previous cases, the RMS error for constant local conditions has an increasing trend with L/D increase. Considering these trends and the relatively high uncertainty of two phase inlet data, no screening criterion can be recommended. Because the two phase inlet experimental data are quite scarce and their errors are not extreme, their impact on the general LUT error assessment is minimal. It can be concluded that this screening criterion is not critical and the value chosen for the LUT 2005 two phase inlet screening criterion is acceptable.

6.5 Summary

Investigation of the L/D effect on CHF has shown that for the same local conditions, the CHF measured in short channels is higher than the CHF in long channels. This difference can be explained by the relative length (L/D) required by the flow to fully develop.

Examination of AECL-OU CHF data suggests that L/D strongly depends on the flow conditions and the CHF mechanism: at subcooled flow, where DNB is the most likely CHF mechanism, the L/D effect lasts for ~30 L/D, while at saturated flow conditions the relative distance required is approximately 70 L/D. Two phase inlet data show no threshold for L/D effect. The L/D threshold values mentioned above suggests that the screening criteria for L/D for CHF LUT could be modified, from 25 to 30 for subcooled CHF and from 50 to 70 for saturated data.

The employment of an L/D correction in conjunction with the CHF LUT approach appears to results in lower data scatter and lower errors, especially at high qualities. Using the Lee L/D correlation (2000) and re-deriving the CHF LUT significantly improved HBM RMS errors (by 1.5%) for saturation conditions. For the same range, the DSM RMS error also shows also an improvement of more than 1.3%; therefore, Lee's correlation or a similar L/D correction factor should be considered for adjusting the short-tube CHF in future LUT updates.

7. LIMITING QUALITY REGION IN CHF LUT

7.1 Introduction

One of the most interesting phenomena observed in CHF studies is called the "limiting quality phenomenon" (LQP). Other terms used for this phenomenon in the literature are "transition zone form dispersed–annular to dispersed flow regime", "limiting quality region" (LQR), or "limiting critical quality". It is characterized by a sharp decrease of the CHF value with a small increase in x (e.g. a steep change in slope in CHF versus x_c). The LQR usually occurs in the intermediate quality region, for water typically from x=0.3 until x=0.7. LQR was observed by Galin and Kirilov (1987), for pressures from 3 to 16 MPa and mass fluxes from 500 to 2500 kg $m^{-2}s^{-1}$ (Tolubinskiy et al, 1980).

7.2 Phenomena and Mechanisms

Most researchers in CHF (Doroshchuk et al.,1970, Bennet et al., 1967, Smolin, 1978, Kitto 1980, Pioro et al., 1999) divided q_c versus quality into three regions (see Figure 7-1), according to CHF mechanism:

Region I

Region I is the first kind (DNB) of critical heat flux. It is a result of transition from nucleate boiling of a liquid to film boiling. At the end of Region I the CHF mechanism changes from DNB-type to entrainment-controlled dryout

Region II

It is the transition from entrainment-controlled dryout to deposition-controlled dryout.

Region III

Region III represents dryout by a deposition-controlled mechanism. It results in a disruption of very thin liquid film that flows near the heated wall. It is characterized by relatively small CHF values.

Most researchers agree that the LQR represents Region II, i.e transition from entrainment-controlled dryout to deposition-controlled dryout. Some differences between Doroshchuk et al., (1970) (Figure 7-1 (a)) – sudden decrease, infinite slope and Bennet et al. (1967) and Smolin et al. (1970) (Figure 7-1b)) – steep but finite slope, are noticeable. According to Doroshchuk et al. (1970), Region I denotes the classical DNB mechanism with a transition from nucleate to film boiling. From the vertical line downward (Region II and III) is characterized by dryout of the film liquid annulus. The end of region I represents the transition from bubbly/slug flow to annular flow, where the liquid film is relatively thick, has surface waves, and nucleate boiling is not completely suppressed. At the start of Region II, hydraulic and thermal forces remove most of the annular water film, leaving only a very thin micro-film behind. The thin microlayer evaporates very fast unless significant droplet deposition from the misty core takes place. At high heat fluxes (the vertical region II) the evaporation of liquid film is so intense that it prevents any deposition of droplets from the vapour core. This way, the liquid film is depleted and dryout occurs. At the end of region II, the heat flux is low enough to reduce the evaporation rate and to allow droplet deposition into the liquid film.

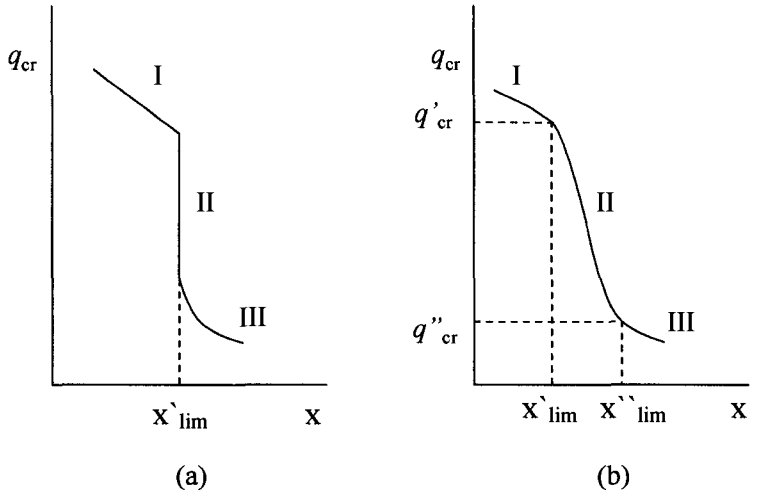

Figure 7-1 Limiting quality region

Other researchers (Smolin et al., 1978, Borishanski et al.,1980, Morozov, 1978, Tippets, 1962) generally agreed with Doroshchuk the LQR mechanism, but argued that region II is not vertical, but a steep slope. Furthermore, Borishanski et al.(1980) developed a heat

transfer model based on the balance of droplets under the influence of inertial forces and the vapour leaving the liquid film surface.

Tippets (1962) explained that the imbalance between dynamic forces at the liquid/vapour interface and surface tension removes the majority of the liquid from the annulus. There were some opinions (Tong and Hewitt, 1972) that LQP was not real, being rather a problem of experimental accuracy. However, most of the experimental data coming from different sources support the existence of this phenomenon.

Currently the LQR is generally accepted, as well as the model proposed more than 30 years ago by Doroshchuk et al (1970)., with improvements. An extensive review of the state of the art in LQP was performed by Peng (2004). He analyzed the AECL-IPPE (Atomic Energy of Canada Limited, Chalk River, Canada, and Institute of Physics and Power Engineering, Obninsk, Russia) CHF database to extract the limiting quality experimental data, including both the lower bound and upper bound and their corresponding critical heat fluxes.

Analyzing the experimental database of limiting quality bounds shows that for some conditions LQP is a very sudden phenomenon, i.e., in a narrow quality range, CHF drops quickly. The LQR selection criterion was that the relative change in CHF is more than twice the relative change in dryout quality:

$$\left|\frac{\overline{X}}{\overline{q}_{cr}}\frac{dq_{cr}}{dX}\right|_{\lim} > 2 \qquad (7.1)$$

Some "obvious" or "strong" LQR were noticed. The criterion to define the strong limiting quality phenomenon was correlated as:

$$\left|\frac{\overline{X}}{\overline{q}_{cr}}\frac{dq_{cr}}{dX}\right|_{\lim} > 10 \qquad (7.2)$$

According to Peng (2004), a strong LQP exists in two separate regimes: one is the low pressure regime where the pressure is smaller than 7000 kPa; the other is the high pressure regime where the pressure is higher than 9800 kPa. The mass flux is roughly from 1000 to

2500 kg m^{-2} s^{-1} in the low pressure regime, but from 500 to 2500 kg m^{-2} s^{-1} in the high pressure regime. Belyakov (1978) reported that at mass fluxes greater than 2000 kg m^{-2} s^{-1}, the LQR was not observed.

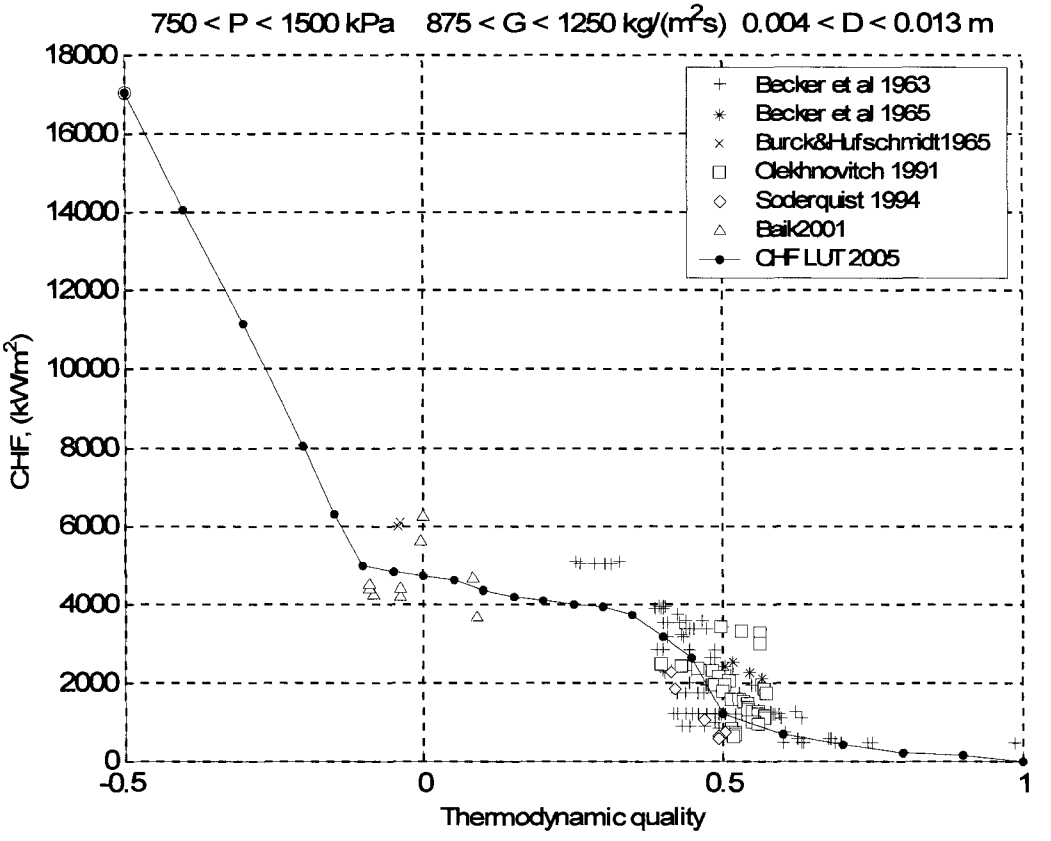

Figure 7-2 Example of LQR at nominal G=1000 kg m^{-2} s^{-1}

Peng (2004) observed two separate regions with strong limiting quality. The shaded area in Figure 7-3 shows the conditions of the LQP on a Pressure –Mass flux map for an 8 mm tube. The strong limiting quality phenomenon regimes are marked as shaded areas. The reason that the strong LQP exists in two separate regimes at low and high pressures respectively is unclear. It maybe due to the complicated interaction between heat flux, droplet sizes, and turbulent transport between liquid film and core vapour flow or an inadequate number of data covering a wide range of qualities at intermediate pressures.

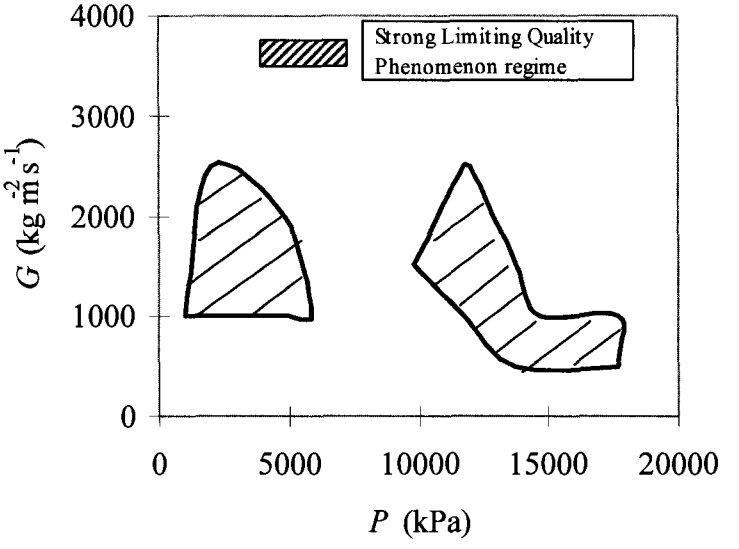

Figure 7-3 *P-G* limiting quality phenomenon regime diagram for 8 mm tube

7.3 Prediction Methods for LQR

Due to the complexity and the importance of the LQR in practical applications, many researchers have developed different methods for predicting the LQR (see Table 7-1). Their methods fall in three main categories:

a) Semi-empirical, based on the ratio of modified Weber number (We) and Reynolds number (Re) and used to predict the transition from large annular film to the micro-film.

b) Empirical, based on polynomial or other type fitting curves. These correlations proved to be more accurate

c) Tables, covering the entire region of LQ

Doroshchuk et al. (1970) Correlation

Doroshchuk et al. (1970) relate the limiting quality phenomenon to the hydraulic resistance crisis: when the steam quality exceeds a certain value, the thick liquid film on the tube wall is converted to a thin liquid film so that the disturbance wave disappears and the hydraulic resistance drops sharply. When the thin film is formed, the ratio between Re and We remains constant, which leads to a correlation with a constant K equal to 3.1×10^{-3} for a 8 mm diameter tube.

Smolin (1970) Correlation

Smolin (1970) found that the limiting quality phenomenon always occurs in the region where the CHF decreases with an increase in mass velocity. The author divides the whole boiling tube into three zones corresponding to three flow patterns, i.e. bubbly, annular, and dispersed flow regimes of steam-water mixtures. The boundary between annular flow and dispersed flow defines the critical hydrodynamic quality, where the limiting quality occurs. The balance between steam inertia and surface tension determines this transition. The similarity principle is then used to derive a correlation for the limiting quality. The coefficient c in the correlation is determined by a method given in a reference which is unavailable to the current authors.

Borishansky et al. (1974) Correlation

Borishansky et al. (1974) developed a semi-empirical correlation for the limiting quality region CHF. Unlike the other local-conditions-type correlations, Borishansky's correlation is inlet-conditions based. The CHF is assumed in the annular regime when the film flow rate is equal to zero and the evaporating rate is larger than the deposition rate. Somewhat similar to the Doroshchuk et al. (1970) correlation, the limiting quality phenomenon is related to the hydraulic resistance crisis and the critical heat flux is assumed to be the sum of the heat flux to bring the inlet quality X_{in} to the quality at the hydraulic resistance crisis $X_{\Delta p}$, the heat flux to evaporate the liquid film, and the heat flux to evaporate the deposition droplets. In the correlation, W_f^0 is the critical film flow rate for the onset of interface wave, W is the total flow rate of the mixture, X_o is the quality from which the deposition starts, X'_{lim} is the quality at which the CHF occurs, L_h is the heating length of the tube, and ξ_D is the local deposition intensity: the deposition rate per unit tube section area.

Doroshchuk et al. (1975) Correlation

Since the Doroshchuk et al. (1970) correlation does not give the correct trend for the pressure effect when pressure is smaller than 5000 kPa, Doroshchuk et al. (1975) subsequently modified the above correlation to the current form. Again, for an 8 mm tube, the constant is found to be 0.015. The same correlation is given in Doroshchuk et al. (1980).

Katto (1982) Correlation

Katto (1982) developed a semi-empirical limiting-quality correlation. For a tube with given length, the constant dryout exit quality at different CHF suggests the dryout exit quality is independent of inlet subcooling.

Morozov (1987) Correlation

While all the previous correlations deal with the limiting quality phenomenon as a hydrodynamic phenomenon, Morozov (1987) first takes the thermal effect into consideration. The limiting quality phenomenon exists over an extended quality range, starting from some rivulets to complete dryout. The thermal effect is represented by a dimensionless group K_q, while the hydrodynamic effect is represented by a dimensionless group K_u. The Morozov (1987) correlation then relates the lower bound of the limiting quality X'_{lim} to the dimensionless group $\psi_{DO} = K_q / K_u$. The $\psi_{DO} < 4$ refers to a region where the interface mass transport (liquid entrainment) plays an important role, but the $\psi_{DO} > 4$ refers to a region where the liquid film dryout occurs due to evaporation only, without entrainment.

Galin-Kirillov (1987) Correlation

An empirical limiting quality correlation, valid from 3 to 16 MPa, is proposed by Galin and Kirillov (1987).

Kitto (1980) Correlation

Kitto's experiments were carried out in a vertical tube with 38 mm ID at a high pressures (152 to 200 bar). Mass flux range was from 543 to 2172 kg m^{-2} s^{-1}.

Yildiz (2004)

For the development of his correlation, Yildiz used 201 experimental data. The independent parameters are pressure and mass flux.

Table 7-1 contains the mathematical expressions of the above mentioned correlations.

An independent assessment of some of the LQR correlations (Peng et al., 2004) revealed that the Doroshchuk et al. (1975) correlation does not provide reasonable results, while the

correlations proposed by Smolin (1970) and Borishansky et al. (1974) contain some coefficients or parameters that are not available, therefore those correlations were not included in their analysis.

Table 7-1 Limiting Quality Correlations

Correlation	Equation	Range applicable	Comments
Doroshchuk et al. (1970)	$(X_{\lim})^2 G \frac{\nu_l}{\sigma} \frac{\rho_l - \rho_v}{\rho_l} = K$ $K = 3.1\times10^{-3}$ for 8 mm tube	G > 600 kg/(m^2 s) for high pressure; G > 1000 kg/(m^2 s) for low pressure (50 bars)	No LQP can be observed at low flow regime
Smolin (1970)	$\frac{X_{\lim}(\rho_l - \rho_v) + \rho_v}{(1 - X_{\lim})^{0.25}} = 1.15 c \rho_l \left(\frac{\rho_l \sigma^2}{D \nu_l G^3} \right)^{1/4}$	27.5 ≤ P ≤176 bars, 1000 ≤ G ≤ 5000 kg/(m^2 s)	
Borishansky (1974)	$q_{cr} = 0.25 G H_{fg} (D/L_h)$ $\left[(X_{\Delta P} - X_{in}) + \frac{W_f^0}{W} + \frac{H_{fg}}{q_{cr}} \int_{X_0}^{X'_{lim}} \xi_D dX \right]$		Conditions for LQP: (1) film flow rate is equal to zero; (2) the deposition rate is smaller than evaporation rate
Doroshchuk et al. (1975)	$(X_{\lim})^2 \left(\frac{D}{0.008} \right)^{0.3} G \frac{\nu_l}{\sigma} \left(\frac{\rho_l}{\rho_v} \right)^{0.5} = K$ $K = 0.015$	10 ≤ P ≤ 166 bars; 750 ≤ G ≤ 3000 kg/(m^2 s)	Obtained by modifying Doroshchuk et al. (1970) corr.
Doroshchuk et al. (1980)	$x_l = [0.39 + 3.53(\frac{p}{p_{cr}}) - 10.3(\frac{p}{p_{cr}})^2 +$ $7.62(\frac{p}{pcr})^3](\frac{\rho w}{1000})^{-0.5}(\frac{8}{d})^{0.15}$		empirical
Levitan et al.	$x_l = [0.39 + 1.57(\frac{p}{98}) - 2.04(\frac{p}{98})^2 +$ $0.68(\frac{p}{98})^3](\frac{\rho w}{1000})^{-0.5}$		valid for 8 mm tubes only
Roko et al. (1978)	$\frac{1 - x_l}{x_l} = [12.01(\frac{p}{p_{cr}})^2 - 5.628(\frac{p}{p_{cr}}) + 0.8623](\frac{G_m}{1000})$	160<G<500 kg m^{-2} s^{-1} 18<p<153 bar	Correlation valid for 10.8 mm tubes only
Katto (1982)	$X_{\lim} = 9.95 \left(\frac{\rho_v}{\rho_l} \right)^{0.133} \left(\frac{\sigma \rho_l}{G^2 D} \right)^{1/3}$	So-called H-regime in Katto flow regime map	Correspond to spray-annular flow regime

Morozov (1987)	$X'_{\lim} = \begin{cases} 0.568\psi_{DO}^{0.25} & \text{for } \psi_{DO} < 4 \\ 0.779\psi_{DO}^{0.022} & \text{for } \psi_{DO} > 4 \end{cases}$ $\psi_{DO} = \frac{K_q}{K_u}$, $K_q = \frac{\rho_l H_{fg}}{k_l}\left(\frac{\nu_l c_{pl}}{q_{cr}}\left\|\frac{d\sigma}{dT}\right\|_s\right)^{0.5}$, $K_u = \frac{G^2 D}{\sigma \rho_l}$	$10^{-2} < \psi_{DO} < 10^5$	Rivulet-spreading mechanism: thermal effect and hydrodynamic effect
Gallin-Kirillov (1987)	$X'_{\lim} = 1 - 0.86\exp\left[-19\left(\frac{G^2 D}{\rho_f \sigma}\right)^{-0.5}\right]$	$30 \le P \le 160$ bars	empirical
Kutadeladze	$Xl=0.3+0.7^{165W}$ where $W = \frac{wg \cdot \mu'}{\sigma \cdot \rho'}(\frac{\rho'}{\rho''})^{1/3}$		Valid for 8 mm tube only
Babcock & Wilcox (Kitto) (1980)	$x_l = 25.5 + 2.54 \cdot (\frac{G}{10^6})^{-1.85}$	152<p<200 bar 543<G<2172 kg m^{-2} s^{-1}	Experiments performed for 38 mm ID
Yildiz (2004)	$x_l = \frac{0.291}{9.85F(P)[G/1000]^{1.39} + 0.39} + 0.55$ $F(P) = 0.0199 + 0.00047P + 0.987\exp(-0.018P^2)$	100<G<400 kg m^{-2} s^{-1} 1<P<7 bar	valid for low pressure and low mass fluxes

The comparative study was performed on Katto, Morozov, and Galin-Kirrilov correlations. The correlations were compared with the experimental data. Peng et at. noticed that the Katto correlation predicts the average limiting quality, but the Morozov and Galin-Kirillov correlations predict the lower bound of the limiting quality regions. The analysis has proved that all three correlations agree reasonably well with the experimental data reported, as shown in Figure 7-4 the Katto correlation over-predicts the average limiting qualities in most cases and the discrepancy increases with the limiting qualities. The Morozov and Galin-Kirillov correlations give reasonable predictions for the lower bounds of limiting qualities. The average errors and RMS errors of three correlations for total 107 experimental data reported by Peng are shown in the Table 7-2.

Table 7- 2 Average errors and RMS errors of limiting quality correlations

Correlation	Average Error (%)	RMS Error (%)
Katto (1982)	17.6	24.0
Morozov (1987)	-0.9	18.3
Galin-Kirillov (1987)	26.0	22.2

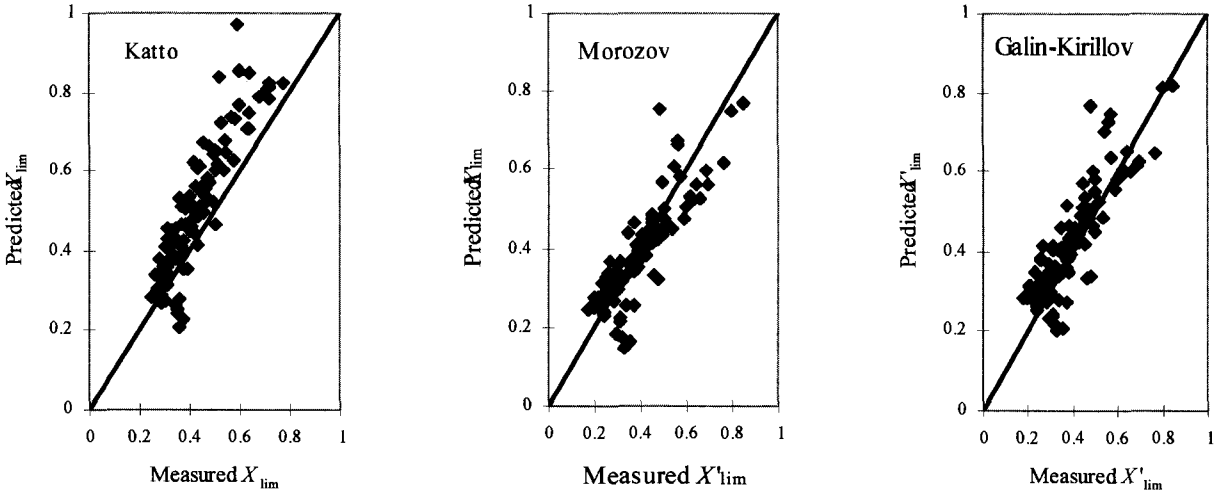

Figure 7-4 Comparison of predictions with limiting quality data

7.4 Limiting Quality Phenomenon and the CHF Look-up Table

In some regions the slope q_c versus x is vertical, as suggested by experiments. Steep changes will affect iterative loops in computer codes where the LUT is used. The current approach in solving this issue was suggested by Shan (2004).

The limiting quality boundaries (lower and upper) X'_{lim} and X''_{lim} were taken from LQR tables. Following steps were taken in deriving the 2005 CHF LUT at conditions near the LQR (see Figure 7-5):

(i) find the adjacent quality x_i to the left of X'_{lim}, and linearly interpolate to find $q_{cr}(x_i)$:

$$q_c(x_i) = q_{cr}(x_{i-1}) + \frac{q_{cr}(x_{i-1}) - q'_{cr}}{x_{i-1} - x'_{lim}}(x_i - x_{i-1}) \qquad (7.3)$$

(ii) find the adjacent quality x_j to the right of X''_{lim}, and replace $q_c(x_j)$ to $q_c(x=0.9)$:

$$q_c(x_j) = \left(r + \frac{1-r}{0.9 - x''_{\lim}} (x_j - x''_{\lim}) \right) q_c(x_j)\Big|_{Smoothed\ table}$$

$$r = \frac{q''_c}{q_c(x''_{\lim})_{smoothed\ table}} \tag{7.4}$$

(iii) linearly interpolate the CHF between x_i and x_j.

(iv) if needed manually modify unusual trends.

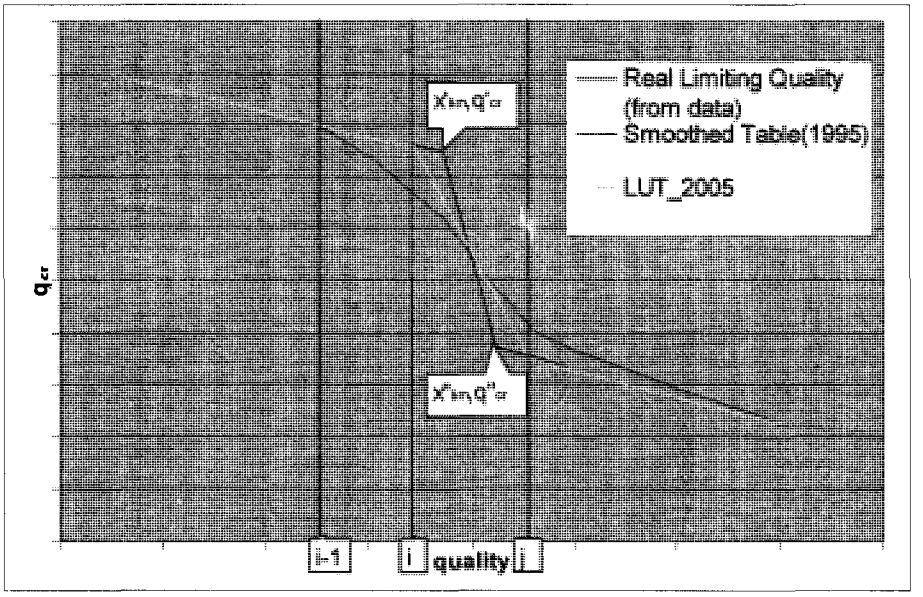

Figure 7-5 Embedding LQR in LUT

The error analysis shown that although the RMS error improves by embedding the LQR in the CHF LUT, the smoothness index is adversely affected by LQR.

Most CHF papers present q_c versus X, but they have not considered CHF versus p or G. This is obvious, since LQR is related to thermodynamic dryout quality, the other parameters being constant. For LUT purposes, however, the plots of q_c versus p and versus G are equally important.

Dependence of LQR on diameter, as some suggested by some researches, may cause difficulties on representing it properly on the LUT. There is no evidences that the "normalization" formula $q_{cD}/q_{c8\ mm}=(D/8)^n$ is applicable in the LQR, or how accurate this is within LQR.

LQR is a major source of errors for the CHF LUT. Because of high data scatter, it is very difficult to predict the CHF value within this region. Figure 7-6 shows a typical LQR at a quality approximately equal with 0.4. Very often at the LQR the experimental CHF show a discontinuity or a positive CHF versus x slope (see data by Kirillov (1984), by Becker(1969), by Zenkevich(1971) or by Soderquist(1994)), which means that at the same local quality there are more than two possible heat fluxes, which can be very different from each other. This makes the prediction of CHF within the LQR subject to high uncertainties.

Examination of the error distribution with respect to critical quality, pressure and mass flux (Appendix 3) reveals that average and RMS errors significantly increase in the LQR. In the plots of error distribution with respect to quality, it can be noticed that prediction within the subcooled and low quality has the lowest errors. Between quality 0.3 and 0.7, the typical LQR quality range, the high data scatter worsen the prediction accuracy. Above 0.6 up to 0.8, the error decreases slightly due lo lower scatter and increases again at very high qualities. The error histograms with respect to pressure and mass flux show the same trends within the LQR: the error shows "peaks" at 2-3 MPa and 12-14 MPa, and 0.5-2 $Mgm^{-2}s^{-1}$, that are the typical regions where a strong LQR exists, as reported by Peng (2004). (see Figure 7-3).

As reported by Shan et al.(2005), and Groeneveld et al. (2005) the CHF LUT 2005 supersedes the CHF LUT 1995. One of the improvements of the CHF LUT 2005 is the embedding of LQR in the LUT, as shown in Figures 7-6 and 7-7. The error histogram comparison with respect to critical quality is presented in Figure 7-8. The LUT 2005 has steeper trends within the LQR, which agree better with the experimental data trends. A smoother trend as shown by LUT 1995, would create a more uniform error distribution within LQR. Also, at qualities around 0.4 and 0.5, the local error in the CHF LUT 1995 is slightly lower than CHF LUT 2005. This effect occurs because a smoother LUT passes through the experimental points, minimizing error at the beginning of the LQR. Due to relatively high number of experimental data obtained in the LQR, the overall impact on error is significant. It may be stated that the main sources of errors for the CHF LUT are LQR and data at very high qualities.

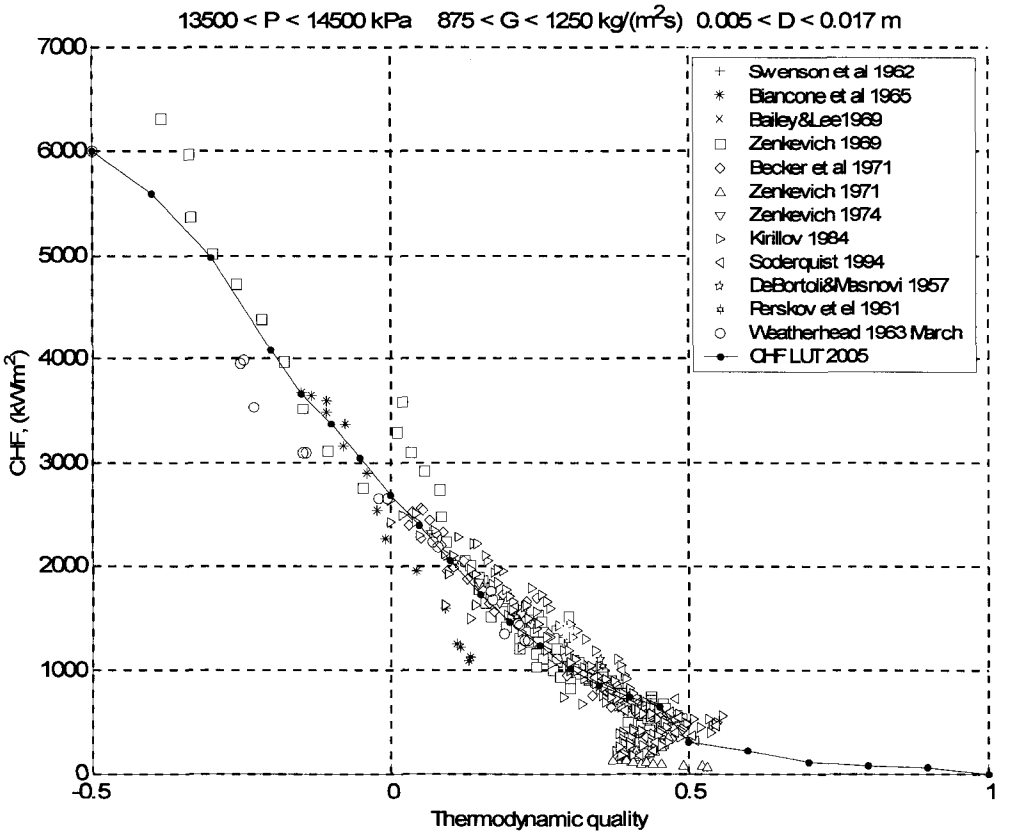

Figure 7-6 Slice showing high scatter of experimental data in LQR

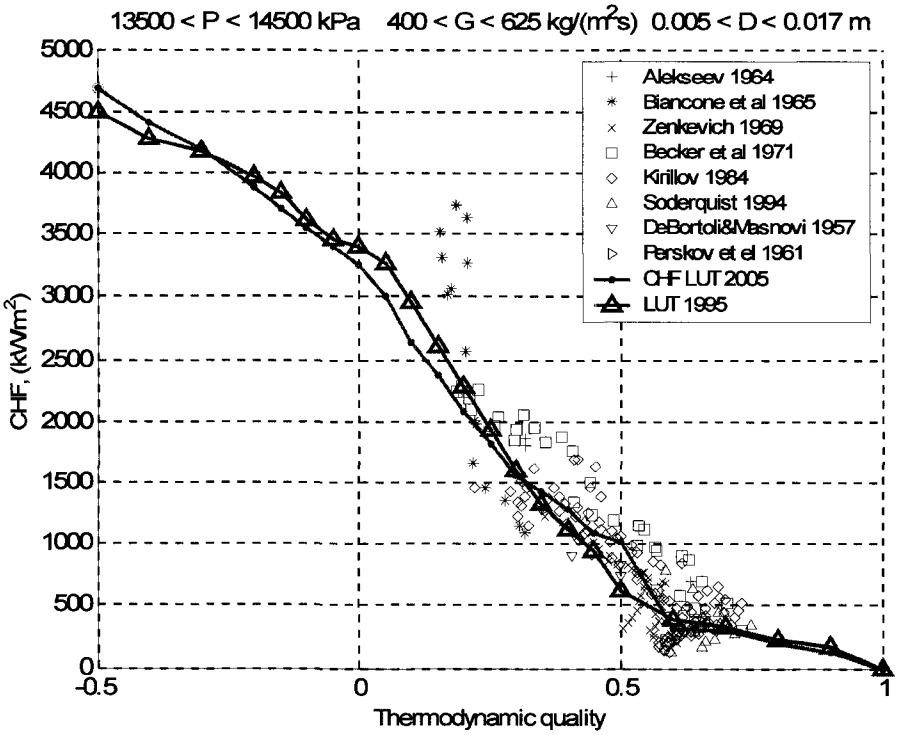

Figure 7-7 Comparison between LQR of LUT 1995 versus LUT 2005

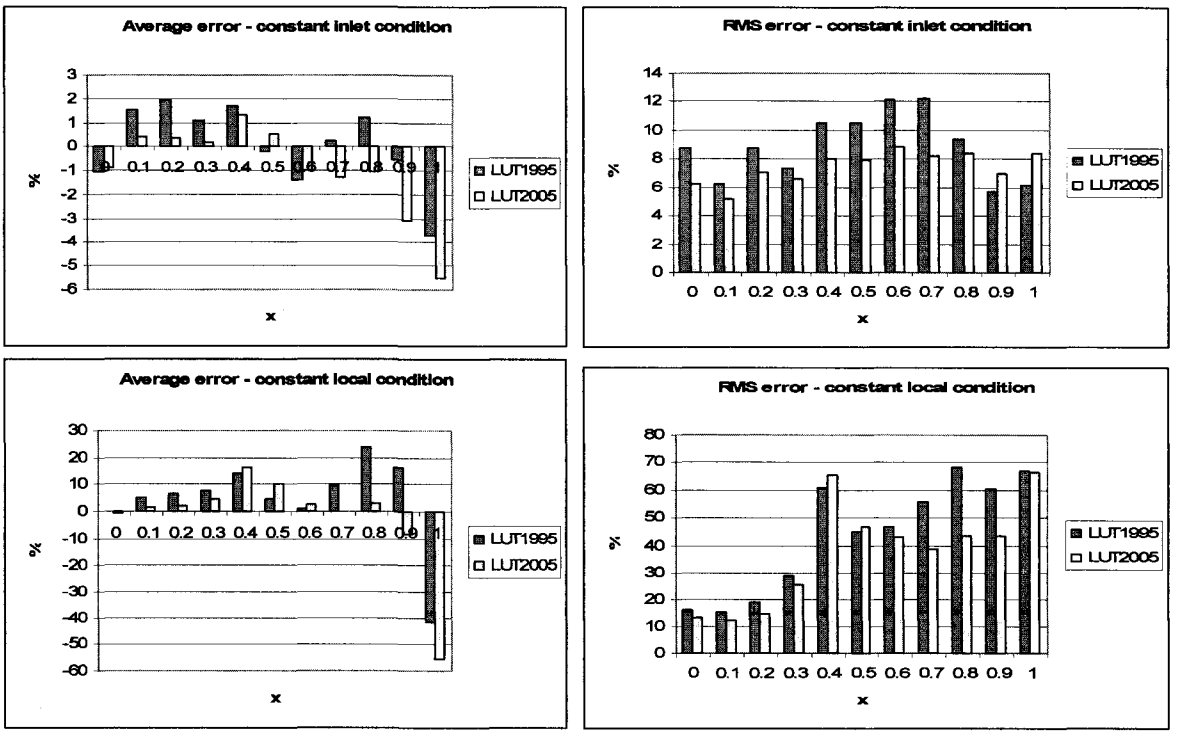

Figure 7-8 Comparison of error distribution in saturated region between CHF LUT 1995 and CHF LUT 2005

7.5 Summary

Limiting quality region is characterized by a sharp decrease of the CHF value with a small increase in x, caused by transition from entrainment-controlled dryout to deposition-controlled dryout.

Prediction of LQR is extremely important in practical applications, such as nuclear reactors, where safety margins are strongly influenced by LQR, therefore many correlations for LQR prediction have been developed. Unlike most of existing CHF empirical models and correlations, the latest versions of CHF LUT has been modified to permit a better prediction of the peculiar behaviour of the CHF in the LQR. However, due to very high data scatter, prediction of CHF within LQR is still subject to relatively high uncertainties. Error analysis revealed that at flow conditions where a strong LQR was observed, the CHF LUT errors are significantly higher (3-6 times higher than subcoled and low quality data, 1.5-2 times higher than LUT overall RMS error, DSM). Because a large amount of experimental data is within LQR, the impact of overall LUT error is significant, LQR being one of the main sources of LUT uncertainties.

An error comparison between CHF LUT 1995 and CHF LUT 2005 has shown that embedding LQR in the CHF LUT has a positive impact on CHF LUT accuracy and trends.

8. CHF AT EXTREME CONDITIONS

8.1 CHF at Low Pressure, Low Flow (LPLF) Conditions

CHF at low pressures and low flows conditions is important with respect to accident conditions of light water reactors and normal and transient conditions for research reactors. Due to peculiarities associated with LPLF regimes – flooding, pool boiling and lower flow stability – the experimental data are scarce and the uncertainties are quite high. Moreover, the range of applicability of most of CHF correlations does not cover the LPLF conditions. This was reflected in the CHF look up table, where those flow regimes were recommended to be used with caution (Groeneveld et al., 2005), being included mainly for interpolation purposes. The current analysis provides an insight in the LPLF literature review, presents a discussion on the main parameters having impact on CHF at those regimes, and compares the trends of the LUT versus some correlations, experimental data, and expected physical trends.
The limit of low pressure – low flow boundary is not clearly stated in the literature; in general experiments at LPLF are performed at pressures between 100 and 500 kPa and mass fluxes up to 250 kg m^{-2} s^{-1}.

CHF characteristics at low pressure are quite different from high pressure. The liquid-vapour density ratio at 0.1 MPa is about 1600, 260 times that at 15 MPa. At low pressures, large bubbles and different flow characteristics in channels of relatively small diameter are present. Low velocity makes the buoyancy effect significant and this factor is taken into account in almost all models for CHF prediction at low flow in vertical heated channels.

The main parameters that influence CHF at low pressure low flow conditions are:

- mass flux
- inlet subcooling
- flow direction
- diameter
- pressure

8.1.1 Effect of mass flux

Chang et al. (1991) and Kim et al. (2000) reported that the CHF increases almost linearly with mass flux for both constant inlet and exit conditions. According to the research conducted by Kim, the mass flux effect is stronger for low L/D ratios. Mishima et al. (1985) performed experiments on a 6mm ID test section and found that at very low mass fluxes the CHF increases very fast as the mass flux increases up to 200 kg $m^{-2}s^{-1}$. After 200 kg $m^{-2}s^{-1}$, the increase is much slower. At low subcoolings, some plots show a slight decrease of CHF up to 250 kg $m^{-2}s^{-1}$, and a monotonous increase for higher mass fluxes.
Moon's et al. (1996) experiments demonstrated that the CHF at high qualities increases with mass flux in the very low mass flow region, then sharply decreases to a minimum and then gradually increases.

8.1.2 Effect of inlet subcooling

The effect of inlet subcooling appears to be less important at LPLF conditions. Chang et al., (1991) found no effect of inlet subcooling at LPLF conditions At low pressures, close to atmospheric, the critical quality of water can not go below -0.2, otherwise the solid state (freezing) occurs. Therefore, the values from LUT for qualities below -0.2 are not possible and any values provided are based on extrapolation and are only useful for LUT interpolation purposes.

The experiment in an annular test section conducted by El-Genk et al.(1988) revealed that the effect of inlet subcooling is inconclusive for mass fluxes less than 140 kg $m^{-2}s^{-1}$ for annulus ratios of 1.575, 1.72 and 2. Kim et al. (2000) found that inlet subcooling has a small effect in general, and this effect decreases with increasing heated length. Mishima et al (1985) reported that for mass fluxes less than 200 kg $m^{-2}s^{-1}$, the effect of inlet subcooling is not significant. There are, however, some indications that the effect of inlet subcooling appears to become significant when the mass flux exceeds 190 kg $m^{-2}s^{-1}$(El-Genk,1988).

channel receives a certain amount of mass and energy per time unit; the fluid mass is heated up and leaves the control volume with higher enthalpy. Usually, during the experiments, the flow conditions are kept as steady as possible, so that heat is not accumulated into the control volume. This hypothesis is no longer valid for zero or very low flow conditions. The heat provided to the test section is not removed by the working fluid, but a significant part accumulates within the control volume (pool) as a temperature increase and/or phase change.

As mentioned, at very low mass fluxes the calculated critical quality tends to be greater than 1, with high scatter, which indicates that the thermodynamic quality is not a useful measure of the flow condition at the CHF location. Hence, most research work at LPLF studies the CHF as a function of inlet conditions (inlet temperature, inlet enthalpy, etc) rather than local conditions. For this reason a direct comparison between CHF LUT and LPLF experimental data is not very straightforward. A helpful observation is that the experiments revealed that at very low flow the impact of inlet fluid temperature (or inlet subcooling) on CHF is weak, and this may suggest that the impact of local quality on CHF is also weak.

According to the mechanisms previously described, there are two possible prediction methods for CHF at zero flows:

1. Pool boiling correlations
2. Zero flow/low flow correlations

Tables 8-1 and 8-2 summarize some of the most common pool boiling and low flow correlations.

8.1.3.1 Pool boiling correlations

As mentioned, pool boiling correlations do not take directly into account either the effect of inlet or outlet subcooling, but the system geometry and fluid/vapour properties. Table 8-2 and Figure 8-3 present some common pool boiling correlations. Figure 8-4 presents the CHF predicted by the LUT 2005 for zero flow conditions. As mentioned before, at zero flow conditions, the local quality has no physical significance and it is still used just for consistency purposes.

Table 8-2 Most common pool-boiling correlations

Author	Correlation
Zuber	$q_c = 0.131 \cdot h_{fg} \cdot \sqrt{\rho_g} \cdot \sqrt[4]{\sigma g \Delta \rho}$
Kutadeladze	$\frac{q_c}{h_{lg}\rho_{lg}^{0.5}[\sigma g(\rho l - \rho g)]^{1/4}} = K$ $K = 0.16$
Borishanskii	$\frac{q_c}{h_{lg}\rho_{lg}^{0.5}[\sigma g(\rho l - \rho g)]^{1/4}} = K$ $K = 0.13 + 4\left\{\frac{\rho_l \cdot \sigma^{3/2}}{\mu^2[g(\rho_l - \rho_g)]^{1/2}}\right\}^{-0.4}$
Rosenhow	$\frac{q_c}{h_{lg}\rho_g} = C\left(\frac{g}{gs}\right)^{1/4}\left[\frac{\rho_l - \rho_g}{\rho_g}\right]^{0.6}$

As found by Mishima (1984, 1985), El-Genk (1988), the inlet subcooling does not have a significant impact on CHF at flows up to 200 kg $m^{-2}s^{-1}$. Examination of Figure 8-4 reveals that in the physically impossible regions (high subcoolings) the predicted CHF is very high 4-8000 kWm^{-2}. In the saturated region, the CHF strongly depends on the local quality, the range of variation being between 1000 to 50 kWm^{-2}, at low pressures. It should be observed that the variation of predicted CHF with pressure is very similar to that of pool boiling correlations. It can be concluded that at zero flow conditions the predictions of the CHF LUT 2005 are close to pool boiling correlations; therefore, it may over-predict the CHF, especially at low local qualities (see also Table 8-1). As mentioned in Section 5.1, at near-zero flow, pool-boiling-like conditions are encountered. Here pool boiling correlations apply for large tube diameters, but for small diameter tubes the geometry prevents the vapour from escaping freely by buoyancy (unrestricted natural convection by buoyancy would have occurred in a pool boiling situation). At near zero flow conditions, although the experimental data are very scarce, they do suggest that future versions of the CHF LUT should predict much lower CHF than the 2005 CHF LUT, (closer to the available experimental data).

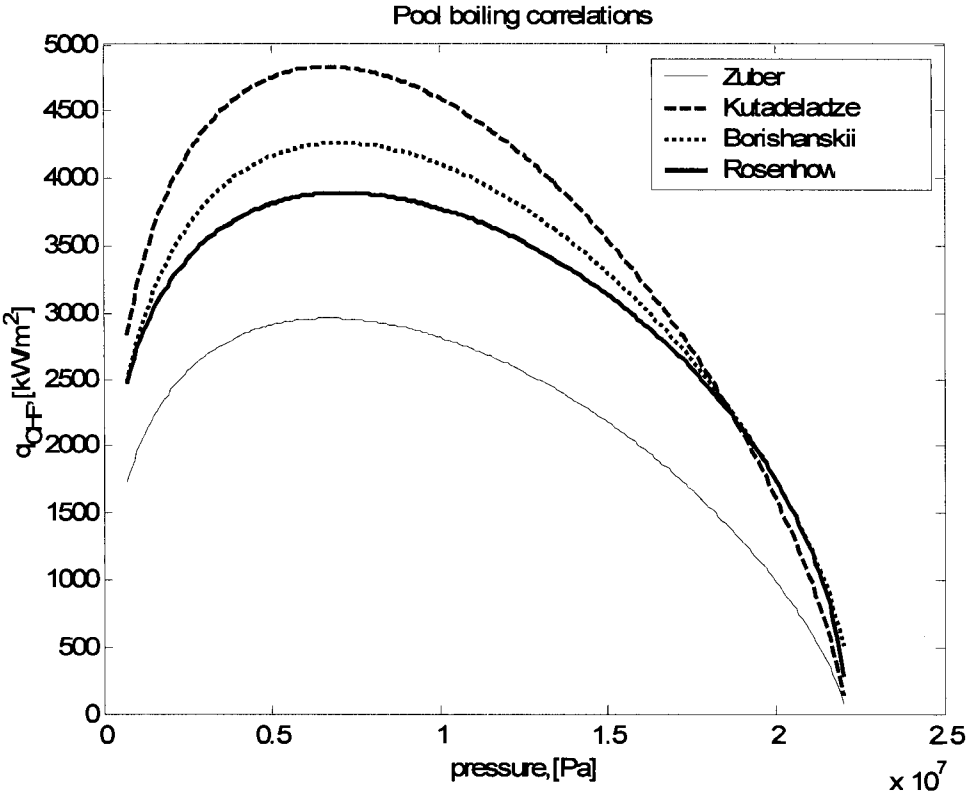

Figure 8-5 Pool boiling correlations

8.1.3.2 Zero flow correlations. Low flow correlations

In general, at zero or very low flow the CHF is governed by the flooding from the top of the heated length. For vertical heated channels with a closed bottom end, Wallis et al. (1969) recommended the following empirical correlation:

$$j_g^{*1/2} + m j_l^{*1/2} = C_W \tag{8.3}$$

where C_W is a constant dependent on the system geometry, typically between 0.73 (rectangular channels) and 1.66 (tubes), constant m is set to unity for turbulent flow, and j_g^* and j_l^* are vapour and liquid dimensionless superficial velocities, defined as follows:

$$j_g^* = j_g \rho_g^{1/2} (gD\Delta\rho)^{-1/2}$$

$$j_l^* = j_l \rho_l^{1/2} (gD\Delta\rho)^{-1/2} \tag{8.4}$$

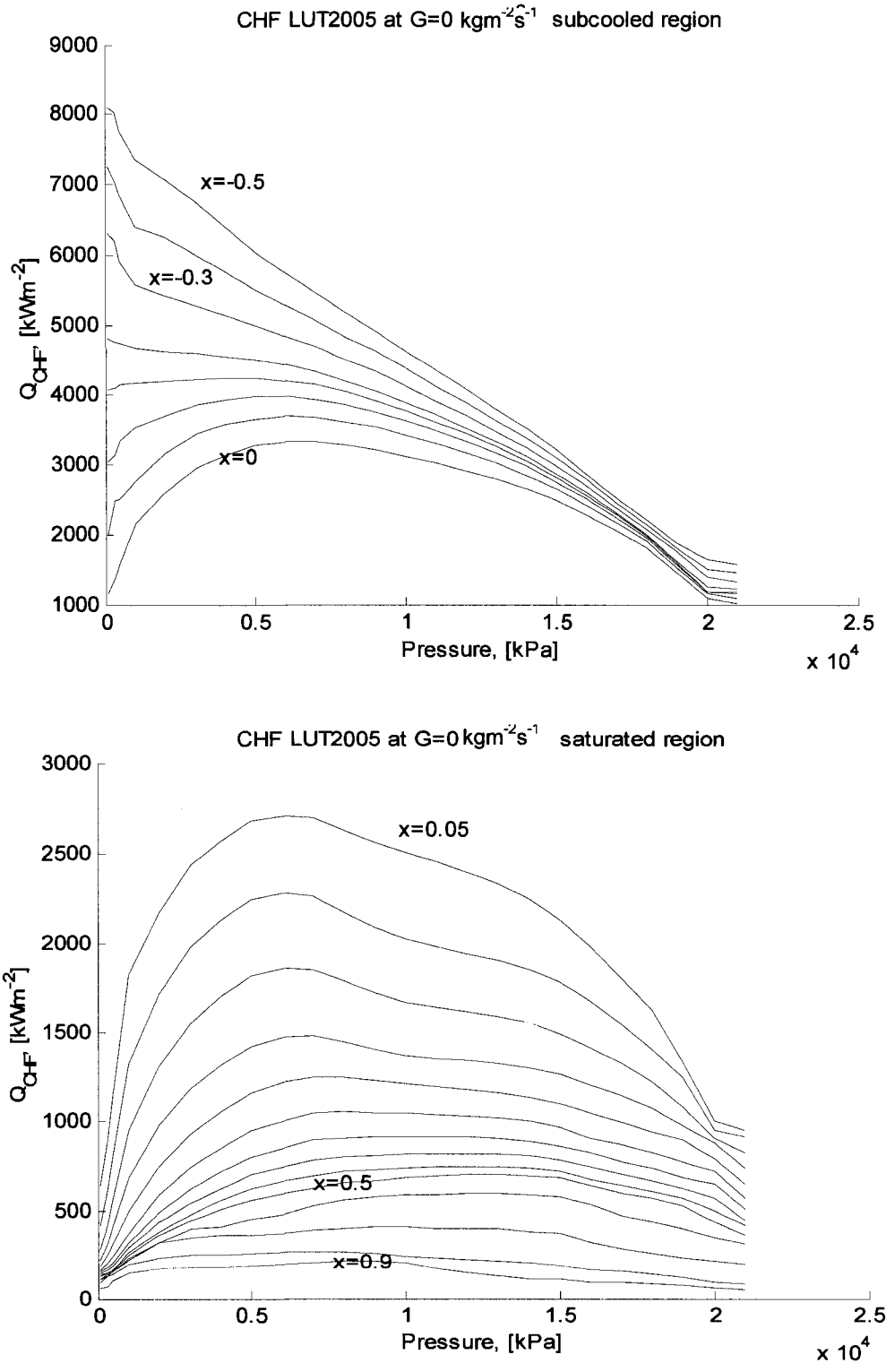

Figure 8-6 CHF LUT 2005, Zero flow, various pressures and exit qualities

where j_g and j_l are vapour and liquid superficial velocities, g is the gravitational acceleration, D is the heated channel diameter and $\Delta\rho$ the difference between liquid and vapor densities. The mass conservation equation for a channel with a closed bottom end can be written as:

$$\dot{m} = \rho_g j_g A_f - \rho_l j_l A_f = 0 \quad \text{or} \quad \rho_g j_g A_f = \rho_l j_l A_f \tag{8.5}$$

where A_f is the cross section area of the heated test section.

The energy conservation equation is:

$$\rho_g j_g A_f = \rho_l j_l A_f = \frac{q_c A_b}{h_{fg}} \tag{8.6}$$

where A_b is the heated area.

Combining equations 8.3, 8.4 and 8.6 one obtains:

$$\frac{q_c}{h_{fg}(gD_{hy}\rho_g\Delta\rho)^{1/2}} = \frac{C_W}{4}\left(\frac{D_{he}}{L}\right)\left[1+\left(\frac{\rho_g}{\rho_f}\right)^{1/4}\right]^{-2} \tag{8.7}$$

where D_{he} is the heated equivalent diameter. The equation has been modified by different experimenters in order to obtain a better fit for their data. Table 8.3 summarizes some flooding limited CHF correlations from literature.

Unlike flooding CHF correlations, in general, low flow correlations include mass flux as an input variable. Some of most common low flow correlations from the literature are presented in Table 8-4. A comparison between the CHF LUT 2005 and some of the low flow correlations has been performed (see Figure 8-6). The plots show a reasonable agreement between the CHF LUT and Griffith and Macbeth correlations. At zero flow conditions, most of the low flow correlations are not applicable, because they contain G and show obviously wrong trends (i.e. CHF=0 at G=0).

In general, at zero and very low flows where the CHF mechanism is CCFL, flooding correlations are most accurate and have correct trends. For higher flows, G-dependent correlations are recommended.

An independent assessment of some well known CHF correlations and models was performed by Kim et al (2000). The results of this study are summarized in Table 8-5.

Table 8-3 Flooding CHF correlations

Author	Correlation	Observations
Wallis (1969)	$\frac{q_c}{h_{fg}(gD_{hy}\rho_g\Delta\rho)^{1/2}} = \frac{C_W}{4}\left(\frac{D_{he}}{L}\right)\left[1+\left(\frac{\rho_g}{\rho_f}\right)^{1/4}\right]^{-2}$	Wallis correlation is the basis for most of flooding correlations
Mishima and Nishihara (1987)	$\frac{q_c}{h_{fg}(g\lambda\rho_g\Delta\rho)^{1/2}} = \frac{C_W^{\,2}}{4}\left(\frac{D_{he}}{L}\right)D^{*1/2}\left[1+\left(\frac{\rho_g}{\rho_f}\right)^{1/4}\right]^{-2}$ $D^* = D_{hy}/\lambda$ $\lambda = (\sigma/g\Delta\rho)^{1/2}$	λ represents the wavelength of Taylor instability. Cw=1.66 for tubes Cw=0.98 for annuli Cw=0.73 for rectangular channels
Nejat (1981)	$\frac{q_c}{h_{fg}\rho_g(gD_{hy})^{1/2}} = \frac{C_W^{\,2}}{4}\left(\frac{D_{he}}{L}\right)\left(\frac{\Delta\rho}{\rho_g}\right)\left[1+\left(\frac{\rho_g}{\rho_f}\right)^{1/4}\right]^{-2}$	$C_W^2=0.36(L/D_{he})^{0.1}$
Tien et al. (1979)	$\frac{q_c}{h_{fg}(g\sigma\rho_g^{\,2}\Delta\rho)^{1/4}} = \frac{C_k^{\,2}}{4}\left(\frac{D_{he}}{L}\right)\left[1+\left(\frac{\rho_g}{\rho_f}\right)^{1/4}\right]^{-2}$	$C_k^2=3.2[\tanh(Bo^{1/4}/2)]^2$ $Bo=D_{hy}(g\Delta\rho/\sigma)^{1/2}$ Bo-Bond number
Imura et al. (1983)	$\frac{q_c}{h_{fg}(g\sigma\rho_g^{\,2}\Delta\rho)^{1/4}} = \frac{C_k^{\,2}}{4}\left(\frac{D_{he}}{L}\right)\left(\frac{\rho_g}{\rho_f}\right)^{-0.13}$	$C_k=0.64$

Table 8-4 Low flow correlations

Author	Correlation	Observations
Lowdermilk (1958)	$q_c = 183.9 \cdot D^{-0.2} \cdot \left(\frac{Lh}{D}\right)^{-0.85} \cdot G^{0.85}$	$G/(Lh/D)^2 \leq 0.2034$ no pressure effect $27.1 < G < 30000$ kg $m^{-2}s^{-1}$
Macbeth (1963)	$q_c = 0.150 \cdot h_{fg} \cdot D^{-0.1} G^{0.51} \cdot (1 - x_c)$	
Griffith (1977)	$q_c = 0.131 \cdot (1-\alpha) \cdot h_{fg} \cdot \sqrt{\rho_g} \cdot \sqrt[4]{\sigma g \Delta\rho}$	Modified Zuber's pool-boiling correlation No diameter effect No subcooling effect
Chang (1991)	$q_c{}^* = q_{cF} + C_1 (D^*)^{C_2} (Lh/D)^{C_3} \cdot \lvert G^* \rvert^{C_4}$ $q_{cL}{}^* = q_{cF} + 0.01351 (D^*)^{-0.473} (Lh/D)^{-0.533} \cdot \lvert G^* \rvert^{1.45}$ $q_{cH}{}^* = q_{cF} + 0.05664 (D^*)^{-0.247} (Lh/D)^{-0.501} \cdot \lvert G^* \rvert^{0.77}$ $q_{cF}{}^* = 1.61 \frac{A}{Ah} \times \frac{\sqrt{D^*}}{\left[1 + (\rho_g/\rho_f)^{1/4}\right]^2}$ $q_c = \min[q_{cL}{}^*, q_{cH}{}^*]$	q_{cL} is for very low G*, q_{cH} is for higher mass fluxes

G*	$\frac{G}{\sqrt{\lambda \rho_g g \Delta\rho}}$
q*	$\frac{q}{h_{fg}\sqrt{\lambda \rho_g g \Delta\rho}}$
D*	$\frac{D}{\lambda}$
λ	$\sqrt{\frac{\sigma}{g\Delta\rho}}$

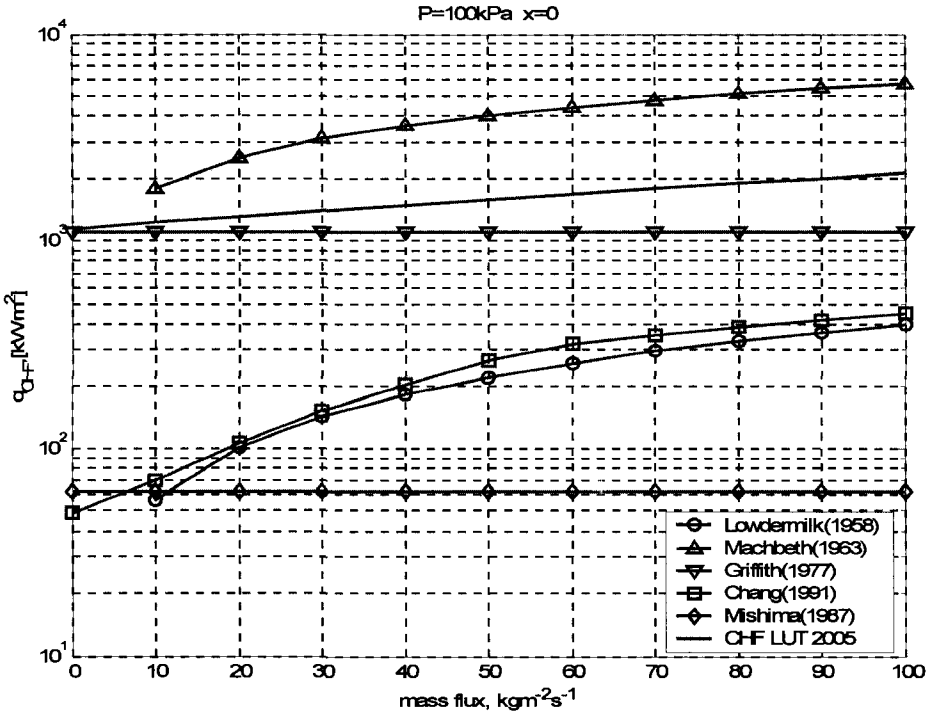

Figure 8-7 Comparison between CHF LUT 2005 and some low flow/ zero flow correlations

Table 8-5 Comparison between different prediction methods for low flow conditions

Correlation type	Table/correlation	Assessment method	No data	Avg	RMS
Local type	Groeneveld et al 1995	HBM	438	11.6	14.1
Local type	Baek et al 1997	HBM	438	5.5	12.9
Inlet type	Bowring (1972)	Fixed inlet	169	12.1	13.2
Inlet type	Katto and Ohno (1984)	Fixed inlet	470	25.2	27.9
Inlet type	Weber and Johannsen (1990)	Fixed inlet	217	13.9	22.3

Inlet type	Chang et al (1991)	Fixed inlet	493	10.5	25
Inlet type	Baek et al (1995)	Fixed inlet	493	9.4	20.3
Mixed type	Shah (1987)	Fixed inlet	513	3.2	10.4
Annular flow model	Katto(1984)	Fixed inlet	513	1	12.4

8.1.4 Effect of flow direction

At low mass fluxes, below 250 kg $m^{-2}s^{-1}$, the flow direction is more important than at higher mass velocities. For mass fluxes above 250 kg $m^{-2}s^{-1}$, no significant effect of flow direction was observed (upflow versus downflow).

When flow oscillations are present, CHF occurs on the lowest flow part of the oscillations. In general, downward flow is more susceptible to flow instabilities, therefore the CHF for downward flow is lower. (Chang et al.,1991). Chang's experiments showed an almost symmetrical behavior of CHF about the line of zero mass flux, which indicates that at low flows buoyancy is not significant for stable flow conditions. The flow direction becomes important only for very low mass fluxes, where the downward flow CHF is generally lower than the upward flow CHF. The difference between the two cases is not significant. This behavior was explained through the susceptibility of downward flow to instabilities and premature CHF due to flow excursions.

8.1.5 Effect of tube diameter at very low flow

The effect of L/D ratio is more important than L or D alone. For fixed inlet conditions, P, G, inlet subcooling, Lh, it was found that CHF increases with a diameter increase (Chang et al, 1991, Kim et al., 2000).

A comparison of the experimental data by Chang with existing LPLF correlations – namely Lowdermilk, Macbeth and Katto, revealed that a good agreement was noticed for Lowdermilk correlation, mainly due to very similar test conditions of Lowdermilk and Chang experiments. However, bigger discrepancies were observed for test sections of higher

diameter (8.8 mm ID) which proves that the Lowdermilk correlation gives higher errors at diameters far from 4.8 mm (Lowdermilk data).

Although no CHF measurements are available for large diameters (> 40-50 mm), it is expected that pool-like CHF mechanisms are valid, hence pool boiling correlations may be more appropriate for predicting CHF. According to Chang et al (1991), flooding CHF or pool-boiling-like mechanisms occur as a function of D and L/D ratio. The threshold value is determined by equality between expressions of CHF for pool boiling and flooding:

$$(L/D) = 31.6 \cdot \sqrt{D} \tag{8.2}$$

For experiments with test sections having 6-12 mm ID, L/D threshold ratios are 3-6, leading to the conclusion that flooding is the most common CHF mechanism at low pressure, low flow in tubes. However, at very small inside diameters (1-2 mm), the bubble slugs may create dry spots leading to CHF conditions, therefore, the mechanism would be neither flooding nor pool-like mechanisms. Figure 8-8 shows a comparison of CHF values at similar inlet conditions for two different diameters, 6 mm and 9 mm, respectively. The CHF measured at higher diameters is higher than the CHF measured for lower diameters. This trend is opposite to that observed at higher flows, where in general, at similar flow conditions, the CHF measured at lower diameters was higher but is consistent with the mechanisms described above.

In annuli experiments El-Genk (1988) concluded that for the same flow conditions, higher annulus ratios (the ratio between outer and inner diameter of the annulus) increased the CHF.

The experiment conducted by Kim et al. (2000) suggested that for a given L/D and inlet subcooling (constant inlet conditions) the variation of CHF with diameter is not significant for tube diameters between 6-12 mm.

It was shown that lower L/D ratios result in higher CHF for the same inlet conditions, but the difference become smaller as L/D increases. For fixed exit conditions there is no apparent effect of tube diameter for fixed L/D ratio. According to Kim et al (2000) the CHF increases with an increase of diameter for a fixed heated length.

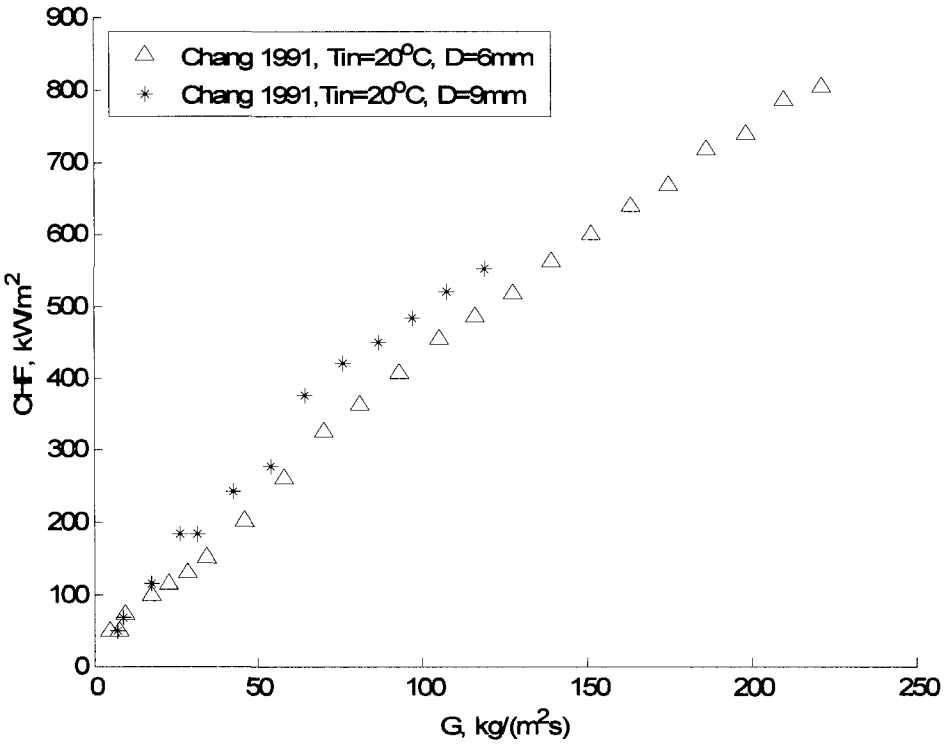

Figure 8-8 Diameter effect at LPLF (Chang, 1991)

Experiments conducted by Mishima et al. (1984, 1985) revealed that for flooding type CHF, an increase in diameter leads to a higher CHF. Indeed, examination of some available experimental data at low flow supports the above conclusion. Obviously, the scarcity of the available experimental data makes it difficult to extrapolate this conclusion for the whole quality or the pressure ranges, but some of the experimental evidence (see Figures 8-9) corroborated with the above mentioned CHF mechanisms lead to the conclusion that at flows below 200 kg $m^{-2}s^{-1}$, for the same local conditions, an increase in diameter leads to higher CHF(see also Chapter 5).

8.1.6 Effect of pressure

CHF is not significantly affected by pressure at LPLF conditions (Kim et al., 2000). Indeed, at very low flow, the entrainment of liquid does not take place, and liquid film thickness decreases by evaporation only.

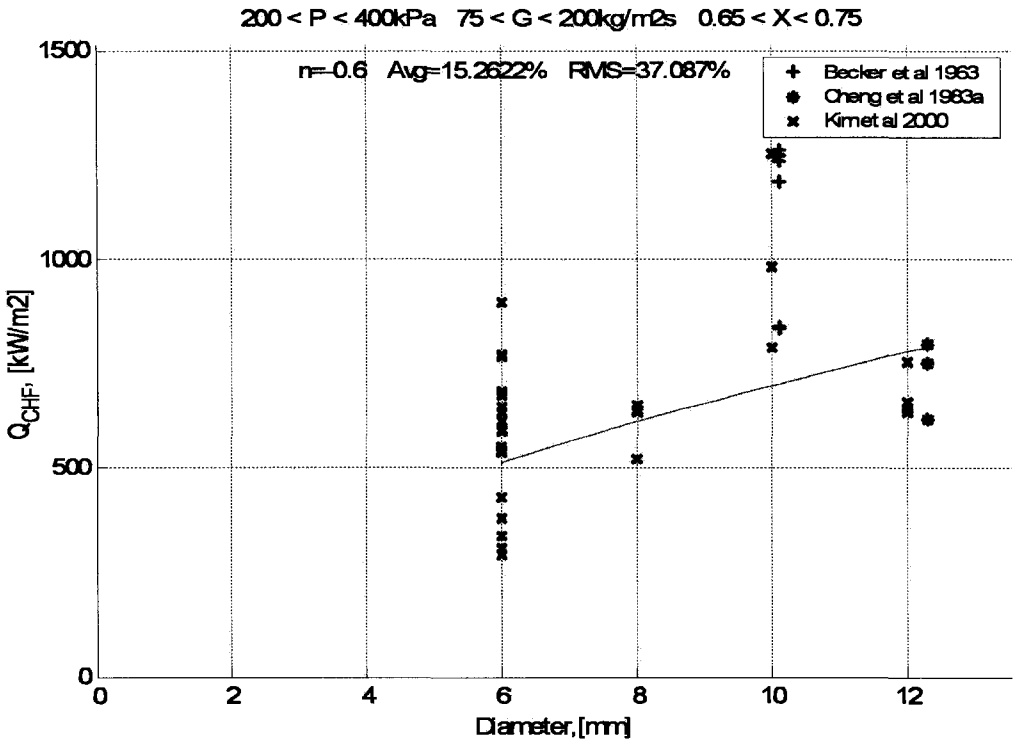

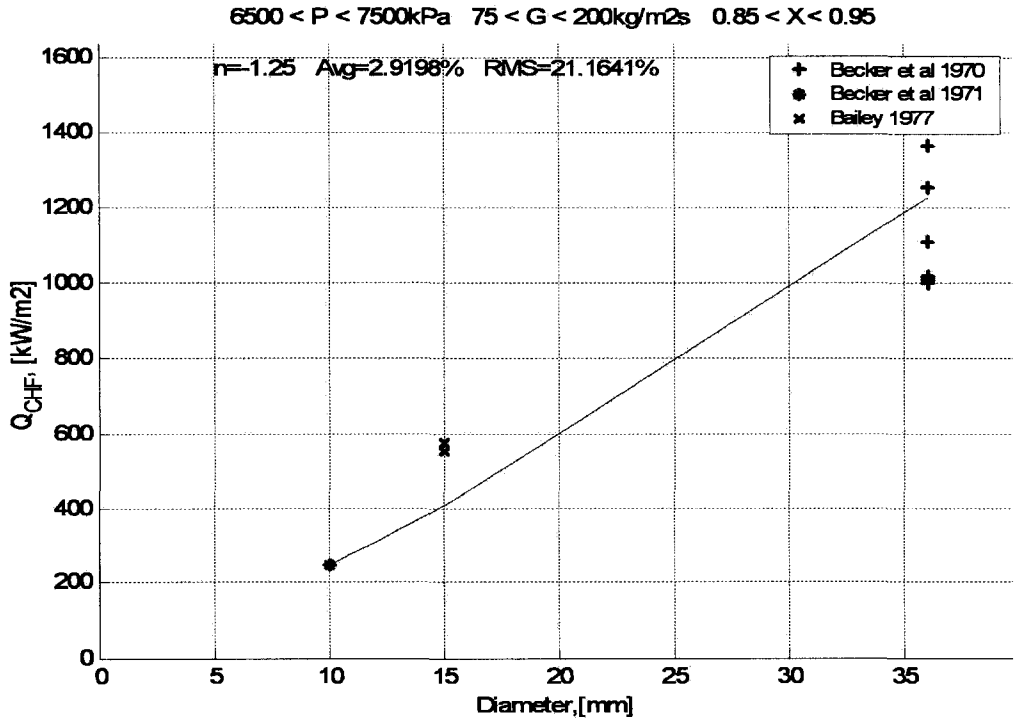

Figure 8-9 Effect of diameter at LPLF conditions

8.2 CHF at High Pressures

CHF at high pressures has become more and more important due to increasing interest in future reactors operating at near critical and supercritical conditions.

The experiments conducted in Freon-12 by Chang (1992) showed that for constant mass flux and exit quality CHF is increasing with pressure until at 1.8 MPa it reaches a maximum and then starts to decrease. This trend can be explained by the following effects:

1) Increase of pressure leads to a lower latent heat (see Figure 8-10), which decreases CHF
2) Increase of pressure increases the vapour density (see Figure 8-10), which increases the CHF
3) Increase of pressure decreases surface tension, which decreases CHF

All these effects, according to the pressure range, play a stronger or weaker role, increasing and decreasing CHF.

A more recent experiment by Vijayarangan et al. (2006) concluded that CHF at very high subcritical pressures is lower than the predictions of the CHF LUT 1986 and Katto-Ohno (1984) correlation. Vijayarangan used refrigerant R134a as the coolant and a test section of 12.7 mm ID and heated length of 3 m. The reduced pressure range for his experiment was 0.24 -0.99, the mass flux 200 -2000 kg m^{-2} s^{-1} and the exit quality from 0.17 – 0.97. A comparative assessment revealed that at high pressures, at P/Pc>0.8 and low flows, the Katto-Ohno correlation may over predict the Vijayarangan data up to 3-3.5 times, and the CHF LUT 1986 up to 4-4.3 times. The overprediction is significant at all mass fluxes. Starting from the Katto-Ohno correlation, Vijayarangan et al. (2006) modified it and using its experimental data derived a new CHF correlation for high pressure conditions:

$$\frac{q_c}{G\lambda} = 0.0051\left[(\rho_v/\rho_l)^{0.133}(\sigma\rho_l/G^2L)^{1/3}\left(\frac{1}{1+0.0031(L/d)}\right)P_R^{\,0.147}\,\mathrm{Re}_l^{\,0.25}\right] \quad (8.3)$$

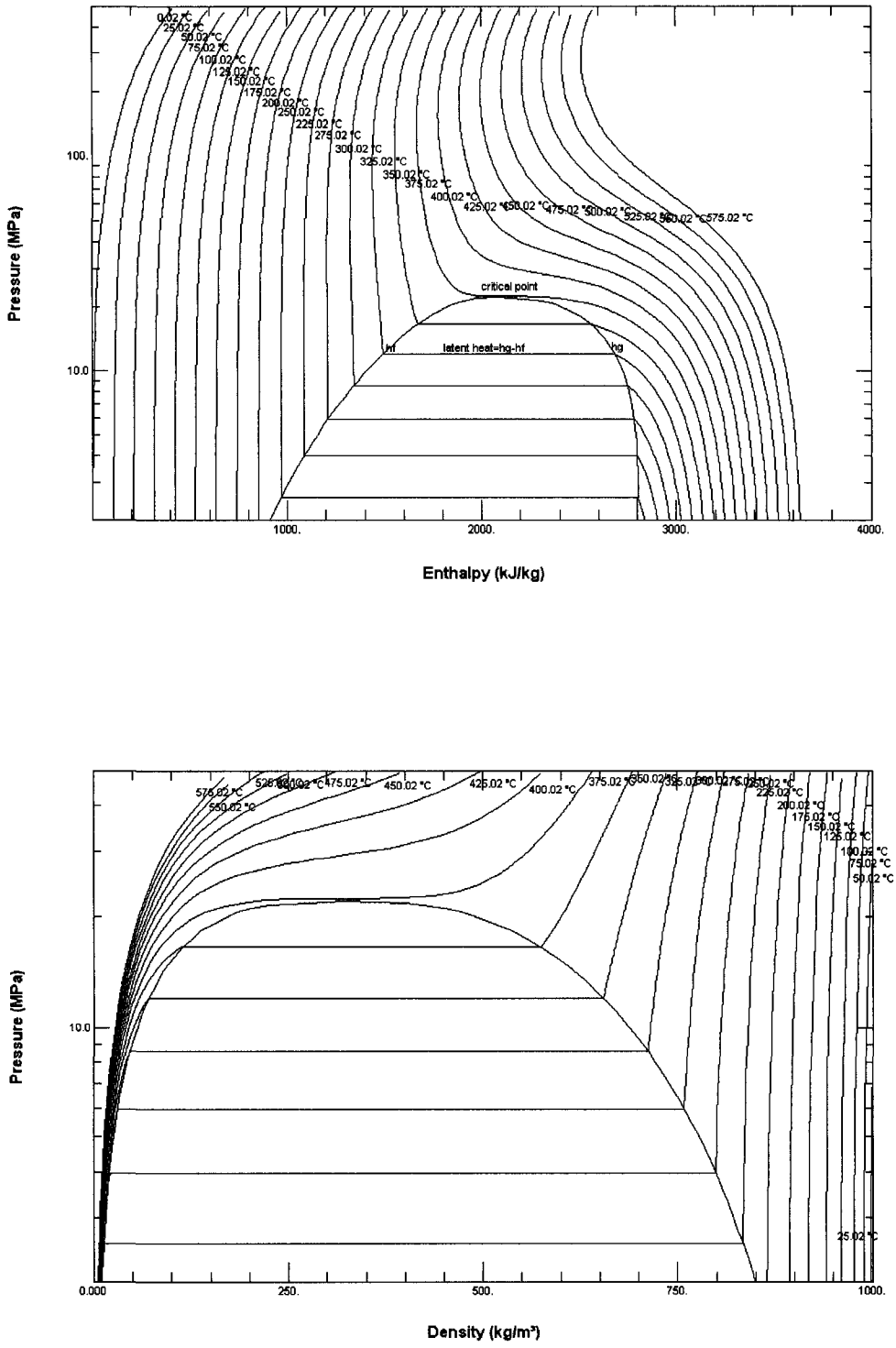

Figure 8-10 The enthalpy and the density as a function of pressure and temperature

It covers the following parametric ranges:

$1.40 * 10^4 < Rel < 7.6 * 10^5$

$1.0 * 10^{-8} < Wel < 1.5 * 10^{-5}$

$6.1 * 10^{-5} < q_c/G\lambda < 8.05 * 10^{-4}$

$0.13 < P_R < 0.95$

$0.01 < \rho\varpi/\rho\lambda < 0.44$

Vijayarangan used the earlier 1986 CHF LUT version. In Chapter 3 it was shown that newer versions of the CHF LUT are derived using an extended database and they have a much better prediction accuracy for all flow regions. Appendix 3 demonstrates that at high pressure RMS errors for both constant inlet conditions and constant local conditions are lower than the corresponding values for the whole CHF LUT, 5.6% and 23%, respectively (see Appendix 3, Tables A 3-2 and A3-5). Furthermore, a straight comparison of the CHF LUT 2005 with experimental data for water at high pressures shows a good agreement (Figure 8-11).

8.3 CHF at Very High Qualities for Medium to High Mass Fluxes

At high thermodynamic qualities the flow is usually annular or dispersed. The available literature approaching this area is very scarce, mainly due to experimental difficulties in obtaining high exit qualities at medium or high mass fluxes. At high exit qualities the CHF mechanism is either flooding-like for very low flows or dryout at average and high mass fluxes. An important characteristic is that the thickness of the liquid film is very small, so no disturbance waves can be formed at the liquid-vapour interface. The entrainment rate is therefore close to zero, the liquid film being depleted only by evaporation and replenished by droplet deposition.

The critical heat flux at very high local qualities is usually small, theoretically approaching zero when the local thermodynamic quality is 1, because no liquid is assumed to exist. However experimental evidence (Becker et al. 1963, Ceresa, 1974, Soderquist et al., 1994) suggests that, at thermodynamic qualities very close to 1, the CHF is of the order of 200 to 500 kWm^{-2} (CHF LUT assumes that at x=1 the q_c =0).

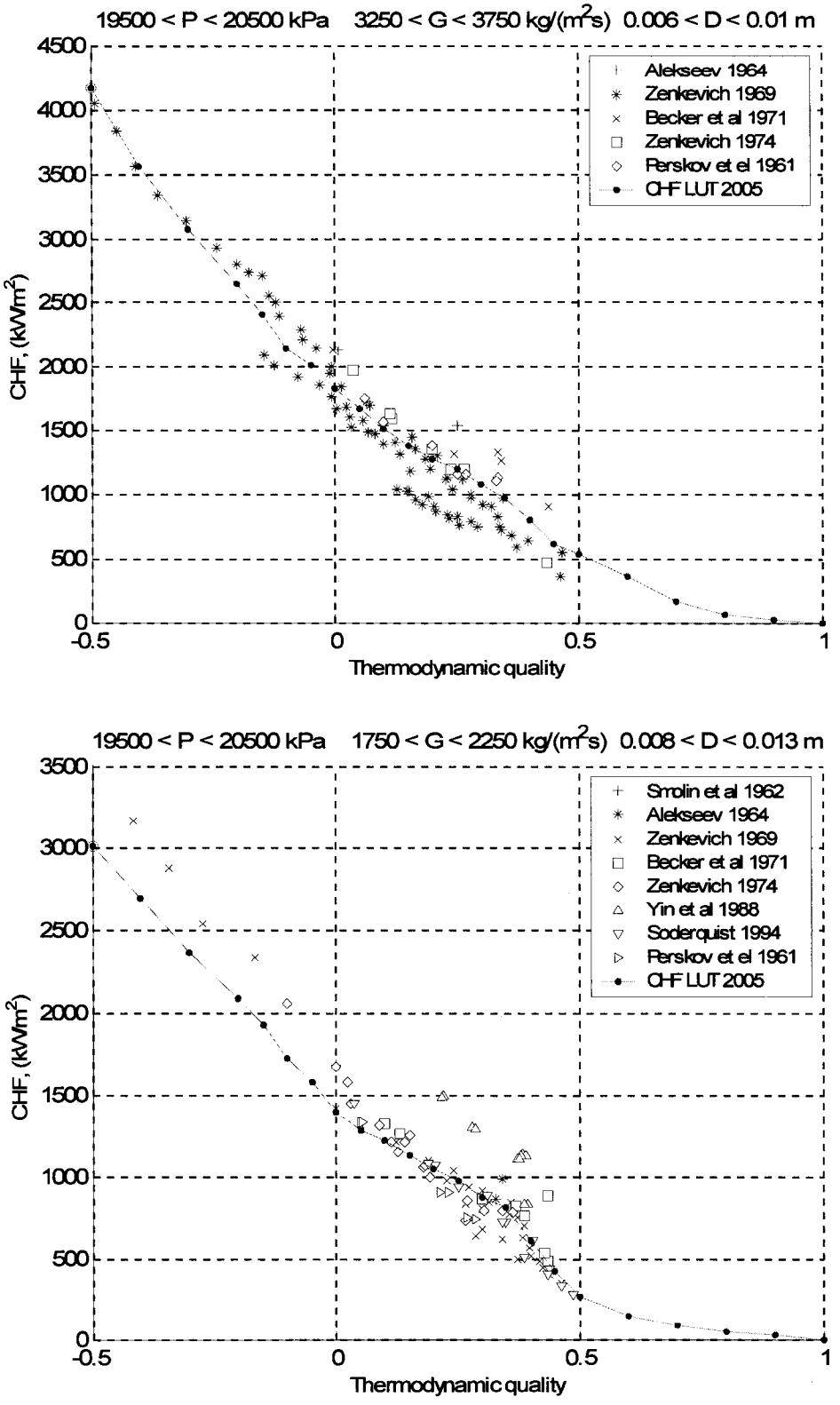

Figure 8-11 Slices showing a close agreement between the experimental data and CHF LUT 2005 at high pressures

Due to relatively low values of CHF, experimental data at high qualities (greater than 0.8) show a significant scatter, leading to higher errors for both constant inlet and local conditions.

There are different sources of experimental errors, negligible at high CHF values, but relatively important at low powers:

- heat losses, that at very low powers reduce the accuracy of the measured test section power, unless they are carefully accounted for and processed
- different types of measurement noises (such as drift signals, electromagnetic perturbations) become more important at low powers. Because of the random nature of some of these perturbations, it is expected that the measured values will be affected accordingly, contributing to data scatter.
- difficulty in detecting CHF at high x where CHF is low and post CHF heat transfer becomes quite efficient. (measurement of CHF becomes subjective as no clear temperature excursion occurs)

As suggested by the experimental data of Becker (1963) and Soderquist (1994), at high local qualities (0.8 – 0.9) situations may be encountered where the CHF is very low or close to zero. The experiments show that at low flows, when the liquid film is disrupted in rivulets, dry spots will occur on the heating surface, leading to the CHF condition. This phenomenon also contributes to high data scattering at high qualities, since the liquid film disruption is dependent on many second order parameters (surface roughness, flow stability), generally not accounted for in the CHF LUT.

It has been found that within the high quality region the calculated relative error of the CHF LUT is very high, for the most of experimental data. The reason is the definition used for the relative error:

$$\varepsilon = \frac{CHF_{\exp} - CHF_{pred}}{CHF_{\exp}} \times 100 \qquad (8.4)$$

At very high qualities, the measured CHF values (CHF_{exp}) are very small and because they appear in the denominator, the relative error is much higher than in other quality ranges. A particular case can be found at x=1, where CHF is always 0. Therefore, for any experimental data different than 0, the relative error is always 100%, regardless of the value of the measured CHF. The error analysis (Appendix 3, Table A3-1 and Table A3-4) shows for high quality very high negative average errors, -5.5% for inlet conditions and -55% for local conditions. The RMS errors are also high (~ 8%) for inlet conditions and 55% for local conditions. It appears that the LQR and the high quality region are the main sources of high errors for the CHF LUT.

8.4 Summary

CHF at LPLF conditions is governed by different mechanisms than CHF at higher flow, hence the CHF parametric trends and values are also different. For the LUT diameter range (3-25 mm ID) the most common CHF mechanism is counter current flow limitation or flooding, caused by upward vapour flow that prevents the liquid from flowing downward (under the influence of gravity) and cooling down the heated surface. For low pressures and very small diameter channels vapour bridging is the most likely CHF mechanism, while for large tube diameters, where sufficient liquid could be supplied to heated surface, a pool boiling-like mechanism occurs. Because the measured CHF in pool boiling experiments is often much larger than the CHF in tubes at low flows, a proper understanding of CHF mechanisms and their limits of applicability is very important.

Experiments have shown that at low flows, CHF is not very sensitive to inlet subcooling, but rather to mass flux and pressure. At the same flow conditions, higher diameter tubes have higher CHF; hence, the diameter effect has opposite trends with high flow conditions.

Comparison between the CHF LUT and zero/very low flow experimental data revealed a good agreement at medium qualities (~0.5); at subcooled conditions and low qualities the CHF LUT overestimates the measured value with a factor varying between 56 and 2.

At high pressures, the CHF LUT 2005 shows a good agreement with available experimental data: the error analysis shows no extreme error within this range. This result has been confirmed by visualization using slice method.

Very high quality data (x_e>0.8) show significant scatter and have very high relative errors, that worsen the error statistics of the CHF LUT within this region, especially the average errors. In spite of this, the absolute errors (the differences between predicted and measured CHF) are still within reasonable limits.

9. CONCLUSIONS AND RECOMMENDATIONS

9.1 Conclusions

1. Previous papers and reports related to the CHF LUT have identified the following areas in which improvements to the LUT derivation can be made, e.g. duplicate experimental data identification, experimental data screening, CHF at low flows, diameter effect and length-to-diameter ratio effect on CHF, and limiting quality region. The present work addresses the above mentioned issues through detailed examination of the steps of the CHF LUT derivation and investigation of the possible areas of improvement.

2. A new methodology for identification and marking of duplicate data has been developed. The method, based on the assessment of five flow parameters (P, G, x_c, dH_{in} and Tin), critical heat flux (q_c) and two geometrical parameters (D, Lh), has shown a very good efficiency.

3. Visualization software that display simultaneously slices of the CHF LUT and experimental data in all three P, G, and x parametric directions have been developed and successfully used in the assessment of the CHF LUT 2005 and its database.

4. An investigation of the diameter effect on CHF using the AECL-UO experimental database and a methodology based on experimental data regression produced a new correlation for diameter correction. The new correlation is based on a general form proposed by Groeneveld (1986) $(8/D)^n$, the exponent n being tabulated as a function of local P, G, and x.

5. Seven correlations for diameter correction have been assessed (Groeneveld (1986), Groeneveld (1995), Kirillov (1992), Tanase (2006), Wong (1996), Becker (1967) and Biasi(1967)) . The error analysis showed that although Wong (1996) gave the best results, there are no significant differences between the most analyzed correlations and the $CHF \sim d^{-0.5}$ appears an acceptable expression. In order to estimate the impact of the diameter correction factor for the CHF LUT, the case where no diameter correction was applied, has been employed as a special reference. An error assessment showed that the reference case (no

correction) has higher errors than the five best correlations assessed. The difference in RMS is 2.5% for HBM and 7.2% for DSM. Since the majority of experimental data are within 7 – 9 mm, it is concluded that this significant difference in errors came from a relatively small amount of data; hence, the diameter effect is important and should not be neglected.

6. The investigation of length-to-diameter effect on CHF suggested that the L/D screening criteria applied for CHF LUT 2005 derivation and assessment are properly chosen. The information on the L/D effect on CHF found in the literature is contradictory, especially for the L/D effect at high qualities. Assessments of the most recent L/D correction factor found in literature (Lee et al., 2000), revealed that it significantly reduced the data scatter at high quality range and slightly improved (1-2% RMS error, DSM) the accuracy of the CHF LUT. The implication is that using an L/D correction factor in conjunction with future versions of the CHF LUT would allow expansion of CHF data used for LUT derivation by relaxing the L/D screening criteria,

7. Most researchers agree that the limiting quality region is caused by the transition from entrainment-controlled to deposition-controlled dryout, when a sudden drop in the CHF value occurs. The CHF LUT 2005 was the first CHF prediction method that embedded the LQR, resulting in more realistic and accurate trends. Moreover, embedding the LQR within the CHF LUT has a positive impact on LUT error. Because of high data scatter, the prediction of CHF within the LQR is subject to high uncertainties.

8. An examination of experimental data and correlations for prediction of CHF at low flow revealed that CHF strongly depends on mass flux and, up to certain extent, on pressure. Inlet subcooling and local quality have a weak influence on CHF at low flows. Unlike medium and high flow, it appears that at very low flows, the CHF increases as heated channel diameter increases, for similar flow conditions.

9. Comparison of the predicted CHF at zero flow with experimental data has shown that CHF values of the CHF LUT are close to the pool boiling predictions, hence they may significantly overestimate the CHF. Further versions of the CHF LUT might use flooding type CHF correlations (such Mishima or Wallis) instead of pool boiling correlations. A table

with an over prediction factor, which can be used for further updating of the CHF LUT, has been produced, too.

10. The most effective way to improve the LUT accuracy is the removal of the small fraction of outlier data. The error assessment proved that the removal of 1% of outlier data improved the accuracy of the LUT by almost 10% for DSM and 1.3% for HBM. It seems that employment of a more elaborated diameter and L/D correction for further versions of the CHF LUT would improve the accuracy within 2-3% (DSM) and would have a positive impact on the LUT trends.

9.2 Recommendations for Future Work

The smoothness index quantifies the smoothness of the CHF LUT and it is an important feature of the CHF LUT. Examination of histograms displaying the smoothness versus P, G and x revealed that smoothness index is significantly affected by the average value of CHF for the range considered. This is obvious at very high qualities, where the smoothness index shows a very high peak without real basis and this may negatively influence the overall smoothness index of the CHF LUT. Future work may consider definition of a smoothness index less dependent on the average value of critical heat flux.

Although many aspects related to diameter or length-to-diameter effect on CHF have been investigated and some correlations for practical applications have been obtained, the physical mechanisms that govern these effects and their interconnection need further study.

Visualization and error analysis proved that employment of an L/D correction factor and new L/D screening criteria for CHF LUT derivation and assessment may lead to lower data scatter and better LUT error statistics, therefore they are recommended.

Future versions of the CHF LUT should reconsider the prediction at zero and very low flows, where the current versions of LUT appear to overpredict CHF due to pool boiling correlations.

REFERENCES

Ahmad, S.Y and Groeneveld, D.C., Fluid Modeling of Critical Heat Flux in Uniformly Heated Annuli, Proceedings of the International Symposium on Two-Phase Systems, Technion City, Haifa, Israel, 1972.

Ahmad, S.Y., Fluid to Fluid Modeling of Critical Heat Flux: a Compensated Distortion Model, Int. J Heat Mass Transfer, 16, pp. 641-662, 1973.

Baek, W.P., Kim, H.C., and Chang, S.H., An Independent Assessment of Groeneveld et. al.'s 1995 Look-Up Table, RCM for the IAEA CRP on Thermalhydraulic Relationship for Advanced Water Cooled Reactor, 1998.

Barnard, D.A., Dell, F.R., Stinchcombe, R.A., Dryout at Low Mass Velocities for an Upward Boiling Flow of Refrigerant-113 in a Vertical Tube, UKEA, AERE-R 7726, 1974.

Becker, K. M., Analytical and Experimental Study of Burnout Conditions in Vertical Round Ducts, Report, AE-178, 1965.

Becker, K.M., Hernberg, Bode, G., and Eriksson, O., Burnout Data for Flow of Boiling Water in Vertical Round Ducts, Annuli and Rod Cluster', Rept., AE-177, 1965.

Becker, K.M., An Analytical and Experimental Study of Burnout Conditions in Vertical Round Ducts, Nukleonik, Vol. 9, No. 6, 257-270, 1967.

Belyakov. V. V. Sokolov, and Koznetsov , A. N., Study of the Drop in Heat Removal Efficiency in Vertical Riser with a Nonuniform Peripheral Heat Supply, Energomashinostroyeniye, No.5, 1978, pp. 37-39.

Bennett, A.W., Hewitt, G.F., Kearsey, H.A. and Keeys, R.K.F., Heat Transfer to Steam Water Mixtures Flowing in Uniformly Heated Tubes in which the Critical Heat Flux has been Exceeded, AERE-R-5373, 1967.

Bergles A.E., Subcooled Burnout in Tubes of Small Diameter, ASME 63-WA-182, 1963.

Biasi, L., Clerici, G.C., Garriba, S., Sala, R. and Tozzi, A., Studies on Burnout, Part 3., Energia Nucleare, Vol 14, pp 530-536, 1967.

Boltienko, E.A., Vinogradov, W.N., Pomietko, R.S., and Katan, I.B., Effect of tube diameter on CHF at various two phase flow regimes, Report IPE-1889, 1988.

V. M. Borishanski, V. M., Gotovsky, M. A., Firsova, E. V., The Heat Transfer Crisis at the Steam Water Flowing Channels in High Steam Content Zones, Proceedings of the 5th International Heat Transfer Conference The Japan Society of Mechanical Engineering and the Society of Chemical Engineers, Tokyo. Japan, 1974, Paper B6.10.

Borishanskiy, V. M., Gotovsky, M. A., Firsova, E. V., Effect of Relative Pitch on Heat Transfer Rod Bundles at Turbulent Flow, Inzhenerno-Fisicheskiy Journal., Vol. 19, No 4, pp. 609-616, 1980.

Bowring, R.W., A Simple but Accurate Round Tube, Uniform Heat Flux, Dryout Correlation over the Pressure Range 0.7-17 MN/m^2 (100 – 2500 PSIA), United Kingdom Atomic Energy Authority, 1972.

Celata, P.G., On the Application Method of Critical Heat Flux Correlations, Nuclear Engineering Design, No.163, pp 241- 242, 1996.

Celata, G.P., Cumo, M., and Mariani, A., Geometrical Effects on the Subcooled Flow Boiling Critical Heat Flux, Rev. Gen. Therm., Vol. 36, pp. 807 – 814, 1997.

Celata, G. P., Cumo, M., Mariani, A., Simoncini, M., and Zummo, G., Rationalization of Existing Mechanistic Models for the Prediction of Water Subcooled Flow Boiling Critical Heat Flux, Int. J. Heat Mass Transfer, Vol. 37, Suppl. 1, pp. 347 – 360, 1994.

Celata, P.G and Mariani, A., Critical Heat Flux, Post Dryout and Their Augmentation, ENEA, 1998

Chandraker, P.K., Vijayan, P.K., Saha, D., Sinha, R.K., An Assessment of Critical Heat Flux Correlations and Lool-up Table, Sixteenth National Convention of Mechanical Engineers and All India Seminar on Future Trends in Mechanical Engineering, Research and Development, Dept of Mech & Ind. Engg, U.O.R, Roorkee, Sept. 29 – 30, 2000.

Chang, S.H., Baek, W.P., Tae Min Bae, A Study of Critical Heat Flux for Low Flow of Water in Vertical Round Tubes under Low Pressure, Nuclear Engineering Design, Vol. 132, pp. 225 – 237, 1991.

Chang, S.H. and Lee, K.W., A Critical heat Flux Model Based on Mass, Energy and Momentum Balance for Upflow Boiling at Low Qualities, Nuclear Engineering Design, Vol.113, pp.35-50, 1989.

Chen, G. Analytical and Experimental Studies of Critical Heat Flux in Complex Geometries, Master dissertation, Ottawa Carleton Institute for Mechanical and Aeronautical Engineering, University of Ottawa, 2001.

Chun, T.H., Hwang, D.H., Bang, J.G., Baek, W.P., Chang, S.H., Prediction of CHF in Fuel Assemblies, Using a CHF Table Method, Proceedings of the Korean Nuclear Society Autumn Meeting, October, 1997.

Chun S.,Y., Moon, S.K., Chung, H.J., Yang, S.K., Chung, K.M., Masanori, A., Critical heat flux under zero flow conditions in vertical annulus with uniformly and non-uniformly heated sections, Nuclear Engineering Design, No. 205, pp. 265-279, 2001.

Chung, J.B., Baek, W. P., and Chang, S. H., Effects of The Spacer And Mixing Vanes on Critical Heat Flux for Low-Pressure Water at Low Velocities, Int. Comm. Heat Mass Transfer, Vol. 23, No. 6, pp. 757-765, 1996.

Collier, J. G. and Thome, J.R., Convective Boiling and Condensation, third edition, Oxford Science Publications, 1996.

De Bortoli, R.A., Green, S.J., Letourneau, B.W., Troy, M and Weiss, A., Forced Convection Heat Transfer Burnout Studies for Water in Rectangular Channels and Round Tubes at pressures Above 500 psia, WAPD-188, 1958.

Doerffer, S., Groeneveld, D.C., Tain, R.M., Cheng, S.C., and Zegel, W., Fluid to Fluid Modeling of the Critical Heat Flux in Simple and Complex Geometries, Trends in Heat and Mass Transfer 1, 45-64, 1991.

Doerffer, S., Groeneveld, D.C. and Cheng, S.C., A Comparison of Critical Heat Flux in Tubes and Bilaterally Heated Annuli, Nuclear Engineering and Design, Vol 177, pp. 105-120, 1997.

Doroshchuk, V. E., Lantsman, F.P., and Levitan, L.L.,. A Peculiar Type of Burnout in Evaporator Tubes, Heat Transfer , Proceedings of the 4th International Heat Transfer Conference (Heat Transfer), Elsevier Publishing Co., Paper B6.1, 1970.

Doroshchuk, V.E., Levitan, L.L. and Lantzman, F.P., Recommendations for Calculating Burnout in a Round Tube with Uniform Heat Release, Teploenergetika Vol. 22 pp. 66-70, 1975.

Doroshchuk, V.E., Levitan, L.L. and Lantzman, F.P., Boiling Crisis in Evaporator Tubes, Heat Transfer-Soviet Research, Vol.12, No.6, 1980.

El-Genk M.S., Haynes, J.S., Kim, S.H., Experimental studies of CHF for low flow of water in vertical annuli near atmosphere pressure, Int. J. heat mass transfer, Vol.31, No.11, pp. 2291-2304, 1985.

Griffith, P., Counter-Flow Critical Heat Flux Related to Reactor Transient Analysis, EPRI 292-2, 1975.

Green, S., Saladna, E, Letourneau, B, and Sherba, P., CHF on a Coolant Channel Simulating a Closely Spaced Lattice of Rods, Proceedings ASME Winter Meeting, Symposium of two phase flow and heat transfer in rod bundles, p 72-80, 1969.

Groeneveld, D.C., Review of Scaling Methods as Applied to Deyout in High Pressure Water, CRNL-33, 1967.

Groeneveld, D.C., Freon Dryout Correlations and their Applicability to Water, AECL-3418, 1969.

Groeneveld, D.C., Similarity of Water and Freon Dryout Data for Uniformly Heated Tubes, ASME, 1970.

Groeneveld, D.C., On the Definition of Critical Heat Flux Margin, Nuclear Engineering Design , Vol.163, pp.45-247, 1996.

Groeneveld, D. C., Cheng, S. C., and Doan, T., AECL-UO Critical Heat Flux Look-up Table, Heat Transfer Engineering, Vol. 7, pp. 46 – 62,1986.

Groeneveld, D.C., Doerffer, S., Tain, R.M., Hammouda, N., and Cheng, S.C., Fluid-to-Fluid Modeling of the Critical Heat Flux and Post-Dryout Heat Transfer, Experimental Heat Transfer, Fluid Mechanics and Thermodynamics , pp.859-865, 1997.

Groeneveld, D. C., Joober, K, Wong, W., Leung, L.K.H., Cheng, S.C., The effect of Fuel Subchannel Geometry on CHF, NURETH-5, Salt Lake City, 1992.

Groeneveld D.C.,. Joober, K., Doerffer, S., Wong, W. , Leung, L.K.H., and Cheng, S.C., The Effect of Fuel Subchannel Geometry on CHF, Proceedings NURETH-5, Vol. II, pp. 683-690, Salt Lake City, Utah, 1992.

Groeneveld, D.C. Yousef, W.W., Spacing Devices for Nuclear Fuel Bundles: A Survey of their Effect on CHF, Post CHF Heat Transfer and Pressure Drop, 1980.

Groeneveld, D.C., Leung, L.K.H., Kirillov, P. L., Bobov, V. P., Smogalev, I. P., Vinogradov, V. N., Huang, X. C., and Royer, E., The 1995 Look-up Table for Critical Heat Flux in Tubes, Nuclear Engineering and Design, Vol. 163, pp. 1 – 23. 1996.

Groeneveld, D.C., Shan, J.Q., Vasic , A.Z., Leung, L.K.H., Durmayaz ,A., Yang, J., Cheng, S.C. , Tanase, A., The 2005 CHF Look-up Table, The 11th International Topical Meeting on Nuclear Reactor Thermal-Hydraulics (NURETH-11), Avignon, France, 2005.

Hall, D. D., and Mudawar, I., Critical Heat Flux for Water Flow in Tubes – II subcooled CHF correlations, Int. J. Heat Mass Transfer, Vol. 43, pp. 2605 – 2640, 2000.

Hejzlar, P. and Todreas, N.E., Consideration of Critical Heat Flux Margin Prediction by subcooled or Low Quality Critical Heat Flux Correlations, Nuclear Engineering Design, Vol. 163 , pp.215 -223, 1996.

Huang, X.C. and Cheng, S.C., Simple Method for Smoothing Multidimentional Experimental Data with Application to the CHF and Postdryout Look-up Tables, Numerical Heat Transfer, Part B, Vol. 26, pp. 425-438, 1994.

Inasaka, F and Nariai, H., Evaluation of Subcooled CHF Correlations for Tubes with and without Internal Twisted Tapes, Nuclear Engineering Design, 163, 1996.

Incropera, F.P. and DeWitt, D.P., Fundamentals of Heat and Mass Transfer, Fourth edition, 1996.

Katto K., Critical heat flux, Int. J. Multiphase Flow Vol. 20, Suppl., pp. 53-90, 1994.

Katto, Y., An Analytical Investigation on CHF of Flow Boiling in Uniformly Heated Vertical Tubes with Special Reference to Governing Dimensionless Groups, Int. J. Heat Mass Transfer, Vol.25, pp. 1353-1361, 1982.

Katto Y., A Prediction Model of Subcooled Water Flow Boiling CHF for Pressure in the Range 0.1-20.0 MPa, Int. J. Heat Mass Transfer, Vol. 35, pp.1115-1123, 1992.

Kim, I.G., Korol'kov, B.P., Enhancement of Steady-State Post-Dryout Heat Transfer in an Annulus with Spacers, Heat Transfer Soviet Res. , Vol.23 , no.5, pp. 649–657, 1991.

Kim, H. C., Baek, W. P., and Chang , S. H., CHF of Water in Vertical Round Tubes at Low Pressure and Low Flow Conditions, Nuclear Engineering Design, No. 199,pp 49-74, 2000.

Kitto J.B., Critical Heat Flux and the Limiting Quality Phenomenon, AICHE Symposium, Heat Transfer, No.199, Vol. 176, pp. 57-78, 1980.

Kirillov, P.L., Bobkov, V.P., Boltenko, E.A., Vinogradov, V.N., Katan, I.B., and Smogalev, I.P., Lookup Tables of Critical Heat Fluxes, Atomnya Energiya, Vol.71, No.1, pp.18-28, 1991.

Kirillov, P.L., Bobkov, V.P., Boltenko, Katan, I.B., E.A., Smogalev, I.P., and Vinogradov, V.N., New CHF Table for Water in Round Tubes, Report IPPE-2225, Obninsk, Russia.

Kirillov, P.L., Bobkov, V.P., Vinogradov, V.N., Donisov, V.S., Ivashkevitch, A.A, Katan, I.B., Paniutchev, E.I., Smogalev, I.P., and Sal'nikova, O.B., On Standard Critical Heat Flux

Data for Round Tubes, Proceedings of the 4th International Topical Meeting on Nuclear Reactor Thermalhidraulics, karlsruhe, F.R.G., Vol.1, pp.103-108.

Kirillov, P.L., and Yushenko, S.S. Diameter Effect on CHF, Working Material Presented at the Second Research Coordination Meeting, IAEA Coordinated Research Program on "Thermalhydraulic Relationships for Advanced Water-Cooled Reactors", Vienna, Austria, 1996.

Kutadeladze, S.S. and Leontev, A.I., Some Applications of the Asymptotic Theory of the Turbulent Boundary Layer, Proceedings of the 3rd Int. Heat Transfer Conference, Chicago, 1966.

Lahey, R. T. Jr., and F. J. Moody. The Thermal-Hydraulics of a Boiling Water Nuclear Reactor. 2nd ed. La Grange Park, IL: American Nuclear Society, 1993.

Lee, D.H., An Experimental Investigation of Forced Convection Burnout in High Pressure Water, Part IV, Large diameter tubes at about 1600 psi, AEEW-R 479, 1966

Lee, D.H., Burnout in a Cannel with Non-uniform Circumferential Heat Flux, UKAEA Report AEEW-R 477, 1966.

Lee, D. H., Obertelli, J. D., An Experimental Investigation of Forced Convective Burnout in High Pressure Water, part 1, Round Tubes with Uniform Heat Flux Distribution , Rept. AEEWR213, 1963.

Lee, Y. H., Baek, W. P., and Chang, S. H., A Correction Method for Heated Length Effect in Critical Heat Flux Prediction, Nuclear Engineering Design, Vol. 199, pp. 1 – 11, 2000.

Lee, C.H., Mudawar, I., A Mechanism Critical Heat Flux Model for Subcooled Flow Boiling on Local Bulk Flow Conditions, Int. J. Multiphase Flow, Vol.14, pp. 711-728, 1988.

Leung, L.K.H., A Model for Predicting the Pressure Gradient Along a Heated Channel During Flow Boiling, PhD dissertation, Ottawa Carleton Institute for Mechanical and Aeronautical Engineering, University of Ottawa, 1994.

Leung, L.K.H., Groeneveld, D.C., and Zhang, J., Prediction of the Obstacle Effect on Film-boiling Heat Transfer, Nuclear Engineering Design, Vol. 235, pp.687-700, 2005.

Lim J.C. and Weisman, J. A Phenomenologically Based Prediction for Rod-bundle Dryout, Nuclear Engineering Design, Vol. 105, pp. 363-371, 1988

Macbeth, R.V., Burnout Analysis, Part 4: Application of a Local Conditions Hypothesis to World Data for Uniformly Heated Tubes and Rectangular Channels, AEEW-R-267, 1963.

Mayinger F., Investigation into the CHF in Boiling Water, Rept. EUR-3347,1967.

Mishima, K., Flow Regime Transition Criteria for Upward Two Phase Flow in Vertical Tubes, Int. J. Heat Mass Transfer, Vol.27, No.3, pp.723-737.

Mishima, K., Nishihara, K, and Michiyosi, I, Boiling Burnout and Instability for Water Flowing in Round Tubes under Atmospheric Pressure, Int. J. heat mass transfer, Vol. 28, no.6, pp.1115-1129, 1985,

Mishima K. et al., Effect of Channel Geometry on Critical Heat Flux for Low Pressure Water, Int. J. Heat Mass Transfer, Vol. 30, no.6, pp.1169-1182, 1987.

Moeck, E.O., Matzner, B., Casterline, J.E., and Yuill, G.K., Critical Heat Fluxes in Internally Heated Annuli of Large Diameter Cooled by Boiling Water at 1000 psia, Proceedings of the 3rd International Heat Transfer Conference, vol III, p 86-97, A.I.Ch.E., New York .1966.

Moon, S.K., Baek, W.P., and Chang, S.H., Parametric Trends Analysis of Critical Heat Flux Based on Artificial Neural Networks, Nuclear Engineering Design, Vol. 163, pp. 29-49, 1996.

Morozov, Y, A Correlation for the Limiting Dryout Steam Quality in Forced Convection in Uniformly Heated Vertical Round Tubes, Int. J. Heat Mass Transfer, Vol.30, No.9, pp. 1885-1893, 1987.

Moshe Simon-Tov, Application of Energy Balance and Direct Substitution Method for Thermal Margin and Data Evaluation, Nuclear Engineering Design, Vol. 163, pp. 249-258, 1996

Ornatskiy, A. P., The Effect of Basic Regime Parameters and Channel Geometry on Critical Heat Fluxes in Forced Convection of Sub-Cooled Water, Heat Transfer – Soviet Research, Vol. 1, No. 3, pp.17 – 22, 1969.

Peng, S.W., Revellin, R., Groeneveld, D.C., Vasic, A.Z., Shang, D., and Cheng, S.C., Effects of Flow Obstacles on Film Boiling Heat Transfer, Nuclear Engineering Design, 222 (2003) 89-95

Peng, S. W., On the Smoothness of CHF/PDO Look-up Tables, Internal report, Department of Mechanical Engineering, University of Ottawa, 2002.

Peng S.W., Flow Boiling CHF and Limiting Quality Phenomenon in Tubes, private communication, University of Ottawa, 2004.

Pioro I.L., Cheng, S.C., Vasic, A.Z., and Salah, I, Experimental Evaluation of the Limiting Critical Quality Values in Circular and Non-circular Flow Geometries, Nuclear Engineering Design 190, 317-339, 1999.

Pioro, I.L., Doerffer, S.S., Cheng, S.C., An Eperimental Investigation of the Lmiting Critical Quality and its Impact on CHF in Horizontal and Vertical Tubes Cooled with Water and R-134a, 11th International Conference on Nuclear Engineering, Tokyo, Japan, 2003

Pioro, I.L., Groeneveld, D.C., Cheng, S.C., Experimental Study of the Effect of Flow Obstructions in a Circular Tube on the Critical Heat Flux, Proc. 9th Int. Topical Meeting on Nuclear Reactor Thermal Hydraulics (NURETH-9), San Francisco, California, 1999.

Pioro, I.L., Groeneveld, D.C., Cheng, S.C., Doerffer.S and Vasic, A., Effect of Flow Obstruction Shape on the Critical Heat Flux, Proceedings of ICONE 8 , 8th International Conference on Nuclear Engineering, April 2-6 , Baltimore, USA, 2000.

Shah, M.M., Improved General Correlation for Critical Heat Flux during Upflow in Uniformly Heated Vertical Tubes, Int. J. Heat Fluid Flow, vol. 8, pp 326-335, 1987.

Shan, J.Q., private Communication, 2004.

Shan, J.Q. ,Vasic, A. , Groeneveld , D.C., Peng S.W, Cheng S.C., and Tanase, A Methods in Improvement of 2005 CHF Look up table, UO-MCG-TH-2004-003, Technical Report, 2005.

Smolin, V.N., Boiling Heat Transfer Crisis in Tubes with Dispersed Annular Flow of Steam-Water Mixtures, Proceedins of the 4th International Heat Transfer Conference Heat Transfer 70. Elsevier Publishing Co., Amsterdam, Netherlands, 1970. Paper B6.8.

Smolin, V. N., Shpanskii, S.V., Esikov, V.I., and Sedova, T K., Comments on VTI Recommendations for Calculation of Critical Heat Flux in a Round Tube, Teploenergetika, Vol. 25, No. 2, pp. 13 – 16, 1978.

Stevens G. F., An Experimental Investigation into Forced Convection Burnout in Freon, with eference to Burnout in Water, AEEW-R 321, 1964

Thompson, B., and MacBeth, R.V., Boiling Water Heat Transfer Burnout in Uniformly Heated Round Tubes: A Compilation of World Data with Accurate Correlations, UKAEA AEEW – R356, 1964.

Tippets, F.E., Critical Heat Fluxes and Flow Patterns in High Pressure Boiling Water Flows, ASME Paper 62-WA-162 presented at the Winter Annual Meeting of the ASME, New York, 1962.

Tain, R.M., Cheng, S.C. and Groeneveld, D.C., Limitations of the Fluid to Fluid Scaling Techniquie for Critical Heat Flux, Int. J. Heat and Mass Transfer, Vol. 38, pp. 2195-2208 1995.

Tanase, A., Nakla, M., Zahlan El, H., Groeneveld, D.C. and Cheng, S.C., Impact of Circumferential Location of a Flow Obstacle on Critical Heat Flux in Tubes, UO-MCG-TH-2006-002, Technical Report, 2006.

Tavoularis, S., Measurements in Fluid Mechanics, Cambridge University press, 2005.

Tong, L.S., Hewitt, G.F., Overall Viewpoint of Flow Boiling CHF Mechanisms, ASME Paper 72-HT-54, 1972.

Tong, L.S, Boundary-Layer Analysis of the Flowing Boiling Crisis, Int. J. Heat Mass Transfer, Vol.11, pp. 1208-1211, 1968.

Vijayarangan, B.R. , Jayanti, S. and Balakrishnan, A.R., Studies on critical heat flux in flow boiling at near critical pressures, Int. J. Heat Mass Transfer, Vol.49, pp.259-268, 2006

Wallis, G.B., One-Dimensional Two-Phase Flow, MaGraw-Hill, New York, pp. 336–342, 1969.

Weisman, J., Pei, B.S., Prediction of Critical Feat Flux in Flow Boiling at Low Qualities, Int. J. Heat Mass Transfer Vol. 26 , pp. 1463-1477, 1983.

Ying, S. H. and Weisman, J. Prediction of the Critical Heat Flux in Flow Boiling at Intermediate Qualities, Int. J. Heat Mass Transfer Vol. 29 , pp. 1639-1648, 1986.

Whalley, P.B and Hewitt, G.F., The Correlation of Liquid Entrainment Fraction and Entrainment Rate in Annular Two-phase Flow, UKAEA Harwell report AERE-R 9187, 1978.

Wong, W.C., Effect of Tube Diameter on Critical Heat Flux, MSc dissertation, Ottawa Carleton Institute for Mechanical and Aeronautical Engineering, University of Ottawa, 1996.

Yildiz,S., Bartsch, G., A new correlation for the limiting quality of critical heat flux at low mass fluxes and low pressures, Int. J Energy Res., No.28, pp. 1101-1112, 2004.

Zuber, N., Hydrodynamic Aspects of Boiling Heat Transfer, Ph.D. thesis, Research Laboratory, Los Angeles and Ramo-Wooldridge Corporation, University of California, Los Angeles, CA,1959.

Appendix 1: Correlations for CHF prediction in bundles

Table A1-1 Correlations for prediction of CHF in bundles

Reference	Expression	Comments
Groeneveld (1995)	$CHF_{subchannel} = CHF_{D=8} F_{enh} MIN[F_{size}, F_{gap}]$ $Fgap = FxMIN[(Fmg)heated, (Fmg)unheated]$ $Fenh = 1 + 1.5K0.5xG0.2x\exp(\frac{-0.1Lsp}{Dhy})$ $Fx = 1 - 0.25K1[1 - Kx]$ $Kx = \begin{cases} 1.0 \\ 0.7942 - 1.375X \\ 0.3 \end{cases}$ $Fmg = MIN[1.0, 0.5 + 6\frac{\delta \min}{d}]$ $Fmg = MIN[1.0, 0.2 + 9\frac{\delta \min}{d}]$ $Fsize = \left(\frac{8}{Dhy}\right)^{1/3}$	Method based on correction factors which modify the CHF 8 mm tubes to account for differences between geometries, CHF mechanisms for tube and bundles K=spacer-plane loss coefficient Lsp= distance to the nearest upstream flow obstruction K1 =1 for similar adjacent subchannels and 0 for very different adjacent subchannels
Hwang (1992)	$\frac{q_c}{q_{ciso}} = 1 + \left(\frac{\partial q_c}{\partial G}\right)_x \frac{Go}{q_{ciso}}(F_G - 1) + \left(\frac{\partial q_c}{\partial x}\right)_G \frac{\Delta h_{iso}}{q_{ciso} h_{fg}}(F_H - 1)$	q_c is CHF for bundle, Go and Δh_{iso} are bundle averaged parameters q_{ciso} is CHF for an isolated subchannel, obtained from LUT at a diameter of heated equivalent diameter of subchannel. The derivatives are calculated from LUT.The

Reference	Expression	Comments
	$F_H = \frac{\Delta hi}{\Delta hiso} = \frac{Fi\left[1+\frac{\omega ij(zc/2)}{GoAi}\left(\frac{Dhi}{Dhj}\right)\left(\frac{Fj}{Fi}\right)\right]}{1+\frac{(\omega ij - wij)(zc/2)}{GoAi}}$ $F_G = \frac{Gc}{Go} = 1 - \frac{wijzc}{GoAi}$	correlation has an iterative solution methodology: calculates CHF for a mean isolated subchannel with a tube correlation. ΔPbundle is calculated and wij is assumed. Zb and xc are calculated and ΔPchannel is then calculated. The iteration is repeated until ΔPbundle =ΔPchannel. The validity range: 2-17 MPa 43-4800 kg m^{-2} s^{-1} 11.8<Dh<13.3 1.8<Lh<4.3
Bobkov et al. (1997)	$\frac{q''_{CHF}(D_{hy},P,G,X)}{q''_{CHF\_Table}(8mm,P,G,Xo)} = \left(\frac{D_{hy}}{8}\right)^n K_{bf}(P,G,X)$ $Xo = X + 0.05(C_o+1)^2(1-0.8P/P_{cr})$ $Co = 1.047(s/D)-1$ $Dhy = 1.103D[(s/D)^2-1]$ $Kbf(P,G,X) = [a + b\frac{P}{Pcr} + c\left(\frac{P}{Pcr}\right)^2 + d\left(\frac{P}{Pcr}\right)^3]\cdot[0.9+0.5(X-0.4)]$ $a=0.361+0.138g-0.01g^2$ $b=-1.59-0.584g+0.269g^2$ $c=4.8473+5.004g-1.367g^2$ $d=-2.46-5.32g+1.24g^2$ $g=G/1000$	The correlation is valid for triangular rod arrangement. The pitch/diameter >1.16 1-20 MPa x=0.4-0.8 G=150-5000 kg m^{-2} s^{-1}Average error=5% RMS=24%
Groeneveld et al (1986)	$q''_{CHF}=q''_{CHF-Table}*CHF_{mul}$	

Reference	Expression	Comments
	$CHFmul = \prod_{i=1}^{7} Ki$ $K1 = \left(\frac{0.008}{Dhe}\right)^{1/3} \quad for 0.02 < Dhy < 0.016m$ $K2 = \min[0.8, 0.8\exp(-0.5X^{1/3})]$ $K3 = 1 + 1.5K^{0.5}\left(\frac{G}{1000}\right)^{0.2}\exp(-0.1\frac{Lsp}{Dhy})$ $K4 = \exp(\frac{Dhy}{L}e^{2\alpha})$ $K5 = \begin{cases} X < 0 \Rightarrow K5 = 1 \\ X > 0 \Rightarrow K5 = [\frac{1}{(z - zo)}\int_{z,x=0}^{z} q''(z')dz'] / q''(z) \end{cases}$ $K6\begin{cases} (G < G1) \Rightarrow K6 = 0 \\ (G > G2) \Rightarrow K6 = 0 \\ G1 < G < G2 \Rightarrow K6 = \frac{G - G1}{G2 - G1} \end{cases}$	

<table>
<tr><th>Reference</th><th>Expression</th><th>Comments</th></tr>
<tr><td>Lee (1999)</td><td>$q"CHF = q"CHF - Table(P,G,Xex)Kcorrectio\ n - factors$
$Khy = \left(\frac{Dhy}{0.008}\right)^{-1/2}$
$Khl = \exp\left(\frac{Dhy}{L}e^{2\alpha}\right)$
$Kbf = AXB$
$A = \min[c1, c1\exp(-1.12X)]$
$B = \exp[-0.073 + 0.035(G/1000)]$
$Kw = \left(\frac{Dhy}{Dhe}\right)^{0.115}$
$Ksp = 0.86(1 + 0.155K^{1.5})$
$Krp = 2.51\exp(-0.82P_{radial\ max})$
$K5 = [\frac{1}{(z - zo)}\int_{z,x=0}^{z} q"(z')dz']/q"(z)$</td><td></td></tr>
<tr><td>Fortini et al. (2002)</td><td>$f_D = \frac{q_{crit\_measured}}{q_{crit\_8mm}}$
$f_D(x) = a_0\left(\frac{D}{8}\right)^{a1+a2x}\left(\frac{Dh}{Dw}\right)^{a_3}\left(\frac{\rho_f\sigma}{G^2Dw}\right)^{a_4}$
<table><tr><th>Region</th><th>a0</th><th>a1</th><th>a2</th><th>a3</th><th>a4</th></tr><tr><td>1</td><td>0.414</td><td>-0.006</td><td>1.526</td><td>0.246</td><td>-0.063</td></tr><tr><td>3</td><td>0.326</td><td>-0.463</td><td>0.337</td><td>0.327</td><td>-0.111</td></tr><tr><td>5</td><td>0.015</td><td>2.813</td><td>8.762</td><td>1.00</td><td>-0.184</td></tr></table></td><td>The regions are delimited by Xo, X1, X2, X3</td></tr>
</table>

Reference	Expression	Comments
	$X1 = 2.7\left(\frac{\rho_g \sigma}{G^2 D}\right)^{0.25}\left(\frac{\rho_g}{\rho_f}\right)^{0.333}$ $X2 = 4.3\left(\frac{\rho_g \sigma}{G^2 D}\right)^{0.204}\left(\frac{\rho_g}{\rho_f}\right)^{0.214} \quad if P < 6MPa$ $X2 = 3.6\left(\frac{\rho_g \sigma}{G^2 D}\right)^{0.28}\left(\frac{\rho_g}{\rho_f}\right)^{0.0119} \quad if P > 6Mpa$ $X3 = 6.11\left(\frac{\rho_g \sigma}{G^2 D}\right)^{0.238}\left(\frac{\rho_g}{\rho_f}\right)^{0.204} \quad if P < 6MPa$ $X3 = 4.53\left(\frac{\rho_g \sigma}{G^2 D}\right)^{0.3}\left(\frac{\rho_g}{\rho_f}\right)^{-0.0367} \quad if P > 6MPa$ $X0 = \frac{\rho_g \alpha\left\{1 + 1.53(1-\alpha)G^{-1}[g\sigma\rho_f{}^2(\rho_f - \rho_g)]^{1/4}\right\}}{\alpha\rho_g + (1-\alpha)\rho_f}$	

Appendix 2: Experimental data sets, as per January 2007

	Source of CHF Data	Number of data points	Tube Diameter	Heating Length	Pressure	Mass Flux	Critical Quality	Inlet Sub-cooling	Heat Flux	Inlet Temperature
	Reference	number	mm	m	kPa	kg m^{-2} s^{-1}	-	kJ kg^{-1}	kW m^{-2}	°C
1	Alekseev (19??) data from Kirillov.	70	10.00 10.01	1.000 4.966	9800 19610	216 7566	-0.866 0.944	57 1398	134 4949	139.77 357.93
2	Becker et al. (1963).	2,659	3.94 20.10	0.100 3.750	216 8973	100 3183	-0.069 1.054	-50 1640	278 7477	25.42 217.80
3	Becker et al. (1965) AE-RTL-778.	1,326	3.93 37.47	0.216 3.750	1128 9905	159.5 5586	-0.005 0.993	-16 2711	503 6620	63.32 288.71
4	Becker et al. (1970) TPM-RL-1260.	116	2.40 36.03	0.500 1.880	3050 7100	93.3 2725	0.207 0.903	371 1065	1026 5130	51.75 113.22
5	Becker et al., (1971) KTH-NEL-14.	1,455	10.00 10.01	1.000 4.966	3000 20000	156 8111	-0.866 1.061	26 1414	135 5476	124.75 358.65
6	Bennett et al. (1965) AERE-R 5055.	201	9.22 12.62	1.524 5.563	6612 7481	623.8 5844.4	0.026 0.948	21 691	589.6 3299.7	157.67 279.45
7	Bergelson (1980) data from Kirillov.	328	8.00	0.241 0.400	170 3080	1927 7078	-0.295 0.090	96 853	3511 14571	28.94 169.20
8	Bergles (1963) ASME 63-WA-182.	117	0.62 6.21	0.011 0.155	140 586	1518.7 24272.4	-0.137 0.111	25 534	4957.1 44713	3.10 116.55
9	Bertoletti et al. (1964) CISE-R-90.	386	4.90 15.20	0.050 2.675	4881 9876	1051 3948.8	-0.083 0.774	-28 769	198.7 7502.8	112.97 302.14
10	Borodin (19??) CRNL-2538.	494	8.92	3.690 3.990	8205 10385	1331.3 6927.4	0.105 0.535	31 456	541.5 2304.4	230.54 308.34
11	Celata, G.P. and Mariani, A. (1993).	88	0.10 22.50	0.002 0.610	90 6890	917 90000	0.007 0.923	88 1023	4000 228000	3.44 245.78
12	Cheng et al. (1983).	150	12.60	0.370 0.740	101 687	50 400	0.187 1.227	42 210	331.2 2115	70.00 154.61
13	Dell et al. (1969) AERE-M 2216.	82	6.17	0.914 5.512	6895	14328.9 4135.8	0.144 0.779	79 365	492.7 3340.4	217.13 270.09

	Source of CHF Data	Number of data points	Tube Diameter	Heating Length	Pressure	Mass Flux	Critical Quality	Inlet Sub-cooling	Heat Flux	Inlet Temperature
	Reference	number	mm	m	kPa	kg m^{-2} s^{-1}	-	kJ kg^{-1}	kW m^{-2}	°C
14	Era et al. (1967).	163	5.98	1.602 4.800	6777 7049	1105 3014.9	0.374 0.952	-1211 565	109.2 1960.9	181.13 509.30
15	Griffel, J. (1965) NYO-187-7.	397	6.22 37.46	0.610 1.972	3448 10343	637.3 18577.2	-0.209 0.592	45 1209	1400.6 8107.3	87.68 287.07
16	Groeneveld D.C. (1985)	118	10.00	1.000 2.000	7900 20000	282 2805	-0.097 0.805	622 1733	1133 5479	120.32 279.79
17	Hassid et al. (1967) CISE-R-236.	191	24.90 25.10	1.590 2.391	2942 6090	369.3 3857.5	-0.035 0.838	1427 3433	1430.9 3444.1	153.89 267.66
18	Hewitt et al. (1965) AERE-R 4864.	442	9.30	0.229 3.048	101 208	90.9 301	0.160 1.083	-41 383	144 4013	13.71 119.39
19	Jens and Lottes (19??) subcooled burnout data.	48	5.74	0.625	3448 13790	1301.8 10603.9	-0.464 -0.015	279 1310	2965.3 11924.4	70.52 285.05
20	Judd and Wilson (1966) BAW-3238-9	49	11.30	1.829	6861 13859	673.9 3428	0.016 0.776	33 730	593.1 2668.8	207.11 323.84
21	Kirillov et al. (1984).	2,470	7.71 8.09	0.990 6.000	6370 18040	494 4154	-0.494 0.981	7 1537	110 7700	79.41 350.90
22	Ladislau (1978) data from Kirillov.	136	4.00	0.200	420 1000	884 5504	-0.051 -0.009	104 638	1860 4631	28.04 149.56
23	Lee (1966) AEEW-R479.	435	14.10 44.70	0.635 1.524	8237 12579	332.2 3410.3	-0.110 0.780	60 451	870.7 3738.2	259.80 318.09
24	Leung et al. (1989).	66	5.45	2.511	5030 9710	1167.6 9938.3	0.210 0.578	6 316	656.2 3058.3	227.85 305.33
25	Leung et al. (1990).	39	8.94	2.490	7030 9580	1956.3 7611.6	0.106 0.414	13 229	904.2 2328	243.79 305.38
26	Lowdermilk et al. (1958).	470	4.00 4.80	0.119 0.991	100	27.2 4865.5	0.030 1.236	317 331	167 9525	20.91 24.24
27	Matzner et al. (1965) ASME 65-WA/HT-30.	99	10.20	2.438 4.877	6893	1193.3 9559.8	0.008 0.693	48 1183	643.5 4041	65.61 275.82
28	Mayinger (1967).	128	7.00	0.560 0.980	1925 10244	2233 3734	0.098 0.405	-239 314	924 5618	233.28 310.09
29	Nguyen and Yin (1975) CWTM-013-HT.	56	12.60	2.438 4.877	6645 8401	929.6 3838.4	0.216 0.738	52 413	677 2023.7	225.06 276.81

	Source of CHF Data	Number of data points	Tube Diameter	Heating Length	Pressure	Mass Flux	Critical Quality	Inlet Sub-cooling	Heat Flux	Inlet Temperature
	Reference	number	mm	m	kPa	kg m^{-2} s^{-1}	-	kJ kg^{-1}	kW m^{-2}	°C
30	Rudzinski (19??) MR1-A Data (Private Communication).	106	8.00	1.745	3073 10127	1232.7 7831.8	0.038 0.727	19 495	1388.2 4511.7	133.52 299.43
31	Smolin et al. (1962).	369	3.84 10.80	0.776 4.000	7840 19610	498 7556	-0.132 0.795	5 1329	230 5652	140.35 350.39
32	Smolin et al. (1979) data from Kirillov.	2,987	3.84 16.00	0.690 6.050	2940 17710	490 7672	-0.136 0.789	4 1362	245 5626	72.72 351.65
33	Snoek (19??) (CRNL-4231).	32	11.90	1.500	9460 9610	980 5060	0.034 0.543	-481 356	422.6 3036.8	246.68 303.95
34	Tong (1964).	266	6.22 12.90	0.380 3.660	5171 13790	678 14002	0.002 0.502	5 1060	587 6139	263.94 330.85
35	Yin et al. (1988) 25th Nat. Heat Trans. Conf.	287	13.40	3.658	1028 21197	1938.9 2081.6	0.075 0.431	0 493	583.3 1863.7	128.42 358.41
36	Zenkevich (1969) data from Kirillov.	5,595	3.99 15.10	0.250 6.000	5880 19610	498 9876	-1.652 0.964	2 1644	136 14760	76.01 361.79
37	Zenkevich et al. (1971) data from Kirillov.	392	7.80 8.05	7.000 20.000	6860 17650	1008 2783	0.262 0.876	18 1549	47 1283	81.96 352.22
38	Zenkevich (1974) data different from the others.	823	4.80 12.60	1.000 6.000	5890 19620	497.2 6694.4	-0.221 0.969	5 1381	230 4740	96.70 358.24
39	Ornatskii and Kichigin (1961)	222	2.00	0.04	1013 7599	5000 30000	-0.654 -0.002	72 1176	6392 70895	2.25 263.8
40	Ornatskii and Kichigin (1962)	169	2.00	0.04	7599 15199	5000 30000	-1.23 -0.026	79 1566	8136 72058	0.88 331
41	Babcock et al (1962)	39	8.00 22.5	0.61	413 6890	2946 11452	-0.187 -0.05	202 639	4876 10546	19 177
2	Swenson et al(1962)	25	10.4 10.5	1.75 1.80	13790	679 1765	0.178 0.502	44 564	587 1063	231 329
43	Hood et al (1962) set 1	61	6.30 25.4	0.61	414 8412	2156 11390	-0.25 -0.05	204 1113	5741 11830	-20 243
44	Hood et al (1962) set 2	24	8.00 22.2	0.60 1.10	6895	664 2726	0.001 0.484	66 1224	3186 4637	7.5 272
45	Alessandrini et al (1963)	753	15.2 24.9	0.80 2.46	4795 5148	1080 4140	-0.04 0.75	-1110 365	206 3689	185 265
46	Ornatskii (1963)	69	2.00	0.04	17732 20265	5000 30000	-2.41 -0.054	175 1811	5579 70314	-21 335
47	Peterlongo et al	349	15.1	1.62	4933	1010	-0.02	-90	895	27

	Source of CHF Data	Number of data points	Tube Diameter	Heating Length	Pressure	Mass Flux	Critical Quality	Inlet Sub-cooling	Heat Flux	Inlet Temperature
	Reference	number	mm	m	kPa	kg m^{-2} s^{-1}	-	kJ kg^{-1}	kW m^{-2}	°C
	(1964)		15.2	4.02	6551	4020	0.608	1038	4115	281
48	Zenkevich et al (1964)	63	6.8 10.0	0.10 0.39	3924 9810	550 6444	-0.02 0.693	131 279	4910 9710	211 286
49	Biancone et al (1965)	245	10.2 17.1	0.78 1.32	7914 14396	465 3167	-0.25 0.662	45 1355	742 6649	48 326
50	Burck and Hufschmidt (1965)	143	10.0	0.35	1100 3090	917 3756	-0.246 0.087	532 939	4500 12200	16.7 60.8
51	Ortnaskii and Viniarskii (1965)	109	0.50	0.014	1013 7194	20000 90000	-0.572 -0.107	321 1942	39542 224459	-20 195
52	Waters et al (1965)	37	11.2	0.61 3.65	6895 10342	6578 9548	-0.033 0.322	-322 1050	2017 5389	87 313
53	Lee (1965)	38	9.50	1.73 3.05	6828 7024	2020 5720	0.002 0.433	75.5 577	1307 3873	161 271
54	Babarin et al (1969)	163	12.0	0.96 1.80	284 310	50 500	0.466 1.091	37.6 495	190 2300	15 124
55	Bailey and Lee (1969)	158	9.30	3.05	6895 18340	958 4242	0.069 0.727	54 604	344 2221	199 347
56	Shlykov et al (1970)	60	3.60	0.10	76.5 386	12865 25494	-0.167 -0.022	149 508	12800 30300	3 98
57	Compolunghi (1973)	218	12.0	15.6 20.5	254 9660	1111 2545	0.296 0.772	19.6 740	155 479	205 260
58	Bailey (1977)	110	15.0	3.77 5.37	1350 7080	49 1383	0.45 0.99	-178 473	84 1134	93 286
59	Williams and Baus (1980)	129	9.50	1.84	2758 15169	324 4663	-0.025 0.929	140 1223	388 4073	90 315
60	Cheng et al (1983)	132	4.80	0.19 0.38	100 700	300 750	0.082 0.765	42 214	889 2131	49.6 145
61	Nariai (1987)	93	1.00 3.00	0.009 0.101	100	6710 20910	-0.134 0.007	149.5 353	4647 69990	15.4 64
62	Inasaka and Nariai (1989)	29	3.00	0.10	290 1050	4300 29900	-0.188 -0.051	266 626	7300 44500	25 78
63	Weber and Johannsen (1990)	55	9.70	0.043	110 1200	10.8 301	0.072 1.53	4.2 577	1495 7572	65 175
64	Inasaka ey al (1991)	8	6.00	0.10	104 114	6520 11364	-0.09 -0.07	250 266	7280 11200	39 41
65	Nariai et al (1991)	7	6.00	0.10	196 1470	7700 9952	-0.24 -0.096	306 618	12110 17230	33 53
66	Olekhnovitch (1991)	479	8.00	0.75 3.50	507 4036	977 6122	0.046 0.761	4 498	523 5550	47 244
67	Jafri (1993)	49	15.8	2.44	317 1060	1439 8102	-0.021 0.28	223 667	1795 5691	19 129
68	Vandervort et al (1994)	210	0.30 2.70	0.002 0.066	131 2277	8438 41810	-0.276 -0.018	169 759	18700 123800	6.4 85

	Source of CHF Data	Number of data points	Tube Diameter	Heating Length	Pressure	Mass Flux	Critical Quality	Inlet Sub-cooling	Heat Flux	Inlet Temperature
	Reference	number	mm	m	kPa	kg m^{-2} s^{-1}	-	kJ kg^{-1}	kW m^{-2}	°C
69	Celata et al (1992) set 1	60	6.00 8.00	0.10 0.15	398 5120	2019 10046	-0.517 -0.106	350 1018	7428 29514	29 81
70	Celata et al (1992) set 2	78	2.50 5.00	0.20 0.40	107 2181	2166 32637	-0.091 0.287	345 790	5347 42777	19 55
71	Celata et al (1993)	78	2.50	0.10	578 2714	11240 40000	-0.357 -0.104	387 844	12113 60579	30 70.5
72	Ruan (1994)	41	9.00	0.40	106 707	12 207	0.469 0.966	15 279	139.4 1955	40 153
73	Soderquist (1994)	1,463	8.00 8.10	1.00 6.00	970 20120	243 6086	-0.169 1.336	35 693	94 3879	112 355
74	Tain (1994)	55	8.00	1.75	6849 10127	2401 7832	0.028 0.378	27 455	1341 4358	191 299
75	Pabisz and Bergles (1996)	10	4.40 6.20	0.11 0.154	627 1284	2417 4994	-0.196 -0.133	567 698	7370 13880	15.3 46
76	Doerffer (1997)	175	8.00	2.05	7890 11237	2685 7625	0.004 0.301	11.66 731	1172 4442	159 309
77	Kureta (1997)	913	1.00 6.00	0.04 0.68	101.3	4.1 19130	-0.147 1.664	0 391	185 158100	6.7 100
78	Yild (1997)	385	6.00 8.00	0.17 0.31	90 721	48.5 411	0.001 0.914	-4.26 1057	533 4381	31 158
79	Doerffer (1999)	116	8.00	1.98	5874 11117	491 5112	0.069 0.951	30 772	547 2355	157 307
80	Mudawar and Bowers (1999)	174	0.40 2.50	0.004 0.031	250 17240	5000 134000	-1.778 -0.062	254 1579	9400 276000	18 70
81	Kim et al (2000)	502	6.00 12.0	0.30 1.77	104 951	21 277	0.397 1.251	0.8 634	130 1598	20 156
82	Baik (2001)	56	6.00 10.0	0.18 0.40	101 3618	497 2032	-0.091 0.099	254 935	2041 7413	5.9 40.2
83	Shan (2004)	24	8.00	1.00	13337 14808	572 4137	-0.022 0.422	97 692	819.5 4511	198 328
84	Stein (2004)	383	9.00	0.13 0.45	1090 7140	24 304.5	-0.002 1	215 1245	237.5 4700.5	134 272
85*	Becker and Ling (1970)	87	24.7	7.10	5000 15000	177 2293	0.248 1.059	37.4 434	204 1264	202 333
86*	Becker (1966)	10	10.0	5.00	6865	752 3050	0.35 0.86	448 618	725 1484	152 191
87*	Clark and Rohsenow (1952)	89	4.60	0.24	689 13789	13 102.3	0.61 0.995	94 1402	113 1199	27 301
88*	Cumo (1979)	190	12.9	8.00 9.87	6720 7400	300 2036	0.44 1.064	94 526	161 869	176 267
89*	De Bortolo and Masnovi (1957)	33	4.70	0.31	13789	284 5696	-0.226 0.665	92 700	959 9022	201 322
90*	Eicheldinger (1962)	26	10.6	0.38 0.76	6860 8274	713 1492	0.022 0.217	316 1033	3470 5899	69 220

	Source of CHF Data	Number of data points	Tube Diameter	Heating Length	Pressure	Mass Flux	Critical Quality	Inlet Sub-cooling	Heat Flux	Inlet Temperature
	Reference	number	mm	m	kPa	kg m^{-2} s^{-1}	-	kJ kg^{-1}	kW m^{-2}	°C
91*	Fiori and Bergles (1968)	12	2.40	0.072	193 634	2034 6103	0.031 0.189	48 230	5457 17224	82 141
92*	Hood and Isakoff (1962)	28	8.00 23.7	0.61	6895	692 2726	-0.032 0.484	66 906	3180 5281	84 264
93*	Isakoff and Measley (1962)	10	7.90 12.9	0.60 1.10	6895	665 2007	0.02 0.419	369 730	3310 4639	125 208.5
94*	Jens and Lottes (1952)	34	23.9	0.20 0.86	103.4	9.8 47.3	0.2 0.83	356	156 943	15.5
95*	Kino (1998)	7	6.00	0.06	600 1100	4994 8888	-0.246 -0.179	494 615	15000 24400	39 42
96*	Little and Trenberth (1966)	13	9.50	0.53	3827 3896	2049 9499	-0.253 -0.05	858 870	7000 18000	45 51
97*	Longo (1957)	20	5.30	0.22	102 791	3051 9046	-0.05 -0.01	110 332	2139 9211	44 122
98*	Mc Gill and Sibbitt (1951)	47	3.60	0.07 0.08	1935 21751	212 10173	0.08 6.47	32 1726	1233 13281	31 340
99*	Peskov et al (1961)	264	8.00 10.0	0.25 2.10	9807 19613	492 5542	0 0.431	24 1238	582 4931	36.5 361.5
100*	Reynolds (1957)	67	4.60	0.23	3558 10687	1165 2889	-0.128 0.47	14 803	3596 9022	111 284
101*	Umekawa (2005)	84	3.00 20.0	0.90	300 400	17 1800	0.183 1.402	226 478	162 1785	30 80
102*	Weatherland (1963) set 1	62	1.10	0.114	1379	3716 15732	0.076 0.663	-647 66	2432 21420	179 194
103*	Weatherland (1963) set 1	232	7.70	0.46	13790	171 2712	-0.817 0.718	0 1398	817 5363	36 335
104*	Hunt et al (1955)	93	4.70	0.32	6895 13789	521 10524	-0.458 0.3	35 1403	852 147633	35 331
105*	Lowdermilk and Weiland (1951)	155	1.00 3.00	0.025 0.152	101 13790	27 5750	-0.181 0.94	0 1249	88 19274	23 234
106*	Epstein et al (1956)	180	1.90	0.15 0.70	10342 18961	1845 4232	-0.507 -0.026	329 1660	2082 6751	21 288
107*	Bergles et al (1958)	200	9.70 20.9	0.61 2.44	3392 6971	-4387 5120	0 0.986	-1136 643	165.5 6021	115 285
108*	Ceresa et al (1974)	167	4.80 7.90	1.83 6.00	4710 5130	198 3036	0.153 1.086	79 885	127 3467	71 251
109*	Lee (1963)	609	6.00 11.0	0.216 2.00	3620 11687	407 4421	-0.135 1.01	11.63 698	911 8095	90 305
110*	Mihaila et al (1970)	149	4.00	0.20	417 1000	821 5583	-0.051 -0.004	100 627	1898 4631	26 147
111*	Tramontini et al (1951)	60	5.70	0.64	3447 13789	1302 10375	-0.474 0.506	-8.6 1307	1563 12048	40 287
112*	Lee (1969)	68	9.30	0.56 3.00	1965 2999	650 1391	0.221 0.833	60 893	806 3775	19 207

	Source of CHF Data	Number of data points	Tube Diameter	Heating Length	Pressure	Mass Flux	Critical Quality	Inlet Sub-cooling	Heat Flux	Inlet Temperature
	Reference	number	mm	m	kPa	kg m^{-2} s^{-1}	-	kJ kg^{-1}	kW m^{-2}	°C
113*	Nilson et al (1970)	588	9.30 10.0	1.98 2.01	2910 9210	199 6151	0.02 1.444	12 562	457 4576	128 300
114*	Weatherhead and Lottes (1954)	92	4.70	0.32	6895 13790	521 9873	-0.459 0.309	35 1402	851 14754	35 331
115*	Zou (2003)	53	14.0	2.10	180 400	90 400	0.439 1.042	-952.8 522.68	202 953	19 144
116*	Belyakov et al (1976)	442	30.0 40.0	6.00 8.00	10395 20790	-1050 1875	0 0.947	-736 1244	50 992	93 362
	All 116 data sets	36510	0.100 44.700	0.002 20.000	90 21,751	4.1 134000	-2.41 6	-1,211 3,433	47 276,000	-21 509.30

The lines 85-116 (marked with *) have been added between 2005-2006

Appendix 3: Detailed error analysis for CHF LUT 2005 and various diameter effect correlations

Detailed error analysis of LUT 2005 using different diameter correction correlations

Be	Becker (1967)
Bi	Biassi (1967)
G86	Groeneveld (1986)
G95	Groeneveld (1995)
K	Kirillov (1992)
N	No correction
T	This thesis
W	Wong (1996)

Table A3-1 Error distribution with respect of critical quality for different diameter corrections, at constant inlet conditions

	X	-0.5	-0.4	-0.3	-0.2	-0.1	0	0.1	0.2	0.3	0.4	0.5	0.6	0.7	0.8	0.9	1
T	Avg	0.66	-0.04	0.21	0.08	-0.29	-0.50	0.40	0.53	0.33	1.49	0.49	-1.29	-1.09	-0.92	-2.34	-4.78
	RMS	5.74	5.41	5.42	5.05	5.19	5.70	5.00	7.50	6.70	8.32	8.05	8.99	8.05	8.10	6.97	7.07
K	Avg	1.99	0.56	2.14	4.20	4.36	4.30	2.70	2.00	1.41	2.53	1.84	0.32	-0.32	-0.40	-2.58	-5.19
	RMS	10.84	9.14	10.67	14.30	17.05	17.70	10.01	8.34	6.97	8.57	8.61	9.00	8.11	8.02	6.67	7.93
W	Avg	1.13	0.18	0.50	0.11	-0.39	-0.39	0.66	0.53	0.21	1.31	0.42	-1.15	-1.45	-1.17	-3.19	-5.59
	RMS	6.99	5.74	5.68	5.07	5.31	5.80	5.04	6.96	6.56	8.03	7.91	8.90	8.32	8.57	7.15	8.55
G86	Avg	0.90	0.18	0.49	0.25	0.01	0.21	1.25	1.21	0.88	2.07	1.35	-0.17	-0.63	-0.65	-2.75	-5.26
	RMS	6.12	5.56	5.62	5.10	5.20	6.12	5.64	7.09	6.52	8.20	8.25	8.80	8.11	8.03	6.80	8.00
G95	Avg	0.66	0.19	0.14	-0.74	-1.12	-0.89	0.43	0.34	0.16	1.34	0.52	-1.00	-1.29	-1.05	-3.06	-5.51
	RMS	5.39	5.46	5.58	5.60	6.55	6.23	5.15	7.06	6.62	8.02	7.92	8.82	8.21	8.41	6.96	8.39
Be	Avg	2.61	2.59	1.78	1.49	1.93	3.41	3.90	3.21	2.35	3.27	2.41	0.71	0.45	0.34	-2.43	-5.13
	RMS	8.11	8.37	6.63	6.47	8.34	10.12	9.76	9.81	8.45	9.31	9.26	9.45	9.07	8.44	6.54	7.82
Bi	Avg	0.70	0.34	0.23	-0.56	-0.76	-0.34	0.85	0.69	0.33	1.46	0.64	-0.91	-1.22	-0.88	-3.10	-5.50
	RMS	5.34	5.60	5.73	5.78	6.64	6.28	5.51	7.48	6.86	8.14	7.97	8.86	8.20	8.33	6.95	8.43
N	Avg	1.43	0.24	1.21	2.43	2.48	2.71	3.11	2.93	2.18	3.41	2.88	1.37	0.46	0.08	-2.18	-4.77
	RMS	8.30	6.78	7.53	9.32	10.52	12.19	11.08	10.61	8.43	9.79	9.94	9.99	8.84	8.25	6.71	7.29

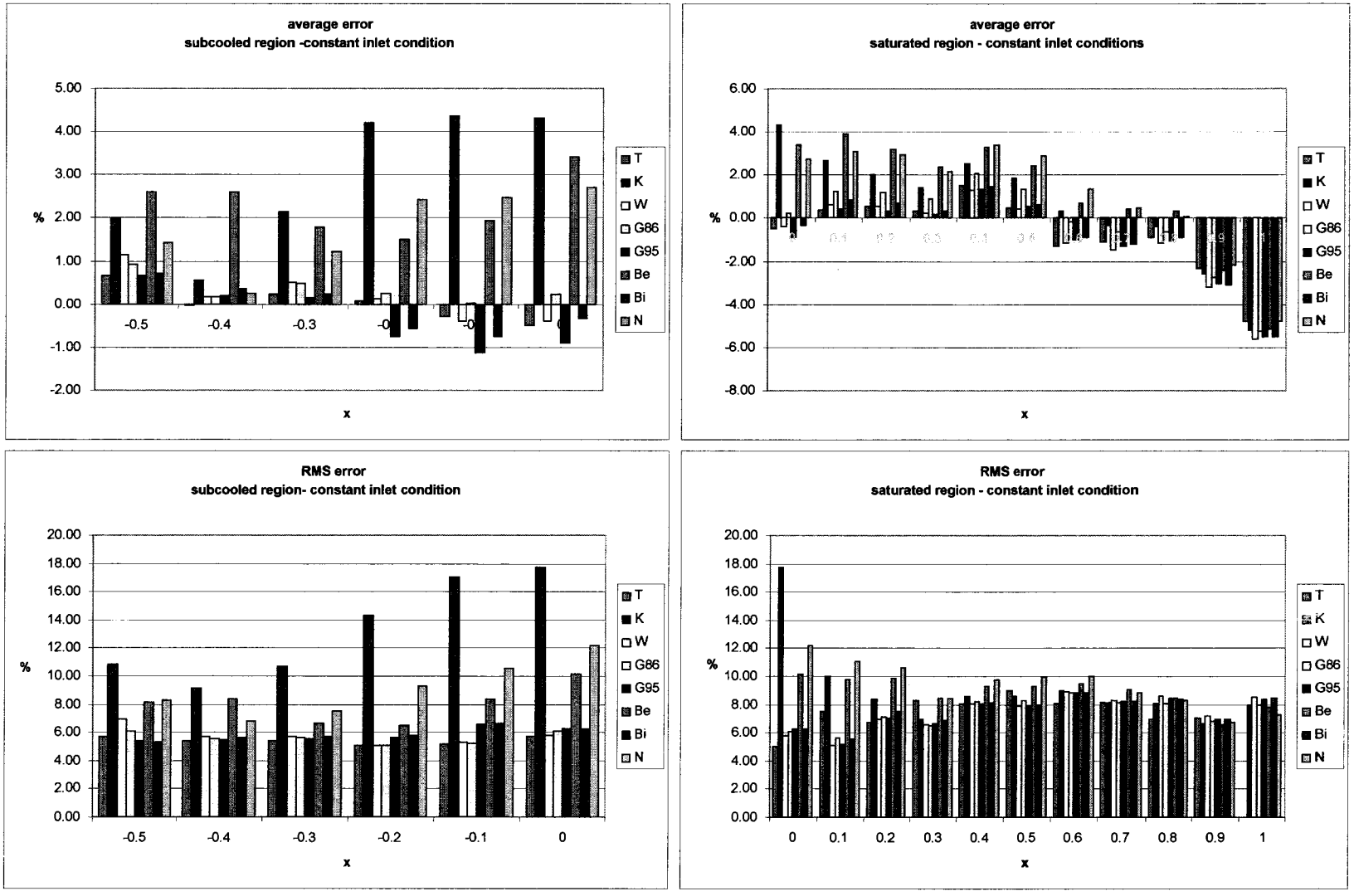

Figure A3-1 Error distribution with respect of critical quality

Table A3-2 Error distribution with respect of pressure for different diameter corrections, at constant inlet conditions

	P [MPa]	2	4	6	8	10	12	14	16	18	20
T	Avg	-1.34	-0.02	0.21	-0.50	0.38	0.92	0.75	-0.90	0.13	0.49
	RMS	12.04	6.44	6.70	4.55	5.62	5.55	5.99	4.94	4.84	5.36
K	Avg	-1.02	2.81	4.02	0.72	1.15	3.32	1.25	0.69	1.05	2.63
	RMS	11.59	10.23	12.84	6.81	7.78	9.18	7.79	6.05	6.56	9.37
W	Avg	-1.89	0.09	0.18	-0.38	0.46	1.11	0.90	1.42	0.06	0.11
	RMS	11.53	6.60	6.86	4.60	5.67	5.58	6.08	5.39	5.09	5.47
G86	Avg	-1.40	1.47	1.58	0.16	0.68	1.82	1.08	-0.52	0.42	1.01
	RMS	11.11	7.47	7.54	4.98	5.50	5.60	6.19	4.94	4.95	5.58
G95	Avg	-1.85	-0.16	-0.11	-0.35	0.45	0.96	0.92	-1.43	-0.09	-0.01
	RMS	11.53	6.54	6.91	4.63	5.89	5.75	6.11	5.39	5.19	5.63
Be	Avg	-0.67	2.90	4.12	1.83	1.86	3.38	2.38	1.18	1.88	3.42
	RMS	12.44	9.44	10.17	7.82	7.41	7.66	7.37	6.32	6.82	7.97
Bi	Avg	-1.77	0.12	0.24	-0.15	0.57	1.19	1.06	-1.25	0.09	0.32
	RMS	11.86	6.67	6.84	4.85	6.03	5.94	6.25	5.27	5.22	5.70
N	Avg	-0.56	4.61	5.08	1.20	1.18	3.52	1.39	1.28	1.37	2.76
	RMS	11.60	12.24	13.26	7.88	6.65	8.16	7.38	6.83	6.64	8.39

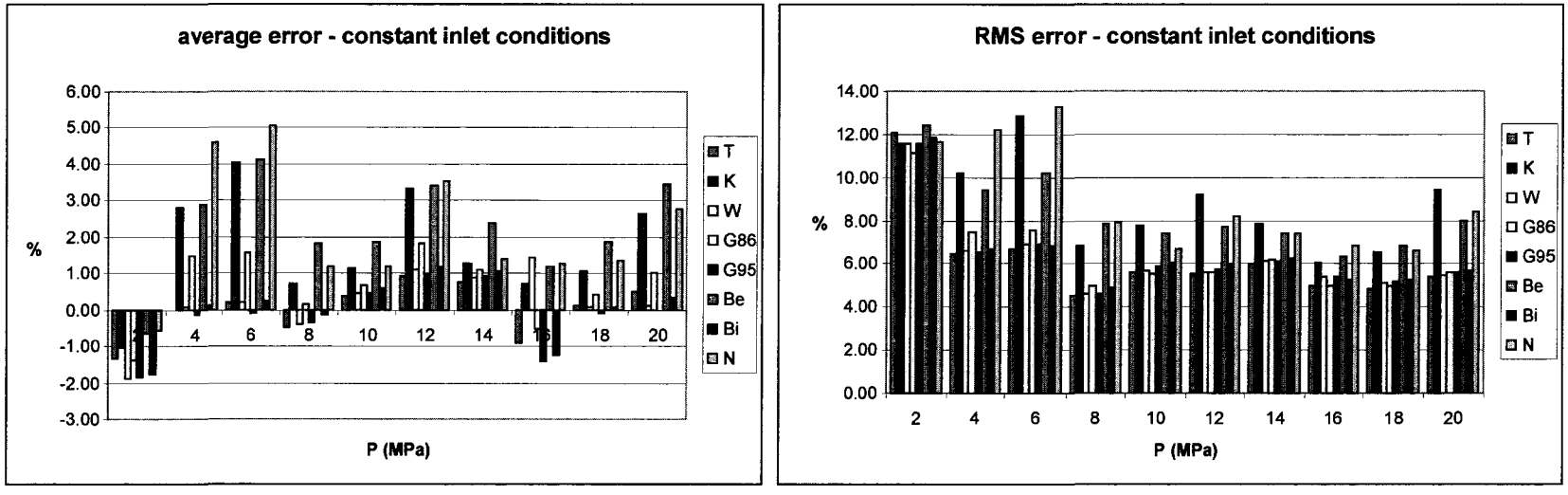

Figure A3-2 Error distribution with respect of pressure

Table A3-3 Error distribution with respect of mass flux for different diameter corrections, for constant inlet conditions

	G [$Mgm^{-2}s^{-1}$]	0	1	2	3	4	5	6	7	8
T	Avg	-1.56	0.37	0.45	-0.04	0.19	-0.70	0.99	-0.54	1.98
	RMS	11.16	7.92	5.48	5.15	5.74	4.93	5.77	7.45	8.86
K	Avg	-0.97	2.40	2.86	1.36	1.12	-1.75	2.61	0.23	2.73
	RMS	10.03	10.06	8.89	10.14	10.25	7.52	9.31	11.14	13.62
W	Avg	-2.59	0.37	0.50	0.14	0.10	-0.25	0.67	-0.65	2.79
	RMS	10.70	7.88	5.62	5.21	5.78	5.12	5.98	7.85	9.63
G86	Avg	-1.56	1.27	1.31	0.39	0.39	-0.60	1.11	-0.60	2.53
	RMS	9.95	7.94	6.10	5.71	6.10	4.87	5.82	7.13	8.38
G95	Avg	-2.40	0.34	0.26	-0.04	-0.07	0.05	0.22	-0.70	3.13
	RMS	10.50	7.98	5.63	5.23	5.94	5.54	6.15	9.13	11.52
Be	Avg	-0.51	2.52	2.34	3.13	1.46	3.97	1.63	0.43	8.41
	RMS	10.68	9.47	7.79	8.48	8.54	10.03	8.68	10.52	15.77
Bi	Avg	-2.25	0.53	0.37	0.20	0.28	0.62	0.07	-0.17	4.38
	RMS	10.60	8.14	5.63	5.32	6.40	5.96	6.64	10.29	13.14
N	Avg	-0.03	3.04	3.41	1.34	1.44	-1.81	2.97	-0.03	2.24
	RMS	10.26	10.21	9.57	9.52	10.12	6.26	8.30	8.80	9.23

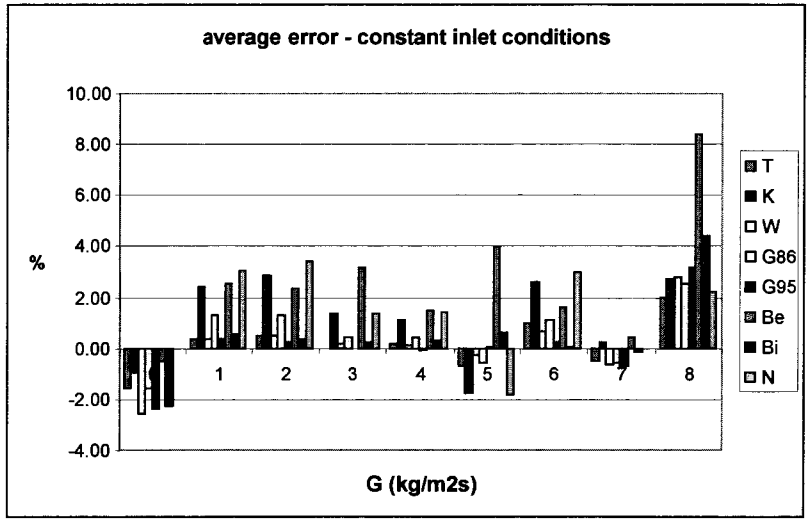

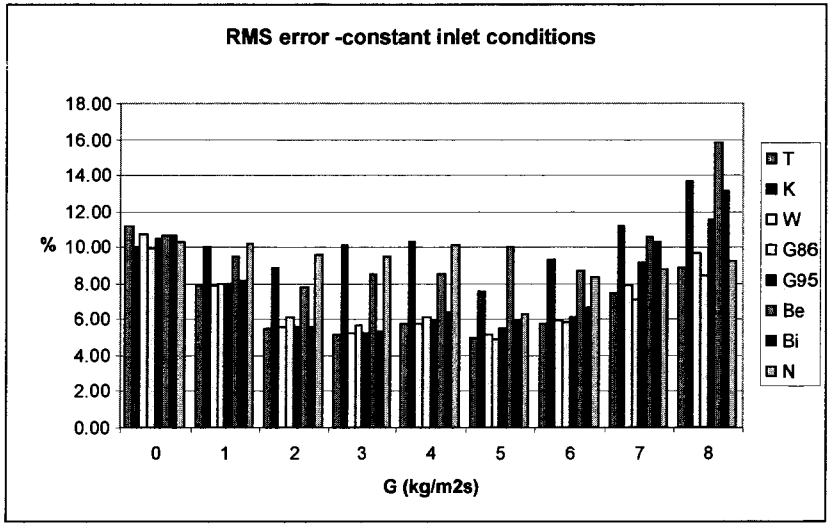

Figure A3 - 3 Error distribution with respect of mass flux

Table A3-4 Error distribution with respect of critical quality for different diameter corrections, for constant local conditions

	X	-0.5	-0.4	-0.3	-0.2	-0.1	0	0.1	0.2	0.3	0.4	0.5	0.6	0.7	0.8	0.9	1
T	Avg	0.53	0.22	0.68	0.37	-0.46	-0.55	1.32	2.11	4.92	16.43	9.58	1.55	-0.45	2.39	-1.40	-49.20
	RMS	10.86	10.78	10.92	10.24	11.36	12.14	11.51	14.59	25.35	65.37	46.42	42.61	36.59	38.95	52.18	70.36
K	Avg	4.50	2.43	5.82	10.13	9.66	10.45	7.39	5.88	8.31	20.76	16.43	8.39	4.02	5.99	-3.47	-52.11
	RMS	23.58	20.66	23.20	30.78	35.00	39.88	28.40	19.13	27.78	67.76	52.05	47.42	40.00	42.06	47.30	66.53
W	Avg	1.60	0.74	1.30	0.43	-0.53	-0.10	1.98	2.30	4.83	16.03	9.52	2.10	-0.62	2.80	-8.95	-55.83
	RMS	13.38	11.64	11.63	10.13	11.47	12.43	11.87	14.47	25.60	65.24	46.47	42.97	39.22	44.17	42.91	66.36
G86	Avg	1.14	0.74	1.28	0.69	0.09	0.86	3.05	3.77	6.59	18.70	3.67	6.00	2.42	4.94	-5.31	-53.49
	RMS	11.66	11.15	11.47	10.27	11.35	12.85	12.58	15.08	26.12	66.34	49.32	45.29	39.39	42.39	45.41	66.27
G95	Avg	0.65	0.74	0.60	-1.07	-1.44	-0.73	1.68	2.09	4.77	16.13	9.92	2.65	-0.09	3.21	-8.11	-55.27
	RMS	10.44	10.90	10.99	10.31	13.01	13.21	12.26	14.69	25.71	65.27	46.67	43.19	39.05	43.59	43.37	66.29
Be	Avg	6.05	6.98	4.73	3.92	5.99	10.01	10.87	10.83	13.22	25.22	19.12	10.37	8.86	11.97	-3.23	-52.26
	RMS	19.21	19.60	14.99	14.19	19.97	23.74	24.04	25.83	34.31	70.53	53.72	48.34	48.29	52.73	48.69	66.85
Bi	Avg	0.84	1.10	0.76	-0.70	-0.67	0.45	2.58	2.84	5.30	16.56	10.34	2.96	0.28	4.03	-8.32	-55.03
	RMS	10.62	11.30	11.25	10.81	13.91	14.19	13.23	15.62	26.28	65.39	46.84	43.19	39.75	55.50	43.57	66.35
N	Avg	2.44	1.06	3.06	5.26	4.59	5.71	7.06	8.47	11.39	25.16	22.81	14.22	8.73	9.90	1.30	-49.22
	RMS	16.51	14.36	15.89	18.67	19.91	24.27	23.32	25.21	32.65	71.68	59.72	53.98	44.57	44.18	52.42	67.33

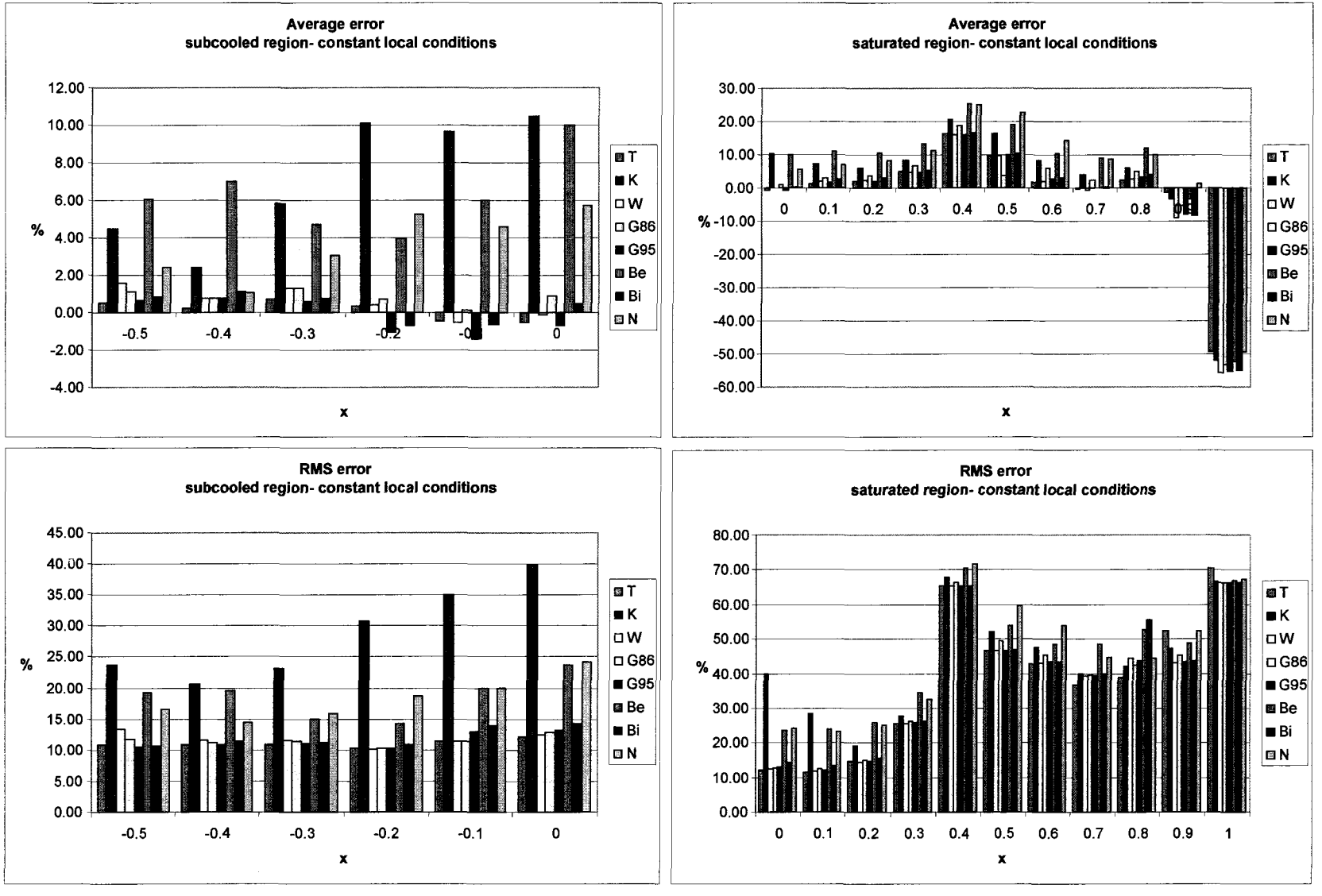

Figure A3 - 4 Error distribution with respect of quality

Table A3-5 Error distribution with respect of pressure for different diameter corrections, for constant inlet conditions

	P [MPa]	2	4	6	8	10	12	14	16	18	20
T	Avg	-0.83	3.31	2.60	-1.82	5.78	8.38	10.06	-0.75	4.41	4.20
	RMS	43.32	39.84	30.48	22.97	36.56	43.35	52.78	23.48	25.94	22.73
K	Avg	0.44	10.45	12.09	3.00	8.41	16.25	12.75	5.49	8.30	14.62
	RMS	44.29	41.87	40.06	29.41	40.29	49.34	55.56	27.62	32.00	47.25
W	Avg	-2.42	1.60	2.15	-1.44	6.23	8.95	10.71	-2.18	3.97	3.52
	RMS	44.29	34.95	29.48	23.35	36.80	43.38	53.02	24.25	26.39	23.27
G86	Avg	-0.66	7.00	6.21	0.73	7.04	11.47	11.49	0.71	5.42	5.94
	RMS	43.83	38.51	32.54	25.30	37.62	44.68	53.57	23.87	26.49	23.71
G95	Avg	-2.25	1.83	1.93	-1.17	6.31	8.78	10.81	-2.17	3.98	3.49
	RMS	44.14	35.17	29.75	23.56	36.96	43.53	53.10	24.28	26.58	23.53
Be	Avg	3.38	12.15	14.76	6.49	11.68	17.71	17.30	8.80	12.28	19.74
	RMS	50.60	43.40	39.99	31.77	41.85	50.08	56.29	30.96	34.82	41.73
Bi	Avg	-1.96	2.66	2.70	-0.66	6.67	9.37	11.30	-1.64	4.61	4.67
	RMS	44.76	35.91	30.05	24.04	37.20	43.64	53.29	24.07	27.00	24.66
N	Avg	3.43	19.72	16.91	5.75	9.14	18.34	13.52	8.35	9.58	13.25
	RMS	45.80	53.19	45.70	34.21	41.39	51.53	56.24	31.82	33.11	37.57

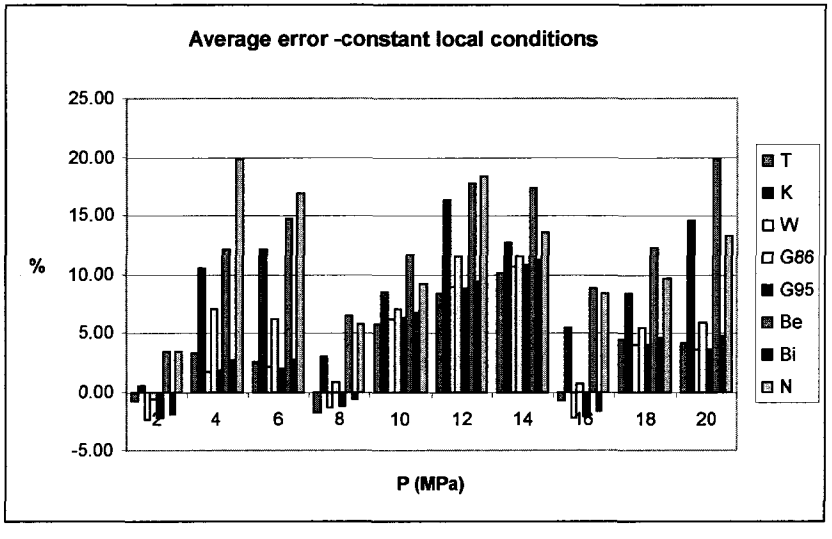

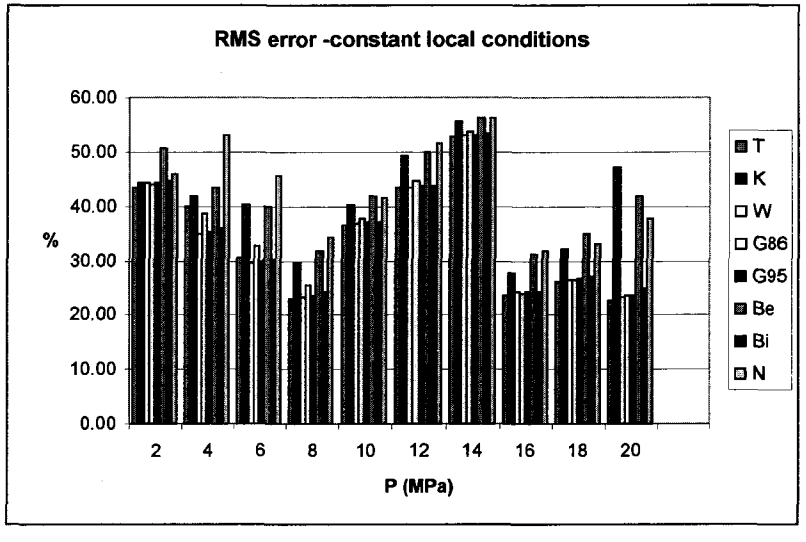

Figure A3 - 5 Error distribution with respect of pressure

Table A3-6 Error distribution with respect of mass flux for different diameter corrections, for constant inlet conditions

	G [$Mgm^{-2}s^{-1}$]	0	1	2	3	4	5	6	7	8
T	Avg	-3.19	7.73	5.20	1.98	0.42	-0.24	1.88	0.25	3.47
	RMS	47.12	49.19	32.19	17.29	13.05	12.55	10.95	11.79	14.83
K	Avg	-0.64	15.52	12.04	5.24	1.84	-3.39	5.60	1.70	4.97
	RMS	46.37	55.92	37.40	32.31	20.17	16.39	17.84	20.26	26.60
W	Avg	-7.46	7.85	5.24	2.84	0.52	1.41	1.30	0.09	4.96
	RMS	45.10	49.38	32.31	18.04	13.77	13.77	11.43	12.44	16.37
G86	Avg	3.56	11.19	7.64	2.94	0.76	0.08	2.07	0.06	4.33
	RMS	44.22	51.33	33.56	18.03	13.45	12.39	11.05	11.18	14.44
G95	Avg	-6.80	7.94	4.74	2.70	0.42	2.46	0.49	0.27	5.75
	RMS	44.75	49.59	32.31	18.22	14.41	14.77	11.69	14.77	19.46
Be	Avg	2.47	17.15	10.65	14.09	3.42	17.39	3.67	2.74	15.54
	RMS	52.51	55.67	36.39	31.32	19.21	33.82	17.55	19.45	26.00
Bi	Avg	6.31	8.51	4.87	3.52	1.38	4.23	0.24	1.31	8.04
	RMS	45.48	49.78	32.25	19.00	16.06	16.68	12.78	17.33	22.73
N	Avg	4.79	19.39	14.48	4.25	2.46	3.95	5.88	0.89	3.21
	RMS	48.97	59.76	39.96	22.92	19.54	13.32	15.60	14.60	16.70

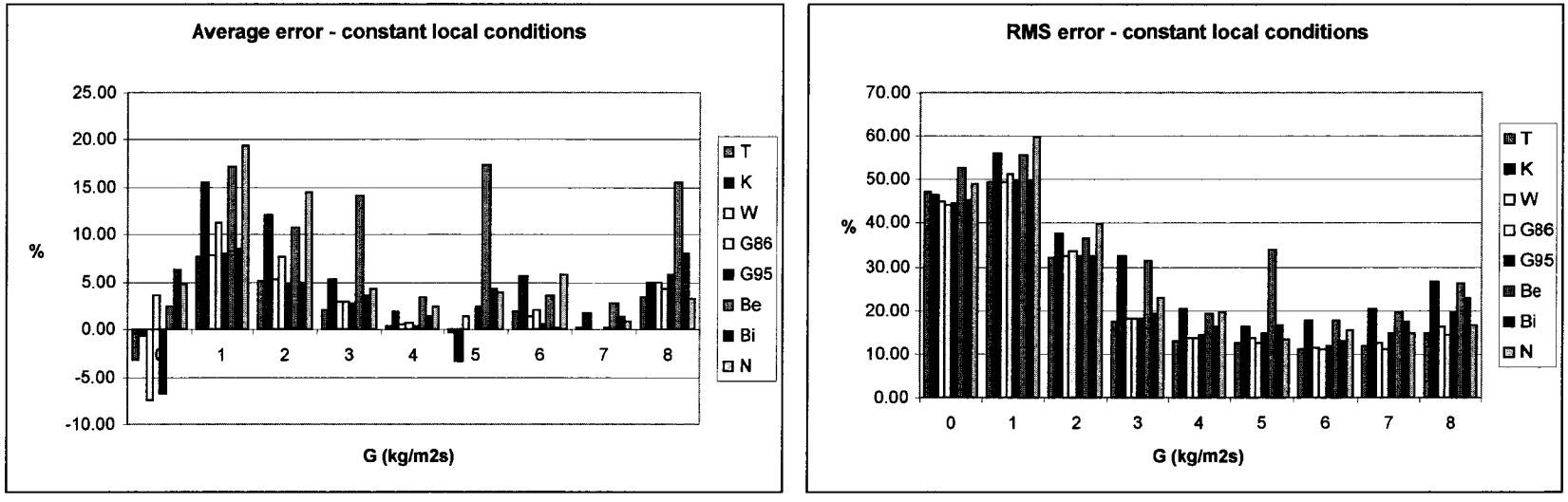

Figure A3 - 6 Error distribution with respect of mass flux

Appendix 4: List of publications authored or co-authored by A. Tanase

Tanase, A., Nakla, M., Zahlan El, H., Groeneveld, D.C. and Cheng, S.C., 2006, Impact of circumferential location of a flow obstacle on critical heat flux in tubes, UO-MCG-TH-2006-002, Technical Report

Shan, J. Q. ,Vasic, A. , Groeneveld , D. C., Peng S.W, Cheng S.C., Tanase, A , 2005, Methods in improvement of 2005 CHF Look up table, UO-MCG-TH-2004-003, Technical Report

Groeneveld, D.C., Shan, J.Q., Vasic , A.Z., Leung, L.K.H., Durmayaz ,A., Yang, J., Cheng, S.C. , Tanase, A., 2005, The 2005 CHF Look-up Table, Proceedings, 11th International Topical Meeting on Nuclear Reactor Thermal-Hydraulics (NURETH-11), Avignon, France, October 2-6,

Groeneveld, D.C. , Vasić , A.Z. , Yuan, L.Q., Leung, L.K.H., Tanase, A. , Shan, J.Q. and Chandraker, D. K., 2007, Tube CHF database compilation and assessment, Paper submitted to the 12th Intern'l Topical Meeting on Nuclear Reactor Thermalhydraulics, Pittsburgh, October 2007

Shan, J.Q., Li, C.Y., Groeneveld, D.C. , Vasić , A.Z. , Yang, J., Tanase, A. Cheng, S.C., Durmayaz, A , Methodology of CHF Look up table derivation, submitted for publication.

Tanase, A., Groeneveld, D.C., Shan, J.Q., Cheng, S.C., Diameter effect on CHF, Technical note in preparation

Tanase, A., Groeneveld, D.C., Cheng, S.C., Length-to-diameter effect of CHF, Technical note in preparation